Study of Mechanical Properties and Erosive Wear Characteristics of Epoxy-Glass Fiber Composites Reinforced with a Nanoclay (Cloisite 15A)

A Dissertation

Submitted in partial fulfillment of the requirements for

the award of the degree of

DOCTOR OF PHILOSOPHY

in

MECHANICAL ENGINEERING

by

Z. Shanti Kiran
(Roll No: 714020)

Supervisors:

Dr. V. Suresh Babu
Professor
&
Dr. K. V. Sai Srinadh
Professor

DEPARTMENT OF MECHANICAL ENGINEERING

NATIONAL INSTITUTE OF TECHNOLOGY,

WARANGAL (TS) - 506004, INDIA.

FEBRUARY 2020

DEPARTMENT OF MECHANICAL ENGINEERING

NATIONAL INSTITUTE OF TECHNOLOGY WARANGAL

CERTIFICATE

This is to certify that the dissertation work entitled "**Study of Mechanical Properties and Erosive Wear Characteristics of Epoxy-Glass Fiber Composites Reinforced with a Nanoclay (Cloisite 15A)"** which is being submitted by **Mr. Z. Shanti Kiran (Roll No. 714020)**, is a bonafide work submitted to the Department of Mechanical Engineering, National Institute of Technology, Warangal in partial fulfillment of the requirement for the award of the degree of **Doctor of Philosophy** in **Mechanical Engineering.**

To the best of our knowledge, the work incorporated in this thesis has not been submitted elsewhere for the award of any degree.

Dr. V. Suresh Babu
Professor
Supervisor
Department of Mechanical Engineering
National Institute of Technology
Warangal- 506004

Dr. K. V. Sai Srinadh
Professor
Co-Supervisor
Department of Mechanical Engineering
National Institute of Technology
Warangal- 506004

Prof. R. Narasimha Rao
Head, Department of Mechanical Engineering
National Institute of Technology
Warangal-506004

APPROVAL SHEET

This Thesis entitled **"Study of Mechanical Properties and Erosive wear Characteristics of Epoxy-Glass Fiber Composites Reinforced with a Nanoclay (Cloisite 15A)"** by **Z. Shanti Kiran** is approved for the degree of Doctor of Philosophy.

Examiners

_____

_____

_____

Supervisor

Dr. V. Suresh Babu
Professor
MED, NIT Warangal

Co-Supervisor

Dr. K. V. Sai Srinadh
Professor
MED, NIT Warangal

Chairman

Prof. R. Narasimha Rao
Professor& Head,
MED, NIT Warangal

Date: 28-02-2020

DEPARTMENT OF MECHANICAL ENGINEERING
NATIONAL INSTITUTE OF TECHNOLOGY
WARANGAL – 506 004

Dedicated to

My Parents Sri Tukaram Zhade and

Smt Durga bai

My beloved wife Meghamala

&

All my teachers

DECLARATION

This is to certify that the work presented in the thesis entitled **"Study of Mechanical Properties and Erosive wear Characteristics of Epoxy-Glass Fiber Composites Reinforced with a Nanoclay (Cloisite 15A)"** is a bonafide work done by me under the supervision of **Dr. V. Suresh Babu and Dr. K.V. Sai Srinadh,** and was not submitted elsewhere for the award of any degree. I declare that this written submission represents my ideas in my own words and wherever others ideas or words have been included those ideas and words were adequately cited and referenced the original sources. I also declare that I have adhered to all principles of academic honesty and integrity and have not misrepresented or fabricated or falsified any idea/data/fact/source in my submission. I understand that any violation of the above will be a cause for disciplinary action by the Institute and can also evoke penal action from the sources which have thus not been properly cited or from whom proper permission has not been taken when needed.

Date: 28-02-2020 (**Z. Shanti Kiran**)

(Roll No.: 714020)

ACKNOWLEDGMENT

I would like to express my sincere thanks and gratitude for my supervisors, **Dr. V. Suresh Babu and Dr. K. V. Sai Srinadh,** Mechanical Engineering Department, National Institute of Technology, Warangal, for their continuous guidance, support, enthusiasm and motivation in my PhD research work.

I am grateful to **Prof. N.V. Ramana Rao,** Director NIT Warangal, who has been a constant source of inspiration for me. I thank **Prof. N. Selvaraj,** Head of the Department of Mechanical Engineering and one of the members in the Doctoral Scrutiny Committee, for his help and continuous encouragement to complete this work. I would like to express my sincere thanks to **Prof. A. Kumar** (Mechanical Engineering Department), and **Prof. N. Narasaih** (Metallurgical and Materials Engineering Department), learned members of my Doctoral Scrutiny Committee for being helpful and generous during the entire course of this work.

My sincere thanks also go to **Prof. C.S.P Rao, Prof. S. Srinivasa Rao** and **Prof. P. Bangaru Babu** former HoDs, Mechanical Engineering Department, National Institute of Technology, Warangal, for their encouragement, for providing access to the laboratory and research facilities. Without their precious support, it would not be possible to conduct this research.

I sincerely thank **Dr. M Raja Vishwanathan**, Department of Humanities & Social Sciences for his help.

I sincerely express my deepest gratitude to my fellow scholar - **Mr. M Kameswara Reddy** for his help and extreme support.

I would like to thank my parents **Sri. Tukaram Zhade** & **Smt. Durga Bai**, my wife **Meghamala,** and my brothers **Srinivas Zhade & Keshav Zhade** for supporting me throughout writing this thesis.

I would like to thank my fellow scholars **K. Nagabhusan**, **K. Ganesh**, **Ravichandra, Ch. Shyam Kumar** and co-scholars for their help and encouragement.

I would like to thank Mr. R. Ravinder, a technician in IC engines lab; K. Yellaswamy, technical officer, workshop; Ravi, technician, IC engines lab; Shyam, technician, workshop; Sathish, technician, IC engines lab for their support and help.

I would like to thank Dr. I. Sriknath, scientist, RCI, Hyderabad; Ivaturi sivaram, Ram Composite Products, Hyderabad; Dakshina Murthy, Succin engineering works, Hyderabad for their help.

I would like to thank Dr. Arockia Kumar, MME Dept., NIT Warangal; Dr. Ajoy Kumar Pandey, MME Dept., NIT Warangal; Dr. Bonta Srinivasa Rao, MME Dept., NIT Warangal; Dr. Gujjala Raghavendra Mech. Engg. Dept., NIT Warangal, for their help.

Above all, I express my deepest regards and gratitude to "**ALMIGHTY**" whose divine light and warmth showered upon me the perseverance, inspiration, faith and enough strength to keep the momentum of work high even at tough moments of research work.

Z. Shanti Kiran
(Roll No: 714020)
Research Scholar
Department of Mechanical Engineering
National Institute of Technology Warangal- 506004

ABSTRACT

The progress in the domain of material technology has led to numerous new and advanced materials. Polymer nanocomposites are one of the emerging classes of materials which are used in different engineering applications. The properties of fiber reinforced thermoset composites make them appropriate for use in diverse fields, namely aviation structures, car parts, marine structures, and so forth. These composites possess notably high strength and stiffness to weight fractions, good creep resistance, erosion resistance, and great damping properties. Fiber reinforced polymeric composites are a good choice in structural constructions.

The present research is focused on the preparation of epoxy-glass-clay nanocomposites (EGCNs) and optimization of their mechanical properties and erosion wear. The experiments are conducted according to Taguchi method and Response surface method and analyzed using ANOVA. These methods were used to comprehend the relation among different controllable variables and to recognize the effective variables that enhance the properties of EGCNs.

A total of six objectives were solved in this study, out of which four are related to mechanical properties and two are related to erosive wear studies of the composites. The effects of selected parameters, i.e., nanoclay wt%, glass fiber vol%, and glass fibers orientation on the selected mechanical properties i.e., tensile strength (σ_{UTS}), flexural strength (σ_f), plane strain fracture toughness (K_{IC}), and microhardness are studied and are optimized for highest value of each property, respectively. The same method is followed for two cases of erosive wear studies, where, in the first case, the effects of composite parameters i.e., nanoclay wt%, glass fiber vol%, and fibers orientation are studied to optimize the parameters for lowest wear rate. In the second case, the testing parameters selected are sand flow rate (f), impingement angle (θ), air stream pressure (P), holding period (t), and stand-off distance (d). The effects of testing parameters were studied and optimized for the lowest wear rate of the composite. For design of experiments, analysis of results, and optimization of parameters Taguchi method and response surface methodology (RSM) were used. For Taguchi analysis Minitab software was used and for RSM analysis Design Expert software was used. The objectives have been taken up after a thorough review of literature.

Taguchi L9 design of experiments has been selected for optimization of each mechanical property. For the selected three parameters, each with three levels, the suitable design is L9 array. The experiments were performed according to the L9 design and the output values were entered in the Minitab software. The software transforms the output values into S/N ratios and based on ANOVA analysis of these S/N ratios it was observed that all the parameters were significantly affecting the mechanical properties except in microhardness testing where the angle of fibers did not affect the microhardness. A linear regression model was generated in each case using which the optimum value of response was computed and validated experimentally.

Taguchi method assumes only a linear relation between control factors and output. In order to check for the interaction effects, response surface methodology (RSM) was used. A central composite design was selected and totally twenty experiments were conducted. After the analysis, the results obtained at the optimum conditions were compared with the properties of the neat glass-epoxy composite (GRE) and a good improvement in the mechanical properties and decrease in erosion wear was observed. The fracture surfaces of the nanocomposite samples have shown critical fracture i.e., matrix-fiber separation is not smooth and surfaces of matrix and fibers were rough. The increase in strength of EGCN due to nanoclay addition to glass-epoxy is explained as follows: i) The amino functional groups present on the surface of the nanoclay, can contribute in the cross linking reaction with the epoxy functional groups present in epoxy matrix resulting in improved interface crosslink density. The improved crossllink density at the fiber-matrix interface results in an improved interface toughness. This enhanced interface toughness due to nanoclay, improve the ability of the matrix to transmit the load uniformly across all the layers by holding the fibers in place. ii) Due to the improvement in the interface toughness more load is required for the specimen to fail, thus strength is improved.

CONTENTS

LIST OF FIGURES

LIST OF TABLES

NOMENCLATURE

Acronyms

MMT	-	Montmorillonite
OMMT	-	Organic modified montmorillonite
DMT	-	Direct mixing technique
EGCNs	-	Epoxy-Glass-Clay nanocomposites
FRPC	-	Fiber reinforced polymer composites
FRP	-	fiber reinforced polymer
GRE	-	Glass fiber reinforced epoxy
HSMT	-	High shear mixing technique
ILSS	-	Interlaminar shear stress
PMCs	-	Polymer composites
SENB	-	Single edge notch bending
NE	-	neat epoxy
ANOVA	-	analysis of variance

Notations

N	-	Nanoclay wt.%
G	-	Glass fiber vol.%
O	-	Orientation angle of glass fibers
V	-	volume
R	-	resin content
r	-	reinforcement
D	-	density of resin
d	-	density of reinforcement

Symbols

σ_{uts}	-	Ultimate tensile strength
σ_f	-	Flexural strength
K_{IC}	-	Plane strain fracture toughness
HV	-	Vickers hardness number
E_r	-	Erosive wear rate
%	-	percentage
V_f	-	volume fraction of fibers

T_d	-	theoretical density
M_d	-	experimental density
S_g	-	specific gravity
*	-	multiplication
<	-	less than
>	-	greater than
+	-	plus
-	-	minus
&	-	and
x, y, z	-	axis directions

Units

mm	-	millimeter
m	-	meter
nm	-	nanometer
µm	-	micrometer
KN	-	kilo Newton
MPa	-	mega pascal
GPa	-	giga pascal
mg	-	milligram
gm	-	gram
kg	-	kilogram
A˚	-	angstrom
s^{-1}	-	per second
mPa-s	-	milli pascal second
g/eq	-	gram per equivalent
g/cc	-	gram per centimeter cube
°C	-	degree centigrade
meq	-	milli equivalent

Chapter 1

Introduction

1.1 Background

In the current era, much effort is invested in developing new composite materials which are superior to existing materials in terms of their mechanical and physical properties. Quite a large number of studies have been published in the area of behavior, characterization, and modelling of composite materials, from metal matrix composites [1–3] to polymer matrix composites [4–7]. There are a number of definitions for composite materials but the common feature of each definition is the presence of two or more constituents with an interface between them.

Conventional composites, such as metal-based composites, can be based on heavy (traditional) engineering materials. For instance, in automobiles or air- crafts, the consumption of fuel is related to the weight of the vehicle. Therefore, the heavier the vehicle the higher is the consumption of fuel. To decrease consumption, conventional materials can be replaced by light-weight materials. Just to give an example of how beneficial it is to develop light-weight materials, current estimates suggest that a 6-8% saving in fuel is possible for every 10% reduction in vehicle weight [8].

The use of glass fibre reinforced epoxy composite in various applications with advantage is undisputed. These may include aerospace materials, ship building materials, automotive industry in seismic retrofit of columns and strengthening of walls, new building frames, and bridges pertaining to civil engineering, etc. GFRP pipes are now in demand for the transport of liquids, especially sea water, for desalination. Further, these materials are now considered for use as insulating material for superconducting magnetic coils in fusion reactors. It will not be out of place to mention here that such a variety of use of the materials is possible owing to its light weight, toughness, insulating properties, specific strength, improved fatigue properties and design flexibility owing to the fact that the material can be tailored to suit the specific application. On account of the above, it is only pertinent that these

materials retain the stability of structure and properties under the unique, specific, and service related environmental exposures over prolonged periods for trouble-free long-life.

Therefore, these materials must be evaluated under stringent environmental conditions of moisture, humidity, temperature fluctuations including thermal shock, nuclear radiations, marine environment and any combination of the above to which they would be exposed during their lifetime.

GFRP consists of epoxy resin as the matrix that houses and holds the glass-fibers in position and this combination offers improvement in properties as listed above, over conventional materials. During operation, both the matrix and fibre must stand the shock effects even under environmental severities. In addition, the glass-matrix interface, where the shock is actually transmitted from the matrix to the fibre, must transfer the shock efficiently and effectively to the fibre without itself getting affected in any way. These can be achieved if materials concerned and process variables are judiciously chosen. An arguer on these fronts requires an in-depth study, experimentation, and evaluation of the material under the injury-prone environment of application [9].

1.2 General Overview of Polymers

1.2.1 Definition and Classification of Polymers

Polymers are composed of large macromolecules, which can interact with each other via intermolecular forces. In a highly crystalline polymer, the polymer chains can be oriented and packed regularly with respect to each other. Conversely, an amorphous polymer will have randomly and irregularly packed polymer chains. A polymer can also be semi-crystalline or in other words a polymer can have both crystalline and amorphous regions. The extent of the crystalline region in a polymer can be indicated by the term degree of crystallinity, which indicates the fractional amount of polymer that is crystalline. Polymeric materials can have different Physico-chemical and thermo-mechanical properties as a function of the degree of crystallinity [10–14]. Polymers are sub-categorized into four classes according to their structure, which is shown in Fig. 1.1

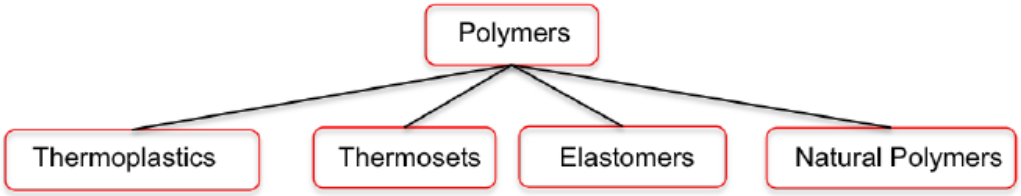

Figure 1.1 Classification of polymer types

1.2.2 Introduction to Epoxy Polymers

Epoxy resins are one of the most widely used thermoset polymers for composite applications. Epoxy resins are characterized by having one or more epoxide end groups in the monomer. The epoxide functional group is a cyclic ether with a three-membered ring, consisting of two carbon atoms and one oxygen atom, as illustrated in Fig. 1.2. The triangular configuration in an epoxide group creates strains within the ring and makes this functional group highly reactive compared with other ethers [15].

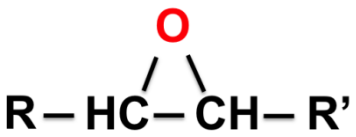

Figure 1.2 Example of an epoxide functional group, where R and R' may refer to a hydrogen atom or other functional groups [15]

Generally used cross-linkers are amines, aldehydes, and anhydrides. Amines contain reactive nitrogen atoms which react with epoxy monomers. Aliphatic amines are widely used amine-based cross-linkers for epoxy polymers. Aldehydes have an aldehyde functional group, which can then react with epoxide functional groups via their oxygen atoms. Anhydrides first react with an alcohol to form a carboxylic group, which can subsequently react with epoxy monomers.

Epoxy monomers and cross-linking agents are mixed in a pre-determined ratio. This ratio depends on the types of monomer and cross-linker pair. The curing temperature can vary

depending on the monomer/cross-linking agent pair. The curing temperature is typically above the T_g value of the material under investigation [16]. The reactive carbon atom present in the methylene group reacts with the nitrogen atom of the amine group of the cross-linker and a hydrogen atom of the amine group reacts with the oxygen atom in the epoxide group. After the curing time has elapsed, the sample is taken out of the chamber and set aside for cooling [17]. Fig. 1.3 depicts a representative illustration of a cross-linking reaction between epoxy and hardener molecule.

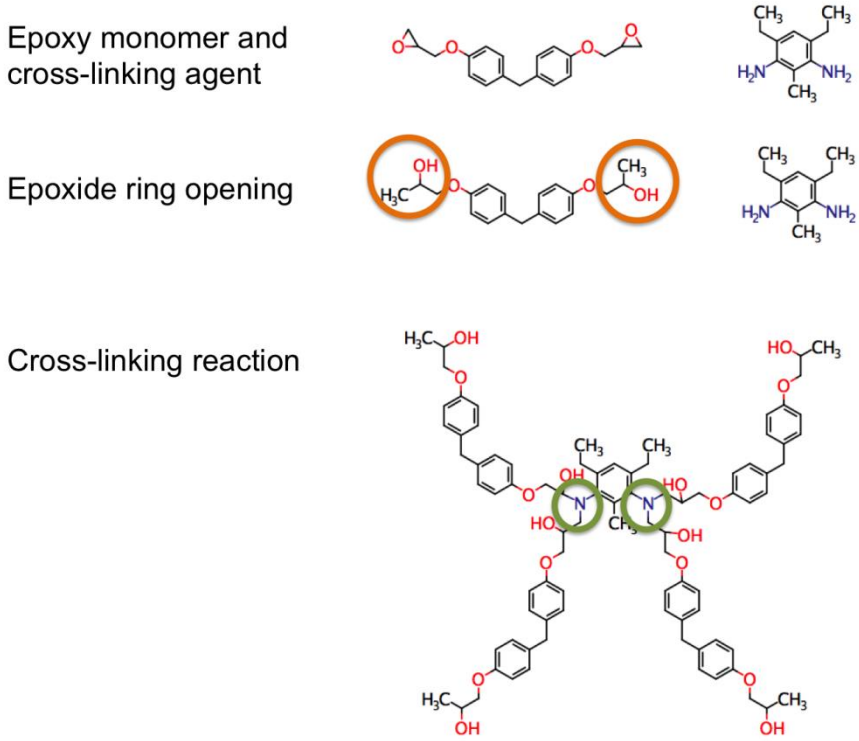

Figure 1.3 Illustration of epoxy monomer and cross-linking agent, ring-opened monomer and the product of the cross-linking reaction [17].

An autoclave is typically needed to produce high-performance composites [18, 19]. The curing reaction includes many factors that can affect the physico-chemical properties of the resultant polymer matrix. Epoxy monomer and cross-linker pairs can react at different rates at different temperatures; therefore, the curing temperature is of paramount importance in the polymer curing process. Molecules can move faster at higher temperatures in the liquid pre-cursor polymer mixture, which increases the chance of collisions between the reactive atoms leading to successful formation of cross-links. The optimum curing temperature can be

determined based on reaction kinetics studies of the polymer sample, which relates the curing temperature to the cross-linking reaction rate [20, 21]. Once the formation of cross-links starts in the reaction chamber, the curing reaction ideally ends when all available reactive atoms react. In practice, this is rarely achieved. The extent of the cross-linking reaction can be expressed via the degree of cross-linking (DOC). In epoxy polymers, the DOC can be, in theory, defined as the ratio between the number of reacted epoxy carbon sites and the total number of epoxy carbon sites in the system. However, in practice, this cannot be readily directly measured in an experimental system. As the number of cross-links increases; the DOC increases, the mobility of the polymer chains becomes progressively more restricted during the curing reaction [22, 23].

The architecture of the polymer network can influence the thermo-mechanical properties of the resultant polymer [24]. In addition to curing temperature, curing time is another important factor determining the ultimate properties of the resultant polymer matrix [25]. At the very beginning of the curing process, the rate of cross-link formation can be high due to the availability of reactive atoms. Over time, this rate tends to decrease as the polymer sample solidifies. This rigidity impedes the diffusion of unreacted molecule; hence, it extends the required time for the formation of new cross-link bonds. Moreover, epoxy polymer samples can be obtained at lower curing temperatures, but this typically requires longer curing time, provided the curing temperature is above the required minimum temperature, which can be determined by kinetics studies. A fast curing of the polymer matrix may lead to the formation of defects in the polymer matrix, such as voids, and these structural changes in the polymer matrix may, in turn, produce inferior thermo-mechanical properties, which may be due to the changes in the viscosity of the polymer matrix during curing [26]. For example, Sun et al. [27] showed that higher heating rate in the curing process produced samples with a higher glass transition value for an epoxy system of E51 (epoxy resin) and 593 (hardener). Also, Liu et al. [28] reported a decrease in the value of tensile modulus as a function of void content in an epoxy-based carbon fibre composite.

1.2.3 Properties of Epoxy Polymers

Several factors, such as the particular epoxy-cross-linker pair, curing temperature, etc. dictate the properties of the resultant epoxy matrix. Moreover, keeping the monomer same and

changing the cross-linker (or vice versa) can impart drastically distinct features to the resultant polymer matrix [29].

The term “epoxy resin” is applied to both the prepolymer and the cured resin; the former contains reactive epoxy groups (see Fig. 1.4), hence the name.

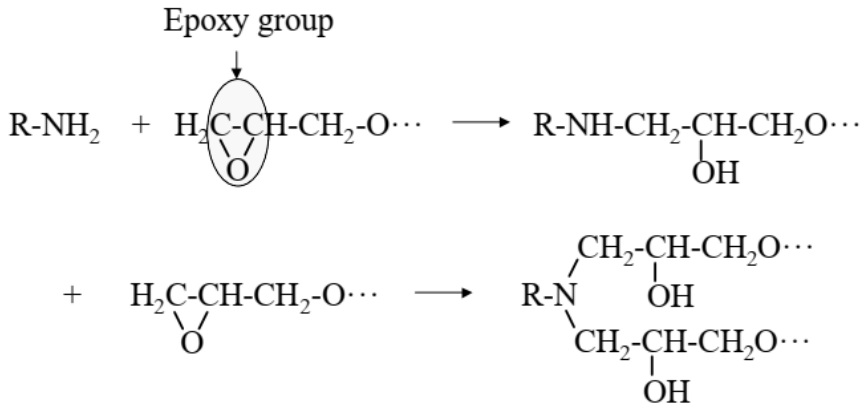

Figure 1.4 Mechanism of cure of epoxy with primary amines. –CH_2O…. indicates that only the reactive epoxy group is shown [30].

In order to convert epoxy resins into hard, infusible thermoset networks, it is necessary to use curing agents. Diamines are the most widely used curing agents because they offer good reactivity with the epoxy groups. Fig. 1.4 illustrates the initial step, which involves the primary amine active hydrogen adding to the epoxy group. This is followed by the resulting secondary amine addition to another epoxy group. Hydroxyls groups, including those generated during cure, accelerate the reaction by favoring the epoxy ring-opening. Epoxy-clay nanocomposites have been extensively studied [31]. The reason for this is that the reactants of epoxy systems have a suitable polarity to diffuse between the clay layer and form an exfoliated nanocomposite upon polymerization.

1.3 Introduction to Glass Fibre: Structure and Properties

1.3.1 Definitions and Properties of Glass Fibre

Glass fiber is available in the form of a mat consisting of fine glass fibers knitted together. The modern commercial glass fiber for modern applications started to be

manufactured after the invention of machine tools. Edward Drummond Libbey made a dress using glass fiber in 1893 which was exhibited at World's Columbian Exposition held in Chicago, USA.

The properties obtained by reinforcing glass fibers in the composite are roughly comparable to the properties obtained by reinforcing high-performance fibers such as carbon fibers in the same matrix. Glass fiber is cheap, but it is highly brittle in nature which reduces significantly when present in the composite. Therefore glass fibers are used as reinforcement in a wide range of polymers.

1.3.2 Fiber Formation

Glass fibers are formed when thin strands of silica based or other formulation of glass are extruded into many fibers with small diameters suitable for textile processing. The technique of heating and drawing glass into fine fibers has been known for millennia; however, the use of these fibers for textile applications is more recent.

Pure silica also can be used to drawn into fibers but it has the drawback of high working temperature which has to be reduced by adding of fluxing agents. The first continuous fiber filaments were made of E-glass and it is also a widely used glass fiber globally. But it easily reacts with chlorine and corrodes, because of which it is not preferable for marine applications. For high strength applications, S-glass is preferred because it has higher strength compared to E-glass. S-glass can be used in civil structures. For applications which require chemical resistance, T-glass and C-glass are preferred.

Games Slayter invented glass wool at the Glass Co., Toledo, Ohio. In 1936 commercial production of glass wool started. The production of continuous fiber filaments started in 1938 with the collaboration of Owens-Illinois Glass Company Corning Glass Works [32]. The two companies formed Owens-Corning Company which is the main producer of glass fiber to date. [33].

E-glass consists mainly of alumino-borosilicate with less than 1% alkali oxides. A-glass contains mainly alkali-lime glass with negligible boron oxide. E-CR-glass contains alumino-lime silicate with negligible alkali oxides (<1%). C-glass consists of high alkali-lime

glass and the boron oxide content is very high. D-glass consists of mainly borosilicate, R-glass is an alumino silicate with no MgO or CaO and S-glass is an alumino silicate with high MgO but no CaO [34].

1.3.3 Chemistry

The basic constituent of glass fiber is SiO_2 which has no true melting temperature but starts degrading at 1200 °C. At 1713 °C, the molecules start moving freely within the crystals. If cooled suddenly at 1713 °C, the molecules will be locked in their positions and unable to form an ordered crystal structure [35]. The glass will have the same energy levels in amorphous and crystalline state and in terms of stability amorphous glass is more stable. In order to impart crystallinity to the amorphous glass, it has to be heated to above 1200 °C [32].

Pure SiO_2 has good properties required for reinforcement but the working temperature of SiO_2 is very high; hence in order to reduce its working temperature, impurities are added. The impurities added also impart some special properties which are required for specific applications. A-glass is the first in such types of glasses, and also goes by the name of soda-lime glass. A-glass easily reacts with the alkalis. E-glass contains alumino borosilicate which consists of <2% of alkali this one used in electrical applications due to good electrical resistance. If the applications require chemical resistance, then C-glass is a good choice [36].

1.3.4 Forms of glass fiber

Fiberglass roving is produced by collecting a bundle of strands into a single large strand, which is wound into a stable, cylindrical package. This is called a multi end roving process. The process begins by placing a number of oven-dried forming packages into a creel. The ends are then gathered together under tension and collected on a precision roving winder.

Woven roving is the fabric form formed from the rovings. This product is used for making FRPs using hand-layup method and other methods which involve panel molds. The woven rovings are again classified based on weave pattern. For high strength in a specific direction, unidirectional fabric is suitable; while for two directions, plain or twill patterns are suitable. There are many other patterns also being developed, for example, tri-axial patterns, which are being developed for special applications.

Fiberglass mats are produced in two forms, one is a continuous fiber mat and the other is a chopped strand mat. The chopped strand mat consists of chopped fibers dispersed on a belt coated with glue. The glue used is generally thermoplastic. The continuous strand mat consists of the deposition of continuous fibers in random orientations maintaining uniform thickness on a thermoplastic glue coated belt. The continuous fiber will get entangled within and the mat becomes densely packed with no way of detaching fiber from the mat. These mats are used in closed mold fabrication methods [37].

1.4 Fiber-reinforced polymer composites (FRPC)

In fiber-reinforced composites, the fibers possess high strength and modulus. Fibers are the main constituent in the composite because fibers carry the load applied on the composite, whereas the matrix acts as a binding agent between fibers while also keeping the fibers in position. In addition, matrix serves to protect the composite from damage. The applied load is transferred to fibers uniformly with the help of a matrix. These properties cannot be obtained with a single material and thus both constituents are needed.

Fiber-reinforced polymer composites (FRPC) have been used for thousands of years [38]; however its application in modern times in aeronautical components was witnessed in 1960s. The applications were limited due to the high cost of production, but with invention of computer-aided manufacturing, the cost has reduced to an affordable amount for any field [39]. The prominent fields of applications are automotive sector, construction sector, naval applications, wind energy sector, etc.

1.4.1 Role of fiber reinforcement in FRP

The improved properties of the composites are attributed to the properties of the fibers. These improved properties are dominated by fibers and hence are called fiber dominated properties. As the fiber volume increases in the composite, fiber dominated properties increase up to a certain extent and then decrease when the optimum quantity of fiber volume is crossed. This decrease in mechanical properties beyond the optimum quantity of fiber volume is attributed to the insufficient volume of matrix, which has to hold the fibers together so that the load may be transferred uniformly. In addition to fiber volume, other factors which

also affect the properties of composites are length of fiber, form of fiber, fiber orientation, etc. [40].

1.5 Nanocomposite Concept

Nanocomposites are materials that are created by introducing nanoparticulates into a matrix. There is a drastic improvement in mechanical properties with the addition of nanomaterials into various matrix materials. In general, the content of nanoparticles that can be added to the composite ranges between 0.5% and 5%. It is because of the high surface area of nanomaterials at a given weight content compared to the micron-sized powder of the same material. Plenty of research is in progress to develop nanocomposites with multiple functionalities.

A nanocomposite is a material consisting of a polymer matrix and a nanofiller or a polymer matrix with two reinforcements, one being a continuous or discontinuous fiber and the other a nanofiller. The nanoparticles should have at least one dimension on the nanometer (nm) scale (10^{-9} m). Based on the nanoparticle dimensions, nanocomposites can be classified as follows: (i) All three dimensions at the nanometer level, e.g., spherical silica; (ii) Two dimensions at the nanometer level, e.g., carbon nanotubes and cellulose whiskers; (iii) One dimension on the nanometer scale, e.g., layered silicates (clay, mica, etc.).

The preparation of nanocomposites is a scientific and technical challenge. In many systems, the chemical nature of the filler is less important than the particle size and shape, the surface morphology, and the extent of distribution within the polymer matrix. The layered silicate nanocomposites have attracted attention due to their inexpensive and abundant availability, high aspect ratio, and excellent barrier properties.

1.5.1 Polymer Nanocomposites

The term “polymer nanocomposite” broadly describes any number of multicomponent systems where the primary component is the polymer matrix and the filler material has at least one dimension below 100 nm [41]. Polymer nanocomposites are generally lightweight,

require low filler loading, often easy to process and provide property enhancements extending orders of magnitude beyond those realized with traditional composites.

1.5.2 Filler

Filler is a term which encompasses a vast number of materials and plays a significant role in improving the composite properties. Fillers help minimize cost, enhance properties, and improve the composites. Fillers also increase the tribological properties and reduce shrinkage of the composites during curing. Proper selection of matrix and filler combination will lead to the creation of composites with high mechanical, tribological, thermo-mechanical properties, etc. which are comparable to metals.

Conventional Fillers

Particulate fillers have played a vital role in the development of commercial purpose polymers. The primary filler types utilized may be classified as natural and synthetic fillers. Calcium carbonate, kaolinite, metakaolin, silica, and calcium sulphate, etc., are commonly employed, natural fillers. Synthetic fillers are prepared by chemical processes, with carbon black being among the most well-known. Carbon black has been widely used as reinforcement in rubber. Synthetic silica is another example of synthetically prepared filler which has found wide application in silicone elastomers [42].

Originally, fillers were primarily considered cheap diluents. However, their ability to beneficially modify polymer properties was quickly realized. Some of the main reasons for using particulate fillers include cost reduction, improved processing, thermal conductivity, controlled thermal expansion, flame retardancy, and improved mechanical properties. Evidently no single filler has provided all of these benefits. Ideally, fillers improve some properties without negatively affecting other properties. The magnitude of the property change observed is not only a function of the filler composition but is strongly influenced also by particle size, shape, and surface chemistry [42]. Particle size, shape, and ability to bond with the polymer matrix are all important factors in determining filler performance.

Nanofillers

In nanocomposites, at least one dimension of the dispersed particles is in the nanometer range. The nanoparticles whose three dimensions are in the order of nanometers are silica, titanium dioxide, carbon black, silicon carbide, zinc oxide, aluminium oxide, and polyhedral oligomeric silsesquioxanes. If two of its dimensions are nanosized and the third is in microns, such particles will be in the form of nanotubes and nanofibers. The third type of nanocomposites is characterized by only one dimension in the nanometer range.

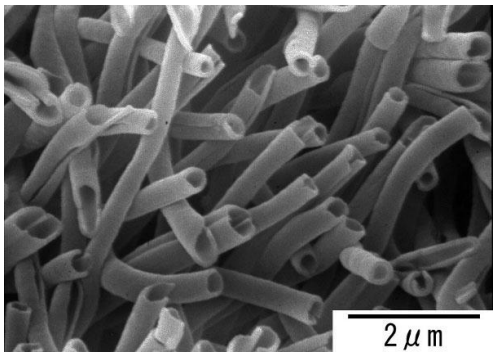

(a) Single wall carbon nanotubes

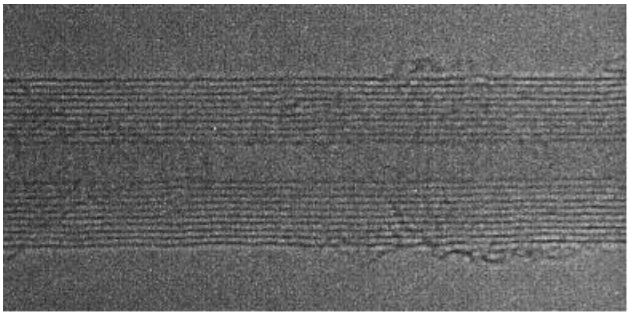

(b) Multiwall carbon nanotubes

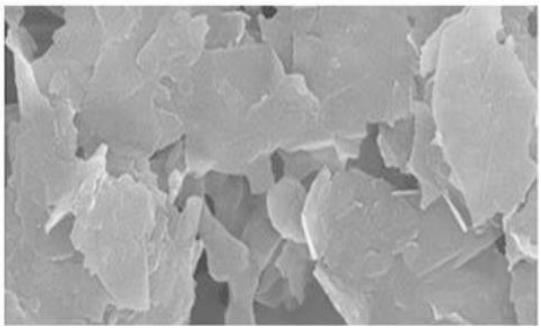

(c) Graphite flakes

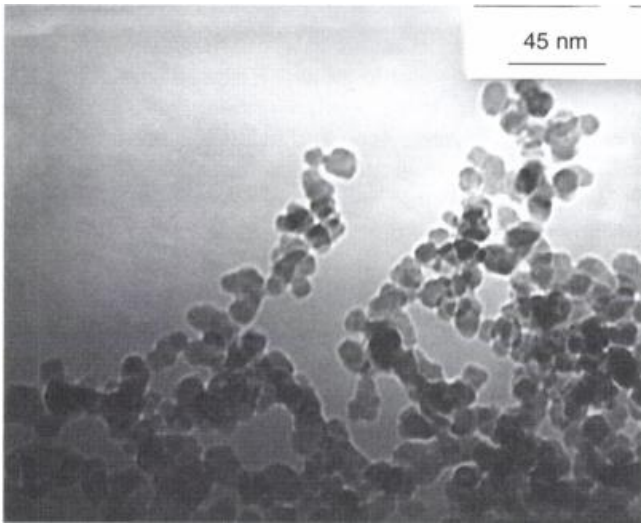

(d) Silica nanoparticles

Figure 1.5 Different types of fillers (a) Single-wall carbon nanotubes (b) Multiwall carbon nanotubes (c) Graphite flakes (d) Silica nanoparticles [43].

If there is only one dimension in nano size, the particles will be in the form of sheets. Silicate platelets, layered double hydroxides, and graphite flakes are examples. Fig. 1.5 shows the types of nanofillers. The ratio of surface area to volume of nanopowder plays a significant role in understanding the structure-property relation of composites. Nanoparticles are added to composites to enhance stiffness and strength. By reducing the particle size from micron range to nano range, novel materials with good properties can be developed [43].

The filler particle size determines the "inner" or specific surface area which is the potential contact area between filler material and surrounding binder matrix. Since nanomaterials tend to agglomerate, resulting in reduced surface area of contact with matrix. Fully exfoliated and perfectly dispersed nanofiller will have the greatest effect on the properties. A comparison between different particles sizes is shown in Fig. 1.6.

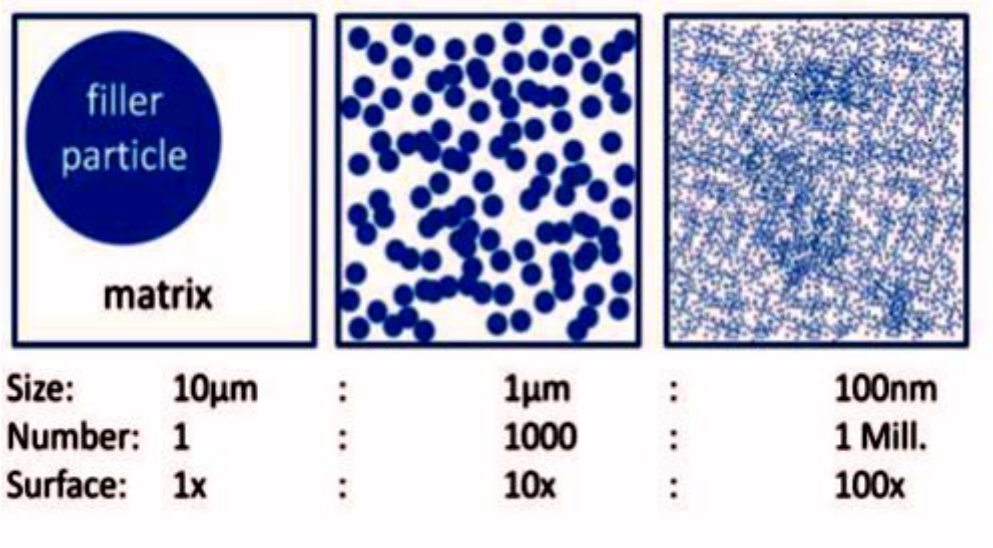

Figure 1.6 Filler particles of same weight and sizes (a) 10µm (b) 1 µm (c) 100 nm [44].

The specific surface area is increased 100 fold when going from 10 µm to 100 nm while keeping the theoretical volume constant. More recently new developments have shown that nanoparticles can lead to special effects which cannot be reached so easily with conventional/traditional fillers. However, often, the optimum effects for reducing both coefficient of friction and the wear rate can be achieved if nanofillers are used in combination with some traditional tribo fillers [44].

1.5.3 Layered Silicates

The generic term “layered silicates” refers to natural clays and also refers to synthesized layered silicates. Natural clays as well as modified clays are being used as reinforcement in polymers. Montmorillonite is natural clay with a high charge density. Charge density is the total number of cations in between the silicate layers of montmorillonite which can be substituted with organic cations. Montmorillonite was discovered by Montmorillon in 1847 in France.

Crystallography

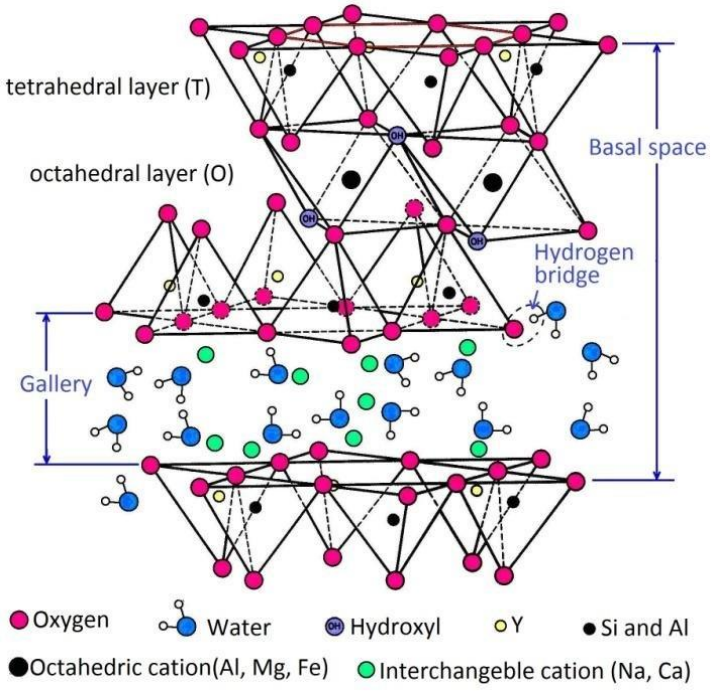

Figure 1.7 Idealised structure for montmorillonite [45].

The crystallographic structure for montmorillonite is shown in Fig. 1.7. It must be emphasised that the structure proposed is idealised and that in reality the lattice is distorted [45]. This model was is proposed by Hoffmann et al. [46]. The structure consists of sandwich type of structure formed by two silica sheets and one alumina sheet. The negative charge is created in the lattice of montmorillonite due to the substitution of silicon in place of aluminum in the silica crystal and substitution of aluminium in place of magnesium in alumina crystal. To balance the negative charge, the positive cations are attracted and adsorbed onto the clay.

There will be Van der Waal gap between the sandwich structures. Montmorillonite is hydrophilic in nature due to which water molecules from the atmosphere get absorbed within the structure.

Cation-Exchange

Montmorillonite has a natural ability to adsorb some cations which can be exchanged with organic cations when the montmorillonite is treated with organic solutions. K^+, Na^+, H^+ Mg^{2+}, Ca^{2+} and NH^{4+} are common exchangeable ions of clay. For example, if clay is treated with a solution containing other ions, these ions substitute the cations present on the clay surface. The exchange between cations as explained above is shown in equation (1).

$$X.clay + Y^+ \rightleftharpoons Y.clay + X^+ \quad \text{……. (1)}$$

The cation-exchange process is controlled by the diffusion of the ion replacing the existing resident on the cation-exchange site. It is considered to occur in two stages [47]:

1. Diffusion from the bulk of the solution through the individual layers (film diffusion) surrounding the clay particles (Nernst diffusion).
2. Diffusion within the particle itself (particle diffusion).

Compatibilizing Agents

Clays are hydrophilic and organophobic in nature and need to be treated with compounds to make them organphilic. These compounds are called compatibilizing agents. The first compatibilizing agents used for nanoclays were amino acids [48]. Numerous other kinds of compatibilizing agents have since been used in the synthesis of nanocomposites. The most popular are alkylammonium ions because they can be exchanged easily with the ions situated between the layers. Silanes have been used because of their ability to react with the hydroxyl groups situated possibly at the surface and at the edges of the clay layers.

Amino Acids

Amino acids are molecules which consist of a basic amino group ($-NH_2$) and an acidic carboxyl group (-COOH). In an acidic medium, a proton is transferred from the –COOH

group to the intramolecular $–NH_2$ group. A cation-exchange is then possible between $–NH^{3+}$ function formed and a cation (i.e. Na^+, K^+…) intercalated between the clay layers so that the clay becomes organophilic.

A wide range of ω-amino acids ($H_3N^+(CH_2)_{n-1}COOH$) have been intercalated between layers of montmorillonite [49]. Amino acids were successfully used in the synthesis of polyamide 6-clay nanocomposites [50]. Thus, the intragallery polymerisation occurs which delaminates or separates the clay platelets in the polymer matrix and a nanocomposite is formed.

Alkylammonium Ions

Montmorillonite nanoparticles are naturally hydrophilic but if treated with alkylammonium ions, the particles become organophilic. The organically treated montmorillonite when dispersed in liquids like epoxy forms gels [51, 52]. The length of the ammonium ions has a strong impact on the resulting structure of nanocomposites. Lan et al. [53] showed that alkylammonium ions with chain length larger than eight carbon atoms favouring the synthesis of exfoliated nanocomposites, whereas alkylammonium ions with shorter chains led to the formation of intercalated nanocomposites. Alkylammonium ions based on secondary amines have also been successfully used [54].

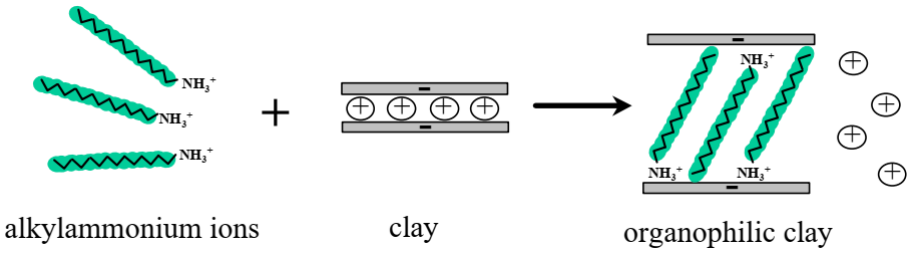

Figure 1.8. The cation-exchange process between alkylammonium ions and cations initially intercalated between the clay layers [55]

A schematic diagram showing substitution of alkylammonium ions in place of interlayer cations is shown in Fig. 1.8. The structure of the organic cations between silicate layers depends on the charge density of clay [55]. In Fig. 1.8, alkylammonium ions adopt a paraffin type of structure due to which the spacing between the clay layers increased by about

10 A°. Alkylammonium ions permit lowering the surface energy of clay so that organic species with different polarities can get intercalated between the clay layers.

1.5.4 Silanes

Silanes have been used in the synthesis of unsaturated polyester-clay nanocomposites. Silane coupling agents are a family of organosilicon monomers which are characterised by the formula R-SiX_3, where R is an organofunctional group attached to silicon in a hydrolytically stable manner. X designates hydrolyzable groups which are converted to silanol groups on hydrolysis.

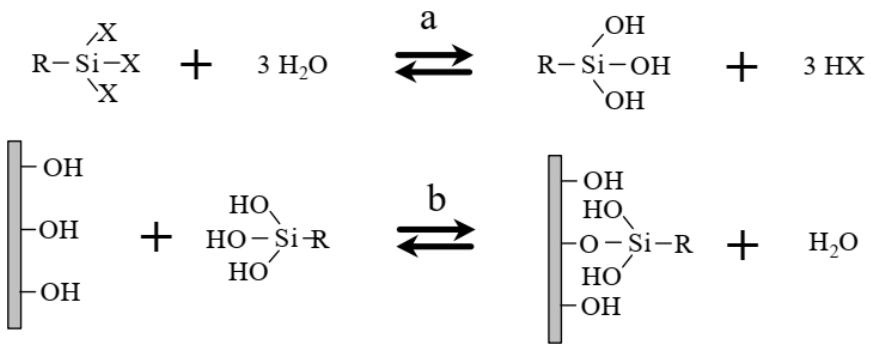

Figure 1.9. The hydrolysis of the silanes (a) and the possible reaction of a silanol group with a hydroxyl group present on the inorganic surface (b).

Silanes have good adherence to inorganic surfaces. The OH groups present on the particle surface react with the silanes and these OH groups are also attached to silicon or magnesium atoms of the inorganic particles. In clays the OH groups are available on the layers and edges of layers. Silane first reacts with water molecules and forms silanol which then forms bond with the OH groups present on clay surface. Fig. 1.9 shows the stepwise reaction as explained.

1.6 Summary

Based on the above discussion, it is observed that out of the three types of surface modifiers alkyl ammonium ions are the most popular because they have higher affinity with silicate layers compared to amino acids and silanes. Depending on the layer charge density of

the clay, alkyl ammonium ions may adopt different structures between the clay layers. Alkyl ammonium ions reduce the electrostatic interactions between silicate layers thus facilitating diffusion of polymer molecule in between clay platelets or galleries [56]. In the present work alkyl ammonium ions treated nanoclay i.e., Cloisite 15A was selected to study its effect on the mechanical properties and erosion wear of epoxy-glass composite.

Chapter 2

Literature Survey

2.1 Introduction

Literature survey was conducted to have the extensive knowledge of polymer nanocomposites, their mechanical behaviour and characteristics. Study by A. K. Dhingra [57] has shown that minimum 20% of cost is saved if polymer composites (PMCs) replace the metal structures and the operating and maintenance costs are also very low. Polymer composites are easy to repair, have good durability, and maintenance is simple. There is a consistent requirement of composites in the industries with invention of new applications. The Composites will continue to find new applications, but the large scale growth in the market place for these materials will require less costly processing methods and the prospect of recycling will have to be solved [58, 59].

Polymer composites have been emerging as materials for structural components in place of metals in various fields. Typical features like light weight and high strength make the FRPs attractive in various structural applications. The controllable anisotropy is one of the credentials. There are many other benefits of composites namely fatigue strength and corrosion resistance. The special characteristic of a composite is that the properties can be tailored according the requirement of end product by selecting a proper combination of matrix and reinforcement.

Generally, a discontinuous phase (reinforcement) is embedded into a continuous phase (matrix). PMCs make up a major portion of composites in various applications. The properties of polymer composites can also be tailored by fiber size, orientation, configuration such as long, short, woven, stranded mat, etc. PMCs exhibit desirable physical and chemical properties that include lightweight coupled with high stiffness and strength along the direction of the reinforcing fiber, dimensional stability, temperature and chemical resistance and relatively easy processing. This chapter consists of detailed explanation about effects of various surface modified nanoclays on various mechanical properties of epoxy based composites.

2.2 Tensile properties

EGCN exhibited 54% improvement in modulus at 10 wt% addition of octadecylammonium treated fluorohectorite (ME-ODA) but there was a 36% decrease in strength while ductility was also reduced. The stress-strain curve of GRE exhibited ductile behavior, and the EGCN exhibited brittle behavior [60]. Bozkurt et al. [61] reported that when MMT is added to epoxy-noncrimp glass fabric composite, up to 6 wt% there was no improvement in strength and stiffness while both decreased beyond 6 wt%. This unchanging behavior is attributed to the dominant effect of noncrimp glass fibers over the nanoclay effect. Shi et al. [62] reported the effect of "Magnetic stirring" and high shear mixing technique (HSMT) on the tensile behavior of EGCN. When the magnetic stirring method was used, the increment in modulus of EGCN was about 19.4%, 22.2%, and 27.7% at 1, 2, and 3 wt% of nanoclay respectively. The increased modulus is credited to good dispersion of clay layers. At 1 wt% nanoclay, the tensile properties were compared between composites; one composite consists of epoxy-clay mixture processed by magnetic stirring, and the other by mechanical stirring. There was about 7.9% and 5.7% increase in σ_{UTS} and modulus for the EGCN with matrix processed by mechanical stirring. The epoxy molecular chains were prevented from moving when the load was applied. The clay layers hindered the molecular chains because of strong adhesion and chemical bond between organoions and epoxy, thereby enhancing the stiffness of the laminate. This mechanism of clay particles hindering epoxy molecular movement was also described by other researchers [63–65]. The formation of clay aggregates at low clay contents, i.e., at 2 and 3wt% clay addition was also reported in some literature [62, 65–67]. The increased tensile properties with addition of various surface modified nanoclays under different mixing conditions and making methods are shown in table 2.1.

Voids are formed while mixing nanoclay and hardener, and increases with clay content; due to an increase in the viscosity of the mixture, the removal of these gas bubbles becomes difficult when kept in degassing chamber. In addition to aggregates and voids, there is a possibility of a decrease in strength by other means, that is, through interruption of crosslinking of chains by silicate layers as a result of reaction of epoxy molecules with organoions, which breaks the continuity of the crosslinks, this claim is not yet fully established though [68–70]. The laminate fabricated from the matrix which was prepared by

HSMT provided the enhancement in strength and modulus by 7.9% and 5.7% as compared to the laminates made by using the matrix prepared by direct mixing technique (DMT) [62].

Gurusideswar and Velmurugan [71] carried out tension tests on laminates with the addition of Garamite-1958 (alkyl ammonium treated clay) at crosshead speeds of 0.5, 5, 50, and 500 mm/min. The stress-strain plot for EGCN at 1.5 wt% of nanoclay and at a testing speed of 5 mm/min was linear elastic with 9.9 % elongation and failed suddenly. At 500 mm/min there was a rise in strength, modulus, and ductility by about 17 %, 10.7 %, and 33.3% compared to the values at quasi-static loading, i.e., at 5 mm/min. σ_{UTS} is more sensitive to strain rate compared to the modulus which is due to dominant behavior of fibers in strength, whereas modulus is influenced by clay. The same behavior was exhibited by glass/epoxy composite (GRE). The increase in clay content by up to 5 wt% did not change the elongation (i.e., 9.9%) at quasi-static loading, but at high strain rates the elongation has reduced (i.e.. 9.6% at 500 mm/min). This is attributed to the high brittleness induced at high clay addition. At 1.5 wt% of nanoclay addition, the inversely proportional behavior between elongation and strain rate was not observed, unlike the case of 5 wt% clay added composite. The increase in strength is mainly attributed to presence of fibers and increase in modulus is mainly attributed to the silicate platelets which restrict the movement of epoxy molecules [72–76].

The optimum value of clay content is 1.5 wt%, whereas all tensile characteristics were improved at high strain rate, the slight decrease in properties above 1.5 wt% nanoclay is attributed to agglomeration and a weak interfacial bond between epoxy and clay. Increase in strain rate in the range of 0.0006 s^{-1} - 0.6 s^{-1} increased the strength and elongation of GRE. Okoli and Smith [77] reported that there was decrease in percentage elongation when GRE specimens were tested at various strain rates. Okoli and Smith [77] added that the decrease in elongation at high strain rates is explained with the help of Eyring theory of viscosity; while formulating this theory, an assumption has been made which states that the molecules of polymer need to cross the potential energy barriers to deform when a load is applied. Based on this assumption a linear model is developed which states that the plot between yield stress and a logarithm of strain rate is linear. This increase in yield stress with the logarithm of strain rate implies decreased plastic deformation of matrix due to decreased movement of crosslinked epoxy molecules at high strain rates. The constrained movement of molecules is ascribed to the lack of time available for the molecules to relax at high strain rates [78–80]. But according

to Gurusideswar and velmurugan [71] this effect was absent at 500 mm/min as there was an increased elongation for GRE at 500 mm/min compared to the elongation at quasi-static loading rate, which implies that 500 mm/min is not high enough to restrict the molecules' relaxation. The high modulus of clay is also one of the attributes for an increase in tensile properties and improved deformation mechanisms [81]. The exfoliated structures have a high surface area of contact between silicate platelets and resin; therefore transfer of load to clay platelets also will be more compared to the load transferred in intercalated structures [82–86]. Withers et al. [87] reported 11.7%, 10.6%, and 10.5% increase in strength, modulus, and elongation with 2 wt% of Cloisite 30B loading into glass-epoxy due to exfoliated morphology.

Gurusideswar and Velmurugan [88] reported the behavior of EGCN with the addition of GARMITE-1958 and at testing speeds varying between quasi-static rate of 0.00167 s^{-1} to very high strain rates of 315 s^{-1}, 385 s^{-1}, 445 s^{-1} which are far higher compared to the strain rates in the range of 0.0001- 0.1 s^{-1}. GRE exhibited about 106% and 67% improvement in modulus and strength at 445 s^{-1} compared to quasi-static conditions. EGCN exhibited about 150% rise in modulus and 84% rise in strength at 1.5 wt% clay addition and at 445 s^{-1} strain rate. This substantial rise in modulus and strength of EGCN is attributed to viscoelastic nature, damage accumulation behavior of epoxy which was also reported by Brown et al. [89] for GRE, restriction of polymers chain mobility in the matrix and at the fiber-matrix interface due to good adhesion between clay platelets and epoxy allowed better stress transfer to all the fibers. Similar findings were reported by many authors [64, 65, 90]. Jeyakumar et al. [91] reported the mechanical properties of EGCNs with the addition of Cloisite 93A into epoxy-glass. Nanoclay was mixed into acetone using a mechanical stirrer for 30 min. Epoxy resin of required weight was added into the acetone-clay mixture and heated to 80˚C and mixed for 1 hr. During this process acetone gets evaporated and epoxy clay mixture remains. The remaining mixture is unltrasonicated for uniform mixing. The testing results of the prepared samples showed that the σ_{UTS} improved by 6.6%, 16.6 %, and 23.58% at 1, 3, and 5 wt% of nanoclay, whereas tensile modulus improved by 8.4%, 14%, and 23.66%. With further addition of nanoclay, decreasing trend started [87, 92].

Achutha et al. [93] attempted to optimize the parameters such as nanoclay wt% and glass fiber content in EGCN. In addition, the samples were also subjected to hygrothermal conditions. A set of samples were soaked in cold water for 70 days and dried and another set

of samples boiled in hot water for 2 hrs and dried. It was reported from these studies that hydrothermal aging conditions showed 42.69% contribution to tensile properties whereas nanoclay content showed 24.57% contribution and fiber content showed 30.23% contribution. Achutha et al. [93] reported that nanoclay does not act as a load bearing instrument but it warrants load transfer to fibers as the interface between matrix and fiber becomes strong, which also hinders crack propagation. The samples treated with cold water exhibited lower σ_{UTS} and those treated with hot water exhibited lowest strength due to the moisture absorbed at the interface which weakens the interface strength. Moisture absorption increases with temperature.

Prabhakar et al. [94] studied the effect of Nanomer I.28E on mechanical properties of EGCN. In addition, the glass fiber was treated with silane and acid to check for the effects of both treatments. The results indicated that a combination of silane treated glass fibers and Nanomer I.28E in the composite exhibited highest σ_{UTS} which was 130% compared to EGCN with untreated glass fiber and unmodified MMT particles. Prabhakar et al. [94] showed that any increase in interfacial bond due to the addition of nanoclay led to increase in both σ_{UTS} and hardness of the composite. The treatment of fibers and organic modifier on MMT formed strong interface.

2.3 Flexural properties

Haque et al. [76] reported 24% and 17% enhancement in flexural strength (σ_f) and modulus at 1 wt% addition of Nanomer 1.28E in EGCN. Kornmann et al. [60] reported 6% and 27% improvement in flexural modulus and σ_f of EGCN at 10 wt% addition of ME-ODA. The increase in σ_f is linked to the existence of nano-silicate layers at the interface of the fiber, which might have improved interfacial properties. Another possible illustration is the fact that the compressive strength of epoxy is enhanced by presence of the silicate layers so that it in turn enhances the bending strength of the laminate. Bozkurt et al. [61] reported 16% and 13% improvement in σ_f and modulus at 6 wt% addition of OMMT. It was observed from the fracture surface that fracture occurred along the fiber-matrix interface and the fracture surface was rough indicating strong interface. The laminate without clay showed smooth fracture surface, which means the interface was weak. The increased flexural properties with the

addition of various surface modified nanoclays under different mixing conditions and making methods are shown in table 2.1.

Manfredi et al. [95] stated that the addition of Cloisite 10A in EGCN laminates caused the flexural modulus and strength to rise by 20% and 29%. The addition of Cloisite 30B did not cause any increment in the modulus of epoxy. It could be because of the collapse of clay particles, i.e. the particles were aggregated and the layers were not separated in the matrix. The modulus of clay nanoparticles is about 170 GPa. Therefore, when a strong bond is formed between matrix and clay it will result in increased modulus of the laminate [96]. The increase in bending strength is attributed to the presence of silicate layers upon the glass fiber surface which improving the adhesion between the interface of matrix and glass fibers. The other possible reason for the improvement in bending strength of laminate could be the increase in compressive strength of the epoxy. Shi and Kanny [62] reported that EGCN showed about 23% and 14% enhancement in modulus and strength at 3 wt% of Cloisite 30B. This enhancement is ascribed to the presence of intercalated silicate platelets of clay which interrupted the molecular motion of epoxy [64], [97]. The composites consisting of matrix processed by HSMT has shown 9.7% and 8.5% improvement in strength and modulus at 1 wt%.

Sharma et al. [98] observed improvement in σ_f up to 5 wt% addition of nanoclay. This increment is attributed to the presence of layered silicates on glass fiber surface enhancing the adhesive bond between the epoxy matrix and glass fibers [97]. In the range of 6 – 8 wt% of OMMT σ_f is reduced which was attributed to the agglomeration of OMMT in the EGCN. The uniform distribution and dispersion of silicate layers in epoxy resin are limited by the weight content of OMMT, when this content exceeds its percolation threshold (the ability of the liquid resin to pass through clay particles so that all the particles get wetted) there is a tendency to form particle aggregates [99]. The increased viscosity hinders the dispersion and favors the formation of agglomerates [100, 101]. The fracture surface of GRE has showed that the fibers pulled out from the matrix had smooth surface texture, whereas EGCN showed that less fiber pullout with rough surfaces of fiber and matrix indicating the strong bond between fiber and epoxy and improved stress transfer between fiber and matrix [102]. At 8 wt% clay addition there were agglomerates formed fully in the EGCN [99].

Table 2.1. Mechanical Properties of Epoxy/Glass/Clay nanocomposites

Author, Year	Nanoclay	Nanoclay wt%	Tension Testing Temperature	Glass Fiber	Observations
Reis et al. [103]	--	0	20 °C, 40 °C, 60 °C, 80 °C	70 wt%	Strength decreased with increase in temperature
Withers et al. [87]	Cloisite 30B	0, 2, 4 wt%	60 °C	---	2 wt% Nanoclay added EGCN composite had high strength and modulus compared to GRE.
Haque et al. [76]	Nanomer I.28E	0, 1, 2, 5, 10 wt%	Room Temp	---	At 1 wt% nanosilicates, there was 44, 24, and 23% improvement in ILSS, σ_f, and fracture toughness compared to GRE.
Bozkurt et al. [61]	MMT	0, 1, 3, 6, and 10%wt	Room Temp	40 – 44 vol %	i) Upto 6 wt% nanoclay addition σ_{UTS} and modulus were not changed. ii) At 6wt% of nanoclay, σ_f and modulus were improved by 16% and 13%. iii) At 10wt% of nanoclay, fracture toughness was improved by 5%

Shi et al. [62]	Cloisite 30B	0, 1, 2 and 3 wt%	Room Temp	55 – 58 vol%	**At 1 wt%** i) The tensile, flexural, and compressive modulus increased by 21%, 27%, 15% respectively. ii) The tensile, flexural, and compressive strength were increased by 18%, 25% and 30% respectively. iii) ILSS was increased by 25% and Impact strength was increased by 6%.
Zulfli and Chow[99]	Nanomer 1.28E	0, 2, 4, 6, 8 wt%	Room Temp	4 layers	i) At 4 wt% of clay, σ_f and modulus were improved by 19% and 9%. ii) At 2 wt% of nanoclay, fracture toughness was improved by 111%. iii) At 4wt% of nanoclay, impact strength was improved by 46%
Kanny and Mohan[104]	Cloisite 30B	0, 1, 2, 3, 4, 5 wt%	Room Temp	6 layers	i) At 3 wt.% of nanoclay, there was about 9%, 21% and 15% increase in tensile strength, modulus and elongation.
Gurusideswar and Velmurugan [71]	Garamite_ 1958	1.5, 3 and 5 wt%	Room Temp	---	i) At 1.5 % clay the modulus and strength increased by 5%, 3% compared to neat epoxy. ii) The modulus and strength of 1.5 wt% EGCN with 1.5wt% clay 5 mm/min crosshead speed

					increased by 8%, 1% compared to GRE.
Kornmann et al. [60]	ME-100	10 wt%	Room Temp	55 vol%	At 10 wt% of nanoclay. i) Flexural modulus increased by 8% ii) σ_f decreased by 27% iii) Flexural strain increased by 19%.
Sharma et al. [98]	Cloisite 30B	1, 3 and 5 wt%	Room Temp	---	i) Upto 3wt% of clay, σ_{UTS} was increased and decreased beyond that. ii) σ_f was increased upto 5 wt% of nanoclay addition.
Manfredi et al. [95]	i) Cloisite 30B ii) Cloisite 10A	3, 5wt%	Room Temp	30 vol%	a. At 30 vol% glass fibre, and 5 wt% of Cloisite 10A i) Flexural modulus and strength were increased by 20% and 29%. ii) ILSS was increased by 8% iii) Impact strength was improved by 23 % b. The properties were not improved by the Cloisite 30B
Gurusideswar and Velmurugan [88]	Garamite_1958	0, 1.5, 3 wt%	Room temperature	--	a. At quasi static strain rate of 0.00167 s^{-1} with corresponding loading speed of 5 mm/min. i) 15% improvement in young's modulus was observed at 3 wt% of nanoclay

					ii) 9% improvement in σ_{UTS} at 1.5 wt% of nanoclay. b. At the strain rate of 445 s^{-1} and at 1.5 wt% of nanoclay the strength was improved by 84% c. At 0 wt% clay and i) At 0.00167 s^{-1} strain rate the strength and modulus were 314.92 MPa, 18.09 GPa ii) At 315 s^{-1} the values were improved by 34%, 58%. iii) At 385 s^{-1} strain rate the values improved by 51%, 92%. iv) At 445s^{-1} strain rate the values were improved by 67%, 106%.
Krushnamurty et al. [105]	Nanomer I.30E	0, 3 wt%	Room temperature	40, 50, 60, 70	At 3 wt% of addition of nanoclay the σ_{UTS} was improved by i) 21% at 40 % of fiber volume ii) 13% at 50% of fiber volume iii) 7% at 60% of fiber volume iv) -2% at 70% of fiber volume At 3wt % addition of nanoclay the σ_f was improved by

					i) 20% at 40 % of fiber volume ii) 14% at 50% of fiber volume iii) 8% at 60% of fiber volume iv) -3% at 70% of fiber volume
Jeyakumar et al. [91]	Cloisite 93	1, 3, 5, 7 wt%	Room temperature	--	Maximum improvement in σ_{UTS} is 30% at 5 wt%. Maximum improvement in tensile modulus is 32% at 5 wt%. Maximum improvement in σ_f is 50% at 5 wt%. Maximum improvement in flexural modulus is 116% at 5 wt%. Maximum improvement in impact strength is 42% at 3 wt%. Maximum improvement in fracture toughness is 136% at 5 wt%.

Achutha et al. [93]	OMMT	0, 2, 4 wt%	a. Room temperature b. Hygrothrmal conditioning before testing	40, 50, 60 wt%	The maximum improvement in the property of EGCN with addition of 4 wt% of OMMT and 60 wt% glass fiber compared GRE with 60wt% fiber a. σ_{UTS} improved by 11.5% at room temp b. σ_f improved by 4.5% at room temp c. For specimens soaked in cold water for 70 days there was 7.5% decrease tensile strength d. For specimens soaked in cold water for 70 days there was 10% decrease σ_f e. For specimens soaked in boiling water for 2 hrs there was 9% decrease tensile strength f. For specimens soaked in boiling water for 2 hrs there was 12.5% decrease σ_f
Prabhakar et al. [94]	a. MMT b. Nano mer I.28E	3 wt%	c. Room temperature	40 wt%	i) Improvement in tensile, flexural, and impact strength values of EGCN compared to GRE a. With the addition of MMT are -54.4%, -19.2%, -20.7% b. With the addition of OMMT are -11.5%, -33.8%, -20.7% c. With the addition of MMT and silane treated glass fiber are -25.36%, -9.2%, -59%

					d. With the addition of OMMT and silane treated glass fiber are 6%, -9.9%, -1.8% e. With the addition of MMT and acid treated glass fiber are -30.7%, -28%, 2.2% f. i) With the addition of OMMT and acid treated glass fiber are -43%, -58.5%, -59.2% ii) Improvement in tensile, flexural, and impact strength values of GRE with addition of silane treated glass fiber -16.6%, 12.5%, 33.75% iii) Improvement in tensile, flexural, and impact strength values of GRE with addition of acid treated glass fiber -26.5%, -5.3%, -40.3%

At 40% and 60% volume of glass fiber reinforcement into epoxy-clay matrix, there was about 20% and 8% improvement in σ_f at 3 wt% of Nanomer I.30E [105]. This increment is attributed to the ability of the matrix to transfer the load to all the fibers. When nanoclay is not present in the matrix, it cannot transfer the load to all fibers and thus crack propagates along the matrix, and there will be low resistance to crack propagation. At low fiber volumes, i.e., at 40%, GRE exhibited interlaminar fracture as the crack propagated through matrix between fiber layers and confined itself to layers near the top of the composite where the loading point is located so that and the load was not transferred to all the layers, whereas EGCN exhibited translaminar fracture as the fiber layers break vertically at the loading point which requires more energy because the load is transferred to all the fiber layers [106].

With increase in V_f of fiber to 60%, there was a reduction in the effect of nanoclay and both GRE and EGCN have failed predominantly in translaminar fracture mode which should occur only for EGCNs. This is because at higher V_f of fibers, the fabric layers are well compacted to fit in the same volume of the composite, thereby the crimp zones present in the fabric will get interlocked with adjacent fabric layers, thus strengthening the interlaminar regions. Hence the crack propagation is resisted along interlaminar regions by the interlocked crimp zones and fracture occurs by rupture of glass fibers along translaminar direction. These interlocks could resist interface shearing; thus, at higher V_f, crack propagation proceeds with the rupture of fiber fabric layers [105]. At further higher fiber volumes, i.e., at > 60%, fiber wetting became difficult, so there is a chance of failure by both mechanisms, i.e., interlaminar and translaminar crack propagation, thereby decreasing strength [107].

Jeyakumar et al. [91] stated that with addition of Cloisite 93A into EGCN there was significant improvement in flexural properties. With the addition of 1, 3, 5 wt% of Cloisite 93A, there was about 10.4%, 41.2%, and 52.3% increase in σ_f and also 18.75%, 62.5%, and 118.75% improvement in flexural modulus. Beyond 5 wt% addition of nanoclay, there was a decreasing trend. Najafi et al. [108] conducted experiments on EGCNs by adding pristine MMT and subjected some samples to hygrothermal conditions which consists of immersing the specimens in distilled water at 80˚C for 10 weeks. The flexural curves for both neat GRE and EGCN exhibited linear behavior, EGCN subjected to hygrothermal conditions exhibited gradual decrease

in slope. At 3 and 5 wt% addition of MMT there was about 8% and 12% improvement in flexural modulus, and 10.7% and 6.3% improvement in σ_f was observed. At 3 wt% of MMT addition the properties were optimum. The samples treated by hygrothermal conditioning exhibited very poor flexural properties due to decreased interface bond strength caused by water absorption. Prabhakar et al. [94] stated that the addition of silane treated glass fiber in epoxy has resulted in improved flexural properties due to enhanced interface bonding between fiber and matrix compared to the composite reinforced with untreated fiber. The addition of Pristine MMT and Nanomer I.28E has not shown any considerable improvement but rather reduced the σ_f. There was about 29% increase in σ_f of epoxy-silane treated fiber composite compared to epoxy-untreated fiber composite.

2.4 Fracture toughness

At 1 and 2 wt% addition of Nanomer I.28E there was about 28% and 32% improvement in fracture toughness of clay-epoxy nanocomposite compared to NE, whereas EGCN exhibited about 20 and 23% improvement in fracture toughness for the same clay contents compared to GRE. Above 5 wt%, there was a decreasing tendency [76]. In the single edge notch bending test conducted by Bozkurt et al. [61] at 10 wt% addition of OMMT, the K_{IC} of EGCN improved by 5 % but MMT did not show significant improvement. The load applied is in in-plane of the specimen. Therefore the fracture mechanism consisted of fiber-matrix debonding, fiber pullout and fracture. The increased fracture toughness of the composites with the addition of various surface modified nanoclays under different mixing conditions and various making methods are shown in table 2.1.

Zulfli and Chow [99] stated that with the addition of nanoclay, K_{IC} improved. This improvement was ascribed to the strengthening of the interface between fiber and matrix by the presence of OMMT at the interface and increased resistance to crack propagation because of OMMT [102]. Swaminathan and Shivakumar [109] stated that the major mechanism for increased toughness in composites was because of the deflection of the crack around clay tactoids. OMMT resists the crack from propagating because of which bowing and pinning of the crack takes place [109]. The toughening effect of OMMT is limited by the agglomeration. Tsai

and Wu [110] reported continuous decrease in Mode-I fracture toughness with the addition of nanoclay due to the brittleness induced in the composite which caused the crack to propagate at a faster rate, whereas pristine GRE composite exhibited ductile nature compared to EGCN with high clay content, so the crack propagation was slow and needed more energy for failure.

Jeyakumar et al. [91] reported that with addition of Cloisite 93A into glass-epoxy, there was a conspicuous increase in fracture toughness of EGCN. For neat epoxy it was 0.9 MPa-$m^{1/2}$, for glass-epoxy it was 1.1 MPa-$m^{1/2}$. At 1, 3, and 5 wt% addition of nanoclay, the increase in fracture toughness of EGCN was about 36%, 63%, and 86% respectively compared to GRE. Beyond 5 wt% addition there was a decreasing tendency. Therefore, it was concluded that the saturation limit is 5 wt% of nanoclay for the experimental conditions adopted by Jeyakumar et al. [91]. Santos et al. [111] reported that with the addition of Cloisite 25A in EGCN, there was a considerable improvement in Mode-I fracture toughness of EGCN. At 2, 4, 6, and 8 wt% addition of nanoclay, there was about 118.85 %, 9 %, 56.55 %, and 38.5 % improvement in fracture toughness. Beyond 8 wt% addition there was a decreasing trend. The increase in fracture toughness is attributed to the fiber bridging effect. At 10 wt% addition of nanoclay there was a decrease in the property, which is ascribed to the poor distribution of matrix between the fiber laminas.

2.5 Interlaminar shear strength (ILSS)

ILSS is a matrix dependent property, which means strengthening of matrix improves ILSS because the interface between the epoxy-clay matrix and the glass fiber becomes strong [112, 113]. Therefore if ILSS of the matrix is enhanced, then ILSS of the composite also will get enhanced. The increase in ILSS of the composite is owing to the enhanced interfacial area between matrix and clay, the enhanced bond between resin and fiber and improved morphology of the matrix. The failure in ILSS mode is acknowledged as a critical mode of failure in FRP laminates. Thus there is a necessity to study the ILSS characteristics of the nanocomposites. It is proved that the shear strength of FRPs is remarkably enhanced with the incorporation of nanoclays [114]. EGCN with 1 and 2 wt% added Nanomer I.28E had shown 44% and 20 % improvement in ILSS compared to GRE. The rough interface between the epoxy-fiber in fracture

surface indicates strong bond, whereas GRE and NE have shown smooth interface which implies a weaker interface bond [76]. The increased ILSS of the composites with the addition of various surface modified nanoclays under different mixing conditions and making methods are shown in Table 1. Bozkurt et al. [61] reported a decrease in ILSS of EGCN with the addition of MMT and OMMT. The ILSS of GRE is noted to be 32.7 MPa. But when clay is added, it is observed that the laminate with the addition of clay reports a small decrease than when MMT is added; the decrease is high when OMMT is added. This decreasing trend is attributed to the creation of air voids at the interlaminar region while making the composite. The susceptibility to form voids in the interlaminar region is observed to be more when OMMT was added and further study is required to establish this phenomenon.

The ILSS characteristics of GRE and EGCN with an addition of Cloisite 10A and Cloisite 30B were evaluated by Manfredi et al. [95] There was a small increase of 7.5% in ILSS of EGCN with the addition of Cloisite 10A, but Cloisite 30B had no influence. The trend of improvement with addition of Cloisite 10A and decrease with the addition of Cloisite 30B was reported in flexural properties section also. Laminates with Cloisite 10A have shown high flexural modulus and high σ_f. The morphologies of the composites indicated that the addition of Cloisite 30B had not provided strong adherence between matrix and fiber, but Cloisite 10A provided strong bonding between matrix and fiber. There is also a high attraction between Cloisite 10A and glass fiber surface since both are ceramic materials. The matrix without clay has shown smooth and brittle surface at failure, whereas the matrix with nanoclay addition has shown rough surface at failure which is also in line with the impact characteristics [95]. EGCN showed 18.5% improvement in ILSS with the addition of 1 wt% of nanoclay by magnetic stirring method. Above 1 wt%, there was a decreasing trend which is attributed to the aggregates of silicate tactoids and voids, whereas EGCN consisting of matrix processed by HSMT exhibited 24% increase in ILSS, which might be attributed to the high shear force, when resulted in good dispersion of nanoclay platelets [62].

Jeyakumar et al. [91] reported that with the addition of Cloisite 93A, the ILSS of EGCN improved notably. At 1, 3, and 5 wt% addition of nanoclay in EGCN, there was about 8%, 16%, and 38% increase in ILSS. The presence of nanoclay brought about strong adhesion amongst

nanoclay and epoxy matrix and in this manner enhanced the shear properties of the composites. Beyond 5 wt% the ILSS stared decreasing which might be due to the non-uniform scattering of nanoclay. Anni et al. [115] stated that with the addition of organic modified nanoclay into woven flax fiber reinforced epoxy, there was a rise in ILSS. Before reinforcing the fibers, some flax fibers were washed in distilled water, some treated with alkali solution, some with saline solution, and some others treated with nanoclay dispersed solution, to graft the nanoclay particles onto the flax fibers. The improvement in ILSS with the addition of these four kinds of treated fibers in ILSS was observed to be 8%, 10%, 17.9% compared to the composite reinforced only with water treated fibers.

Santos et al. [111] reported that with the addition of Cloisite 25A into EGCN there was a significant increment in ILSS property of EGCN. There was increasing trend in the property upto 2 wt% addition of nanoclay, after that it started decreasing. At 2 wt% of nanoclay addition there was about 70% increase in ILSS of EGCN. ILSS mainly depends on matrix behaviour if the matrix is tough, the ILSS is increased. Addition of nanoclay makes the matrix tough because the crack propagation is hindered by the clay platelets and the stress distributed to the fibers will be uniform as the interface becomes stronger. At 10 wt% addition of nanoclay, the ILSS decreased by 3 % compared to GRE. Lim et al. [116] showed that the geometry of interface between epoxy-nanoclay platelets may also influence ILSS.

2.6 Impact strength

The impact strength of the composite depends mainly on the strength of the matrix and the ability of the fiber-matrix to withstand the impact loads. At 5wt% addition of Cloisite 10A, the EGCN has exhibited 23% improvement in impact strength; this improvement is attributed to the creation of a complex path for the fracture propagation, as the layered silicate platelets hinder the extension of microcracks created in the matrix [117–119]. The increase in the strength of the fiber-matrix interface has decreased the resistance to impact force. Manfredi et al. [95] stated that the failure strength of EGCN depends on two factors, one being tortuous path formed by clay platelets, and another being the fiber-matrix interface strength. The well-dispersed nanoclay platelets hinder crack propagation by diverting the crack to a longer path or split it into sub cracks

which require more energy, whereas strong fiber-matrix interface reduces the impact resistance. The laminates were made with low fiber content hence the properties of the laminate are mainly dependent on the matrix behavior. An improvement in the impact characteristics of the nanocomposite with no glass fiber reinforcement was observed. The enhancement in the impact characteristics was observed for laminates with nanocomposite matrix irrespective of the clay type [95].

Shi and Kanny [62] carried out izod impact test at high strain rate to study the impact characteristics of EGCN. When the matrix incorporated into the laminate was processed by magnetic stirring, the impact strength of the laminate was noticed to be decreasing with the addition of Cloisite 30B. A sudden decrease in impact strength of 27% is observed for the laminate at 1 wt% clay; further addition of clay did not affect impact strength. The sudden decrease at 1 wt% clay is attributed to the agglomeration and air voids in the matrix, Siddiqui et al. [100] addressed the same finding, whereas 44.9% improvement in the impact strength at 1 wt% nanoclay was observed when the laminate prepared was incorporated with a matrix processed by HSMT [62]. The changes in the impact strength of the composites with the addition of various surface modified nanoclays under different mixing conditions and making methods are shown in table 2.1.

Zulfli and Chow [99] reported that the impact strength of the laminates with Nanomer 1.28E incorporated in the matrix exhibited higher value compared to GRE. This improvement in the impact characteristics was ascribed to strong adhesion between Nanomer 1.28E and epoxy which implies that the resin has wetted all layers of the nanoclay particles. This therefore enhances the energy required to debond the fiber and matrix due to the strong bond. Yasmin et al. [65] stated that the enhanced impact strength of the laminate is because of the complex path for cracks to propagate through the matrix. The OMMT and glass fiber provide a synergistic increment to the impact characteristics. OMMT at the fiber matrix interface acts as an interfacial modifier while the stress transfer from the matrix to fiber gets enhanced through clay particles; thus as the clay content at the fiber matrix interface increases, higher stress levels can be taken by the composite because of which better characteristics were attained [120]. But the content of clay that can be added to the epoxy is limited by the agglomeration and air voids that are formed while

mixing the clay into the resin. Rafiq Ahmad et al. [121] added Nanomer I.30E into EGCN to evaluate its effect on the impact strength of EGCN. The laminates were stroked with low speed impact forces ranging between 10 – 50J. Optimum property was obtained at 1.5 wt% of nanoclay addition with 23 % improvement in the maximum load required to damage the specimen and 11% improvement in stiffness. Also a notable decrease in physical damage was observed for EGCN compared to GRE.

Najafi et al. [108] studied the effect of the addition of pristine MMT into EGCN on impact strength. To study the effect of hygrothermal aging, some EGCN specimens were immersed in distilled water at 80˚C for 10 weeks. At 3 wt% nanoclay addition there was about 7% increase in impact strength for EGCN. At 5 wt%, the impact strength reduced nearly by 5% compared to the value obtained at 3 wt% and this decrease was attributed to agglomerates. Also, the brittleness of EGCN increased with addition of nanoclay, causing the energy absorption to decrease [122]. The 3 wt% and 5 wt% nanoclay added EGCN subjected to hygrothermal conditioning exhibited 7.23% and 10.47% decrease in impact strength compared to the control specimen which was dry GRE. The conditioned GRE exhibited about 13% decrease compared to dry GRE, whereas for 3 and 5 wt% added, conditioned EGCN exhibited about 14% and 8% increase compared to conditioned GRE. In both dry and conditioned states, the 3 wt% added EGCN's exhibited good impact strength compared to the control specimen. Prabhakar et al. [94] stated that EGCN reinforced with acid treated glass fiber and MMT exhibited highest impact strength out of all the composites made using neat glass fiber, silane treated glass fiber, and acid treated glass fiber, MMT and Nanomer I.28E. Neat GRE exhibited second highest impact strength value. The next highest impact strength was exhibited by EGCN with silane treated fiber and Nanomer I.28E. Compared to neat GRE the former one was 2% superior in property and the latter one is 2% inferior in property. Prabhakar et al. [94] stated that decrease in impact strength was compensated by improvement in hardness of composites added with Nanomer I.28E and silane treated fiber, because the increase in hardness increases the brittleness, thereby reducing the energy absorption capability.

2.7 Summary

After reviewing the existing literature available on EGCNs reinforced with various surface modified nanoclays, it is clear that the interfacial bond between reinforced fiber and the matrix is enhanced which resulted in enhancement in the mechanical properties of the composite. According to the study reported by Khanjanzadeh et al. [123]**,** at 3 wt% addition of Cloisite 15A into polypropylene-wood flour composite; the tensile and σ_f enhanced by 21% and 25%. According to the research conducted by Idiyatullina et al. [124], 5 wt% addition of Cloisite 15A into poly(1-butene) enhanced the young's modulus of poly(1-butene) by 100%. Based on the literature survey, it is observed that the addition of Cloisite 15A into glass-epoxy composite is not reported in the literature. Since Cloisite 15A is noted for its ability to enhance the mechanical properties of various polymers composites for which few examples were mentioned. Therefore it is expected that the addition of Cloisite 15A into glass-epoxy might also increase its mechanical properties. In addition, there is a good chance that tribological properties may also improve because of the ability of nanoclay to enhances the bonding between fiber and matrix. Therefore it is also of interest to study the effect of Cloisite 15A on the erosive wear characteristics of EGCNs. There are other parameters which also affect the properties of composites significantly i.e., volume of fibers and orientation of fibers. The reason for the selection of glass fiber orientation is because in practice, the loads will be applied in various directions of a component and not limited to one direction. Therefore it is necessary to study the properties in various directions of fibers as well.

Thus the priority of this work is twofold.

(1) To develop a polymer composite with glass fiber and Cloisite 15A as reinforcement materials. Selected mechanical properties such as tensile strength, flexural strength, plane strain fracture toughness, and microhardness with reinforcements are evaluated and reported.
(2) The potential of the developed composites for solid particle erosion test with reinforcements have been carried out and reported in this thesis.

The experiments were designed using Taguchi method and response surface methodology. The optimization of three parameters, i.e., glass fiber volume, angle of glass fibers, and weight content of nanoclay is done using the two methods. The Taguchi method is used to fit the linear model to the input variables and response variable and to check the significance of each parameter. Response surface method is used to fit the quadratic model to the data.

Chapter 3

Materials and Methods

3.1 Introduction

In this chapter, the details about the materials selected, i.e. epoxy, triethylenetetramine, glass fiber, and nanoclay are discussed. The physical properties of these materials were also discussed. Further, the experimental methods used for mixing of nanoclay into epoxy resin and fabrication of composites and corresponding ASTM standard for each testing are also discussed in detail.

3.2 Materials

3.2.1 Epoxy

Epoxy resins are relatively low molecular weight pre-polymers capable of being processed under a variety of conditions. Two important advantages of these over unsaturated polyester resins are: first, they can be partially cured and stored in that state, and second, they exhibit a low shrinkage during cure. However, the viscosity of conventional epoxy resins is higher and they are more expensive compared to polyester resins. The cured resins have high chemical, corrosion resistance, good mechanical and thermal properties, outstanding adhesion to a variety of substrates, and good electrical properties. Approximately 45% of the total amount of epoxy resins produced is used in protective coatings while the remaining is used in structural applications such as laminates and composites, tooling, molding, casting, construction, adhesives, etc.

The type of epoxy resin used in the present investigation is Araldite LY-556 which chemically belongs to epoxide family. Epoxy resins are characterized by the presence of a three-membered ring containing two carbon and one oxygen atoms (epoxy group or epoxide or oxirane ring).

Figure. 3.1 Photograph of epoxy resin and hardener

Epoxy is the first liquid reaction product of bisphenol-A with an excess of epichlorohydrin and this resin is known as Diglycidyl Ether of Bisphenol-A (DGEBA). DGEBA is used extensively in industries due to its high fluidity, processing ease, and good physical properties of the cured of resin. The hardener triethylenetetramine has been used with the epoxy designated as HY 951. This has a viscosity of ~20 mPa.s at 25ºC. Both the epoxy and hardener were supplied by Fine Finish organics Pvt. Ltd., India.

Table 3.1 Properties of epoxy resin

Characteristic	Specification
Viscosity at 25ºC	10,500 mPas
Epoxy Content	185 g/eq
Density at 25ºC	1.20 g/cc
Flash Point	> 200 °C

Table 3.2 Properties of Triethylenetetramine

Characteristic	Specification
Viscosity at 25ºC	~ 20 mPas
Density at 25ºC	0.98 g/cc
Flash Point	115°C

The terminology, epoxy, in polymer refers to a family of monomers that consists of an epoxy/oxirane ring, which is a three-membered ring comprising two carbon atoms and an oxygen atom bonded with two and one hydrogen atoms respectively as displayed in Figure 2.2 [125] [126]. The functionality of epoxy resin depends on the number of these oxirane rings per epoxy resin, which can be situated internally, terminally or in cyclic structures [126].

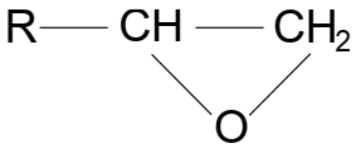

Figure 3.2 Epoxy/Oxirane ring –Chemical structure.

3.2.2 Glass fiber

E-Glass is the most common fiber used in polymer matrix composites. Its advantages include its high strength, low cost, high chemical resistance, and good insulating properties. In the present investigation E-glass fabric of 380 gsm was used which was supplied by saint Gobain ltd, which is shown in Figure 3.3. The fibers were cut to sizes 180× 150 mm from the long sheet.

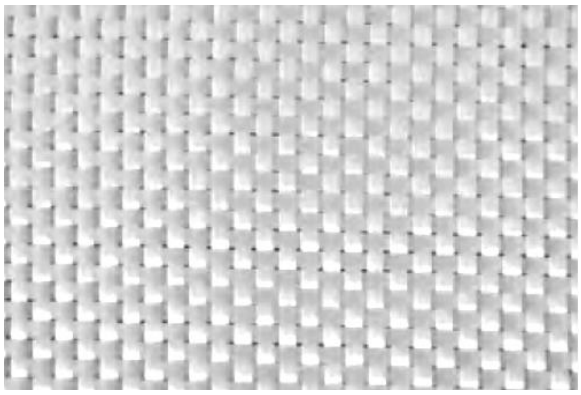

Figure 3.3 Photograph of E-Glass fabric

Table 3.3 Properties of E-glass

Density	Ductility	Glass Temperature	Thermal expansion (μm/m·°C)	Tensile strength (MPa)	Compressive strength (MPa)
2.58 gm/cc	0.028	1123 °C	5	3445	1080

3.2.3 Cloisite 15A

Cloisite 15A (C15A) is a surface treated montmorillonite nanoclay particles with alkyl ammonium ions. Physical Properties of Cloisite 15A are given in table 1.

Table 3.4 Properties of Cloisite 15A

Organic modifier	**Modifier concentration**	**% moisture**	**% weight loss on ignition**	**Density**	**Particle size**
Dimethyl Dihydrogenated tallow	125 meq/100 gms of clay	< 2%	43%	2.8 gm/cc	< 80 nm

3.3 Preparation of epoxy-nanoclay mixture

The nanoclay has a layered structure with a gap between subsequent layers called intergallery or d-spacing. The clay is hydrophilic and organic modification makes it both hydrophobic and organophilic, and also the intercalation of organic cations such as alkylammonium ions which can be introduced into the intergalleries by organic surface modification of clay which increases the d-spacing allowing epoxy monomers to intercalate easily while mixing. During mixing two types of clay morphologies would form in the composite one is intercalated and the other is exfoliated structure. In intercalated morphology, the epoxy

molecules were diffused into the intergallery, and the intergallery expands within the Van der Waals limits of the clay layers, whereas in exfoliated morphology the intergalleries are expanded to such an extent that there will be no more Van der Waals forces are present between clay layers, i.e. the layers are completely separated.

The properties of the composites depend on the intercalation of the matrix into the clay layers. The maximum improvement in the properties would be observed at the completely exfoliated morphology as the matrix will wet all the layers and the distribution of particles will be more uniform. The morphology of composites depends on the processing of the mixture. Azeez et al. [127] stated that the critical speed for the mixing of clay into the resin is 3000 rpm above which the clay layers break rather than to get separated. Therefore, a calculated amount of resin and nanoclay particles were mixed by a mechanical stirrer at 3000 rpm for 1 hr. At that point, the hardener in the proportion of 10 parts for every 100 parts of resin was added and blended further until it is mixed uniformly. Eight plies of fibre mat were utilised to acquire 3 mm thick laminates. The composite was made using hand lay-up method followed by ambient temperature curing for 24 hrs. The specimens of required dimensions for each test were cut from the laminates utilising a diamond tipped cutter.

3.4 Composite preparation

The glass fiber mat is cut into pieces of size 180 mm x 150 mm. The prepared epoxy-clay mixture is finely coated by means of coating brush on the bottom of the mold. The glass fabric is kept upon the coated mold; again a fine thickness of mixture is applied onto the glass fabric. The process of keeping a glass fabric piece and coating with epoxy-clay mixture continuous until the required thickness of the composite is attained i.e. 4 mm. The mold is closed and a weight of 10 kg is placed on the mold so that this applied load keeps the mold closed tightly and also ensures that the expansion of the matrix due to curing reaction is also suppressed. In this state, the composite is left to cure at room temperature and after 24 hrs the mold is opened and the composite plate is ready. The fiber content is ranged between 10.5 vol% to 31 vol%, nanoclay content is ranged between 0.5 wt% to 2.5 wt%, and angle of fibers ranged in between $0^{\circ}/90^{\circ}$ to $45^{\circ}/-45^{\circ}$. The glass fiber contents are experimentally verified by performing burn off test.

3.5 Testing procedures

3.5.1 Density and void content

The void content in the composite is calculated according to ASTM D 2734-09 standard. According to this method, the equation to calculate void content in the composite is given below:

$$V = 100(T_d - M_d) / T_d \quad \text{..... .(1)}$$

V represents the volume percentage of voids in the composite, T_d is the theoretical density and M_d is the experimentally measured density. T_d is calculated using equation (2):

$$T_d = \frac{100}{\left(\frac{R}{D} + \frac{r}{d}\right)} \quad \text{.....(2)}$$

where T_d represents theoretical density, R represents resin content in the composite in weight per cent, D represents the density of resin, r represents reinforcement in composite, weight per cent and d represents the density of reinforcement. The experimentally measured density is calculated according to the ASTM D 792-08 using equation (3):

$$\text{Density } (M_d) = S_g \text{ x Density of water} \quad \text{.....(3)}$$

Here S_g represents the specific gravity of the composite, which was measured using the equation (4):

$$S_g = \frac{a}{(a + w - b)} \quad \text{.....(4)}$$

where S_g represents specific gravity of the composite, a represents the weight of the sample, w represents the apparent mass of the partially immersed wire in distilled water, b apparent mass of specimen completely immersed and of the wire partially immersed in distilled water.

3.5.2 Tensile testing

From each NC loading levels (0.5, 1.5 and 2.5 wt.%) and glass fiber vol.% contents (10.5, 21, 31.5), and glass fiber orientations (0°/90°, 22.5°/67.5°, 45°/-45°), EGCN panels of size 180 mm length, 150 mm width and 4 mm thick were manufactured and were cut for in-plane tensile testing. The orientation angle of glass fabric, NC content, and volume of fiber in the specimens were the preferred parameters for the assessment of strength. Testing of the specimen was carried out on a hydraulic universal test machine with a load cell capacity of 100 kN. The instrument was made by M/S Jin Ahn Testing company, China and its model number is WDW-100S. The tensile testing conducted was consistent with ASTM D 638, which is a standard testing method for tensile properties of fiber reinforced polymer composites. For each test five specimens were tested and average value is considered for analysis. The speed of testing used was 5 mm/min.

Figure 3.4 Universal Testing Machine

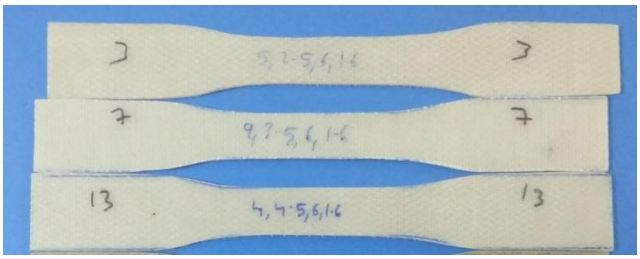

Figure 3.5 Photograph of tensile specimens

3.5.3 Three point bend test

Flexural strength was tested using the same Universal Testing Machine with a crosshead speed of 10 mm/min. A 100 KN load cell was used and a three-point bending fixture was attached to the equipment for this test. In each case, five samples were tested and the average value was tabulated. The sample size is 128 x 20 x 4 mm^3 which was cut in accordance with ASTM D 790 standard.

Figure 3.6 Photograph of three-point bending specimens

3.5.4 Plane Strain fracture toughness test

The single edge notch bending (SENB) samples were tested using the three-point bending test fixtures according to ASTM D5045. In order to establish that a valid K_{Ic} has been determined, the following relation must be satisfied according to ASTM D5045.

$$B, a, (W - a) > 2.5 (K_Q/\sigma_y)^2$$

B = thickness of specimen which is taken as 2 cm

W = width of specimen which is taken as 2 cm

a = crack length (cm)

a/W ratio is taken as 0.5 which gives rise to a = 1 cm

σ_y = yield strength of specimen

K_{Ic}= fracture toughness (MPa-$m^{1/2}$)

Fig. 2.7 shows the specimen whose dimensions are 88 mm x 20 mm x 20 mm. The specimens are prepared in a mold of size 100 mm x 100 mm x 20 mm and Fig. 2.8 shows the diagram of three-point bending set up. The test specimen was placed symmetrically on the two supports of span 8 cm. A force is applied at midspan with a crosshead speed of 2 mm/min. This test speed was chosen because the SENB specimens usually fail at a very small load (<100 kN) due to small dimensions and brittle behaviour of the materials. A 5 kN load cell was used to record the applied load and the corresponding deflection of the specimen during the test was recorded using the crosshead displacement of the machine. These data was logged to a computer for analysis.

Figure 3.7 Photograph of SENB specimen

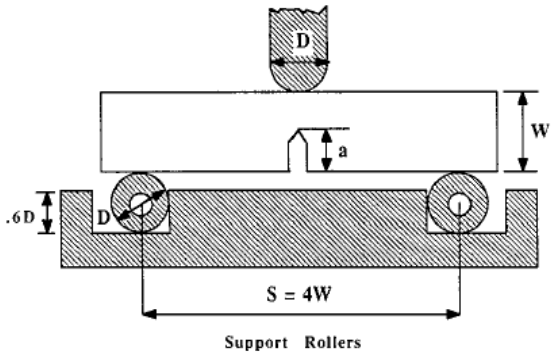

Figure 3.8 Bending Rig for SENB

3.5.5 Microhardness

Microhardness was measured using Leitz microhardness tester according to ASTM E384 standard. The indenter is made of diamond and is in a pyramid shape with 136° angle faces which is pressed onto the specimen surface with 500 gms load for 10 seconds [128]. The instrument is made by Shimadzu Corp., Japan and the model is HMV-G20ST.

Figure 3.9 Photograph of Microhardness tester

3.5.6 Erosive wear test

Solid particle erosion tests were run according to ASTM G76 standard. This test method utilizes a repeated impact erosion approach involving a small nozzle delivering a stream of gas containing abrasive particles which impacts the surface of a test specimen. This test method can be used over a range of specimen sizes and configurations. The abrasive material to be used shall be uniform in essential characteristics such as particle size, moisture, chemical composition, etc. The test temperature shall be the normal ambient value. The nozzle tube shall be of at least 50 mm long. The test gas shall be dry air. The test time shall be until steady state conditions are reached and final erosion crater should be no deeper than 1 mm.

The erosion test was conducted on Airjet Erosion Test Rig which is made by Magnum and the model is TE-400-HMI, the equipment is shown in Fig. 2.9. The erosion testing equipment has a provision for mixing air and sand in a mixing chamber. The mixture is passed through a nozzle where it gets accelerated and comes out with high speed and hits the specimen surface. The specimen size is 20 mm x 20 mm x 4 mm. The erosion loss is measured as erosive wear rate (Er) which is defined as the ratio of mass lost due to erosion to the mass of erodent. It is expressed as specimen weight lost due to erosion in milligrams per kg of erosive medium. The erosion of the EGCNs was studied at 2 and 4 gm/min mass flow rates of sand particles where silica sand is used as erosive medium with the size of the sand particles being 200 µm. L9 design is selected to optimize the composite parameters for the lowest E_r possible; the testing parameters were maintained constant throughout the experiments at 2gm/min, 30° impinging angle, 2 bar pressure, 1 min holding period and 30 mm stand-off distance. At the optimized composition, the erosion test was conducted using L18 design to optimize the erosion testing parameters.

Figure 3.10 Photograph of Airjet Erosion Test Rig

3.5.7 Scanning Electron Microscope

Figure 3.11 Scanning Electron Microscope

The morphology of the fracture surfaces of specimens failed in tensile, flexural, fracture toughness testing, and worn in erosion testing was analyzed on a scanning electron microscope made by Tescon and the model is VEGA 3 LMU shown in Fig. 2.10.

3.6 Taguchi method

Classical experimental design methods are too complex and are not easy to use because a large number of experiments have to be carried out. To solve this problem, the Taguchi method uses a special design of orthogonal arrays to study the entire parameter space with only a small number of experiments. Taguchi's experimental design is an analysis tool for modeling and analyzing the influence of control parameters on the output.

For the design of experiments, the control factors directly affecting the characteristic to be analyzed are required to be identified and selected. Three parameters were selected in this study, namely, nanoclay wt.%, glass fiber volume %, angle of fibers. The selection of levels of parameters is explained in detail in section 4.2.1 of chapter 4. Three levels are selected for each parameter. According to the Taguchi method, if there are three parameters and three levels for each parameter, L9 orthogonal array should be employed for the experimentation. The tests were carried out according to the L9 experimental design and the effect of these parameters was studied.

The experimental outcomes are transformed into the signal to noise ratio (S/N ratio). Signal means the desired output characteristic, whereas noise means the undesired output characteristic. The S/N ratio indicates the quality characteristic, which implies whether the output desired is maximum or minimum or intermediate. In Taguchi method, there are three quality characteristics that were defined as higher-the-better, lower-the better, and the nominal-the-better. The S/N ratio indicates the variation in the output due to error where the smaller the variation due to error, the better the output is. When the outcome is a mechanical property then higher the better quality characteristic suits better, and hence, S/N ratio characteristic should be selected such that the larger the S/N ratio, the better the strength, calculated by equation (1).

$$(S/N)_{HB} = -10 \log[\frac{1}{R}\sum_{j=1}^{R}(1/Y_j^2)] \quad \text{.....(1)}$$

When the outcome is erosive wear then the lower the better quality characteristic suits better, and hence, lower the better S/N ratio characteristic should be selected which is given by equation (2).

$$(S/N)_L = -10 \log[\frac{1}{R}\sum_{j=1}^{R}(y_j^2)] \quad \ldots\ldots\ldots\ldots (2)$$

In this study the properties selected for studying the effects of selected parameters are tensile strength, flexural strength, microhardness, erosive wear for the EGCNs. For studying the effects of testing parameters on erosion wear of EGCNs L18 array was selected. Five testing parameters were selected i.e., sand flow rate (f), angle of hitting (θ), air stream pressure (p), holding time (t), and distance between specimen and nozzle (d); out of which, for 'f' two levels are selected and for remaining four parameters three levels are selected. For this set of parameters and levels the suitable design is L18. For doing Taguchi design and analysis Minitab 17 software is used.

3.7 Response Surface Methodology

Response surface methodology (RSM) is a collection of mathematical and statistical techniques for modeling and analyzing engineering problems. In this technique, the main objective is to optimize the response surface that is influenced by various process parameters by careful design of experiments. The objective is to optimize a response (output variable) which is influenced by several independent variables (input variables). RSM also quantifies the relationship between the controllable input parameters and the obtained response surfaces. The design procedure for the RSM is as follows:

i) Designing of a series of experiments for adequate and reliable measurement of the response of interest.
ii) Developing a mathematical model of the second order response surface with the best fittings.
iii) Finding the optimal set of experimental parameters that produce a maximum or minimum value of response.
iv) Representing the direct and interactive effects of process parameters through two and three-dimensional plots which are also called as response surface plots.

In this study Central composite deign is selected which is a one of the designs in RSM. For three parameters and three levels twenty experiment were generated which is shown in chapter 4. This experimental design and analysis of results were carried out using Design Expert 7 software.

3.8 Summary

The materials used in this study are given with details. This chapter explained about the composite fabrication method and nanoclay-epoxy mixing method used in the present study. The materials used were epoxy resin as matrix and triethylenetetramine as a hardener. Glass fiber was used as major reinforcement and Cloisite 15A was used as a minor reinforcement. The physical properties and chemical compositions are given for all the materials. The testing methods to evaluate the mechanical properties and erosive wear of the composites are given in detail. The measurement of void contents in the composites was explained. The instruments used to conduct the tests were shown with figures along with the specifications. Taguchi method and RSM methods were discussed briefly.

Chapter 4

Mechanical Behaviour of Epoxy/Glass/Clay Nanocomposites

4.1 Introduction

The present chapter gives the detailed discussion on investigation of mechanical properties, their optimization, and characterization of the fracture surfaces of epoxy–glass-clay nanocomposites (EGCNs) with the addition of Cloisite 15A. For optimization, Taguchi and RSM methods are used. Suitable design of experiments are selected based on Taguchi and RSM methods, and the obtained results were analyzed using ANOVA analysis to identify whether the parameters have a significant effect on particular mechanical property.

4.2 Optimization of Tensile Strength (σ_{UTS})

The tension test is generally performed on flat specimens. The most commonly used specimen geometries are the dog-bone specimen. A standard testing method, ASTM D 638 was used according to which the dimensions of the specimen used are 165 x 13 x 4 mm. The tensile test is performed in universal testing machine M/S Jin Ahn Testing DW-100S. The tests were performed at a crosshead speed of 5 mm/min. For each test, five samples were tested and the average value was taken for analysis. For Taguchi method L9 array is selected and central composite design is selected as response surface design. Pilot experiments were conducted to identify the effective ranges of parameters. After these ranges are fixed, the experiments were conducted according to Taguchi and RSM designs. The effect of each parameter is quantified using ANOVA and significance of the effect of each parameter is evaluated. A linear model is fitted in Taguchi method and a quadratic model is fitted in RSM method. The strength of fit of each model is quantified by the R^2 value. The fracture surface is studied using SEM micrography.

4.2.1 Pilot Experiments

The three parameters selected are nanoclay weight percentage, glass fiber volume percentage, and angle of orientation of glass fibers. Nanoclay content is indicated in terms of weight percentages, and glass fiber content is indicated in terms of volume percentage. The range of each parameter is obtained after performing the pilot experiments which consist of fixing two parameters at certain values while the third parameter is varied. In this way, the range of each parameter is identified in which the property has an increasing trend. Fig. 4.1 shows the curve between σ_{UTS} and nanoclay weight content, here glass fiber volume and glass fibers orientation are fixed at 10.5 vol% and 0˚/90˚. Fig. 4.1 shows that the σ_{UTS} has increased up to 2.5 wt% addition of nanoclay and started decreasing after that. Fig. 4.2 shows the curve between σ_{UTS} and glass fiber volume; here nanoclay weight and glass fibers orientation are fixed at 2.5 wt% and 0˚/90˚. Fig. 4.2 shows that the σ_{UTS} has increased up to 31.5 vol% addition of glass fibers and started decreasing after that. The third parameter selected is the angle of orientation of glass fibers which

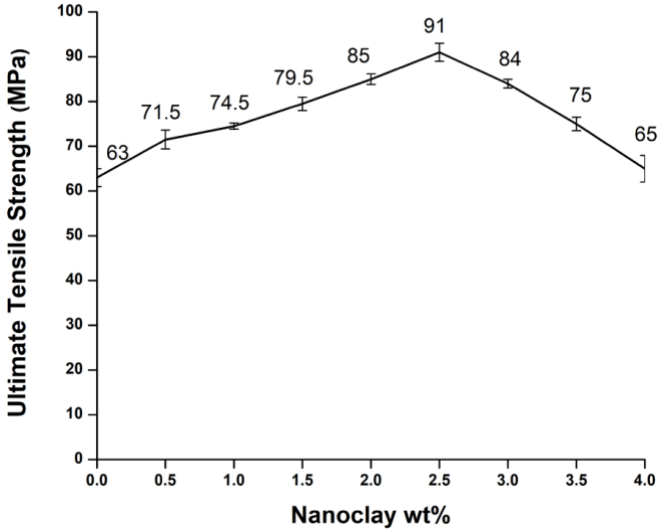

Figure 4.1 σ_{UTS} of the composite vs. nanoclay wt% (G = 10.5 vol%, O = 0˚/90˚)

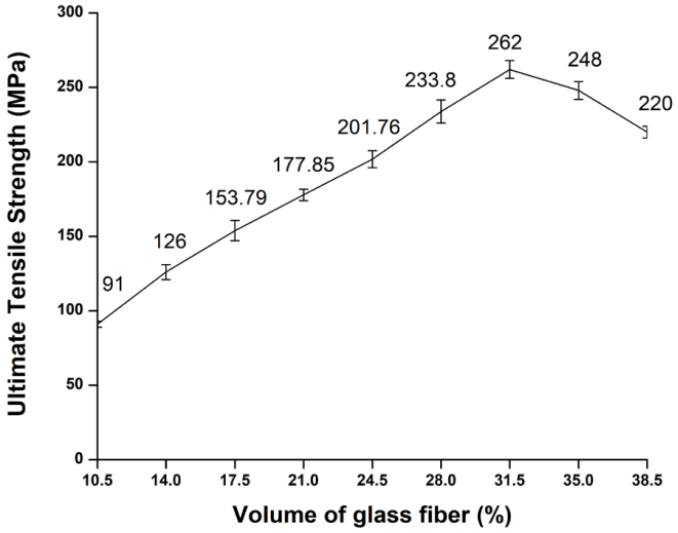

Figure 4.2 σ_{UTS} of the composite vs. glass fiber volume (N = 2.5 wt%, O = 0˚/90˚)

was selected to quantify the mechanical properties and erosion wear in three selected directions. The reason for the selection of glass fiber orientation is because in practice the loads will be applied in various directions of a component and not necessarily in one direction. Therefore it is necessary to obtain data on the properties in various directions of fibers as well.

4.2.2 Taguchi Design

Taguchi design of experiments was selected for optimization of σ_{UTS} of EGCNs. Three parameters were selected; each with three levels is shown in table 4.1. Suitable Taguchi design for the parameters is given in table 4.1 is L9 array. Table 4.2 shows the L9 experimental design and the σ_{UTS} of each composite. Fig. 4.3 shows the stress-strain plots for all the nine composite specimens indicated in table 4.2. It is evident from Fig. 4.3 that EGCNs in which fibers oriented at 0°/90° indicated with serial numbers 3, 5, 7 in table 4.2 show high σ_{UTS} values, whereas when fibers oriented at 22°/67.5° in the composites indicated with serial numbers 2, 4, 9 in table 4.2 show intermediate σ_{UTS} values. When fibers oriented at 45°/-45° in EGCNs indicated with serial numbers 1, 6, 8 in table 4.2 show low σ_{UTS} values. The effect of nanoclay wt% and glass fiber vol% were not that evident as it was evident for fibers orientation in Fig. 4.3.

Table 4.1. Selected Composite parameters.

Test Parameters	Ranges
Nanoclay wt%. (N)	0.5–2.5
Glass fibre volume % (G)	10.5–30.5
Orientation angle of fibres (O)	45°–90°

Table 4.2. Experimental design using L9 orthogonal array for σ_{UTS}.

Sl. No	N	G	O	σ_{UTS} (MPa)	S/N Ratio
1.	0.5	10.5	45°	61.58	35.78879
2.	0.5	21	67.5°	125.58	41.97841
3.	0.5	31.5	90°	241.29	47.65079
4.	1.5	10.5	67.5°	110.28	40.84994
5.	1.5	21	90°	189.18	45.5375
6.	1.5	31.5	45°	180.54	45.13147
7.	2.5	10.5	90°	159.44	44.05195
8.	2.5	21	45°	132.62	42.45218
9.	2.5	31.5	67.5°	230.55	47.2553

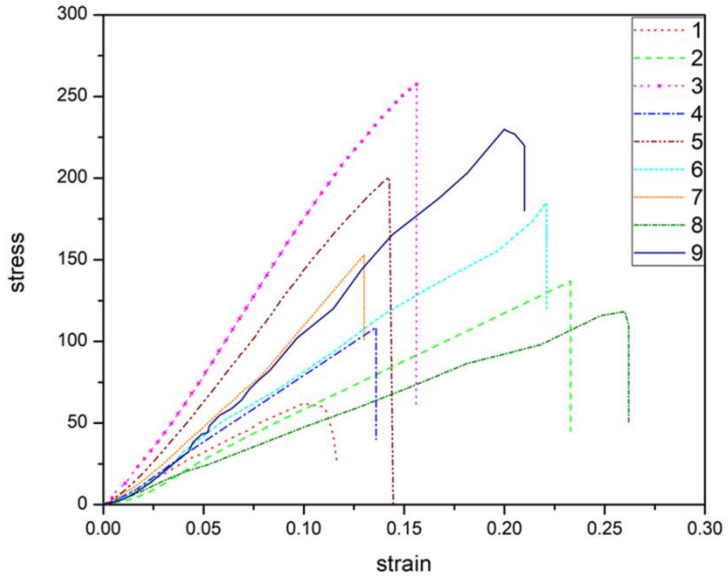

Figure 4.3 Stress-strain graph of EGCNs (numbers 1,2,3, etc. refer to serial nos. in table 4.2)

The experimental outcomes are transformed into the signal to noise ratio (S/N ratio). Signal means the desired output characteristic, whereas noise means the undesired output characteristic. The S/N ratio indicates the quality characteristic, which implies whether the output desired is maximum or minimum or intermediate. In Taguchi method, there are three quality characteristics which were defined as higher-the-better, lower-the-better and the nominal-the-better. The S/N ratio indicates the variation in the output due to an error where the smaller the variation due to error, the better the output is [129]. As the outcome is the tensile strength for which the higher the better quality characteristic suits better, and hence, S/N ratio characteristic should be selected such that the larger the S/N ratio, the better the strength, calculated by equation (1):

$$(S/N)_{HB} = -10\log[\frac{1}{R}\sum_{j=1}^{R}(1/Y_j^2)] \quad \text{.....(1)}$$

Mean σ_{UTS} values and corresponding S/N ratios obtained in Taguchi analysis depicted graphically in Figs. 4.4 & 4.5. These figures show the trend of each parameter's effect on σ_{UTS} and Fig. 4.6 shows the residual plots of S/N ratios. Residual plots indicate that the residuals are closer to the normal distribution line which means that the assumption of normal distribution is satisfied [130].

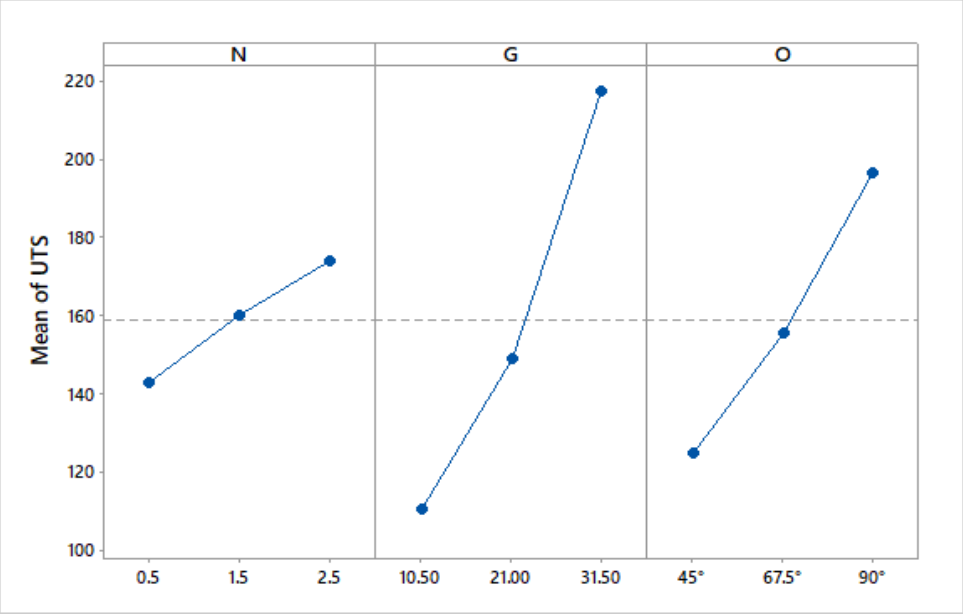

Figure 4.4 Main effect plot for σ_{UTS}

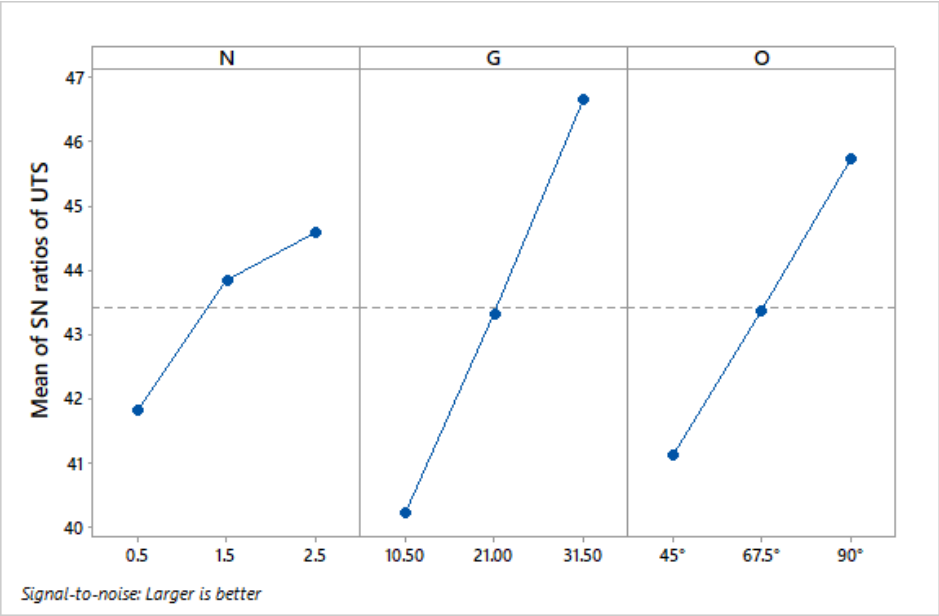

Figure 4.5 S/N ratio plot for σ_{UTS}

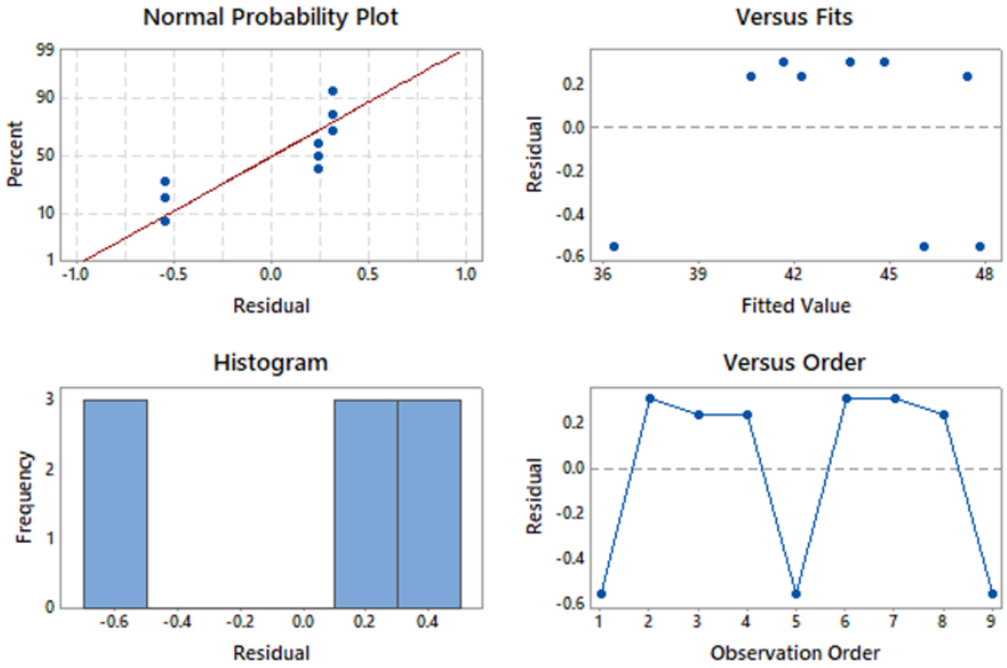

Figure 4.6 Residual Plots for S/N ratio's of σ_{UTS}

ANOVA for σ_{UTS}

Table 4.3 shows the ANOVA table for S/N ratios of σ_{UTS} which is produced using Minitab 17 software. The p-value indicates whether the particular parameter is significant in influencing the σ_{UTS}. If P-value is less than 0.05, it indicates that the null hypothesis is false because the probability of null hypothesis to be true is less than 5%. F-value in table 4.3 indicates the ratio between variance due to parameter to variance due to error and there is an inverse relation between F-vale and P-value which can be observed from table 4.3. The p-values for N, G, and O are 0.099, 0.021, and 0.041 respectively, which means the probability that the parameters N, G, and O do not influence the σ_{UTS} is 9.9%, 2.1%, and 4.1% respectively. This implies that there is 90.1%, 97.9%, and 95.9% probability that the parameters N, G, and O influence the σ_{UTS}. The percentages of contribution values are also significant. Hence all three parameters are showing a significant effect.

Table 4.3. ANOVA table for S/N ratios of σ_{UTS}.

Source	DF	Seq SS	Contribution	Adj SS	Adj MS	F-Value	P-Value
N (wt %)	2	12.425	11.47%	12.425	6.2123	9.07	0.099
G (vol %)	2	62.419	57.65%	62.419	31.209	45.58	0.021
O (deg)	2	32.064	29.61%	32.064	16.032	23.41	0.041
Error	2	1.369	1.26%	1.369	0.6847		
Total	8	108.28	100.00%				

Optimal design for σ_{UTS}

The optimal setting of parameters is selected based on the trend observed in Fig. 4.4 or Fig. 4.5. In both figures, the set N3, G3, and O3 has the maximum S/N ratio or mean value. Hence, this is the optimum setting for the maximum σ_{UTS}. At this set of variables, the optimum values of S/N ratio and σ_{UTS} are predicted using the equations (2) and (3).

$$\text{S/N Ratio} = 43.411 - 1.605\,N1 + 0.429\,N2 + 1.176\,N3 - 3.18\,G1 - 0.088\,G2 + 3.268\,G3 - 2.287\,O1 + 0.049\,O2 + 2.336\,O3 \quad \text{……..(2)}$$

= 43.411+1.176+3.268+2.336

= 50.191

σ_{UTS} = 159.01 - 16.19 N1 - 0.99 N2 + 15.2 N3 - 48.57 G1 - 9.88 G2 + 58.45 G3 - 34.09 O1 + 3.54 O2 + 37.63 O3 …… (3)

= 159.01+15.2+58.45+37.63

= 270.29 MPa

Confirmation tests for σ_{UTS}

The predicted value of σ_{UTS} at optimal conditions is confirmed by performing experiments at those conditions. Five samples were tested and the average σ_{UTS} of these five samples is obtained as 262 N/mm^2 and corresponding S/N ratio is 48.36. The obtained values fell within ±5% of the predicted σ_{UTS} value and predicted S/N ratio. Hence, the fitted model validated the experimental value.

4.2.3 Response surface methodology

Table 4.4. Actual and coded levels of the design parameter

Factors	Levels			Axial points α = 1	
	Low (-1)	Central (0)	High (+1)	-α	+α
Nanoclay wt%	0.5	1.5	2.5	-1	+1
Glass fiber vol%	10.5	21	31.5	-1	+1
Fiber angle	+45°/-45°	67.5°/22.5°	0°/90°	-1	+1

Table 4.5. Experimental design according to CCD and corresponding response

Run	Nanoclay wt% (N)	Glass Fiber Volume % (G)	Angle (O)	σ_{UTS} (MPa)
1	1.5	31.5	67.5°	215.43
2	1.5	21	45°	120.38
3	2.5	31.5	45°	185.52
4	1.5	21	67.5°	154.88
5	0.5	31.5	45°	164.73
6	2.5	10.5	45°	73.34
7	0.5	21	67.5°	134.58
8	2.5	31.5	90°	262.37
9	1.5	21	67.5°	143.96
10	0.5	31.5	90°	249.29
11	1.5	21	67.5°	151.67
12	0.5	10.5	45°	61.58
13	2.5	21	67.5°	138.48
14	1.5	21	90°	183.54
15	1.5	21	67.5°	148.83
16	1.5	21	67.5°	140.55
17	1.5	21	67.5°	148.76
18	2.5	10.5	90°	159.44
19	0.5	10.5	90°	148.76
20	1.5	10.5	67.5°	110.28

Table 4.4 displays the parameters whose levels are shown in coded form and actual form. Table 4.5 shows the generated experimental design according to central composite design and the corresponding σ_{UTS} for each EGCN. The input parameters are nanoclay wt%, glass fiber vol%, and fibers orientation which are indicated in ANOVA tables, 2D, and 3D plots as N, G and O respectively. ANOVA analysis was performed to evaluate the effect of parameters and the confidence level selected is 95%. Based on the obtained p-value whether the particular parameter is significant or insignificant is evaluated. If the p-value is less than 0.05, it indicates that there is greater than 95% probability that the input parameter affects the σ_{UTS}. If the p-value is greater than 0.05, it indicates that there is less than 95% probability that the input parameter affect the σ_{UTS}. If

any of the parameters are insignificant, then those parameters should be eliminated and analysis should be repeated with the remaining ones.

ANOVA and regression model for σ_{UTS}

Tables 4.6, 4.8-4.9 show the ANOVA analysis tables obtained after the first, second, and third step of analysis by eliminating terms that were not effective on σ_{UTS}. It can be noticed from table 4.6 that the probability values for terms N, G, and O were more than 99%. The term N*N is effective with P-value 0.04 and the term G*G is effective with P-value <0.0001 but the term O*O was insignificant as its p-value is >0.05. There were no significant interactions between variables because all the corresponding p-values are >0.05. Moreover, "Lack-of-Fit" of the quadratic model was insignificant as its P-value is 0.26. Hence, the quadratic model fits the data satisfactorily.

Table 4.6. ANOVA table obtained for σ_{UTS} in the first step of analysis

Source	Seq SS	DF	Adj MS	F-Value	P-value
Model	45295.06	9	5032.785	133.4716	< 0.0001
N	362.5244	1	362.5244	9.614302	0.01
G	27451.31	1	27451.31	728.0205	< 0.0001
O	15828.46	1	15828.46	419.7776	< 0.0001
N*G	16.33061	1	16.33061	0.433095	0.52
G*O	9.658013	1	9.658013	0.256135	0.62
N*O	17.61211	1	17.61211	0.467081	0.51
N*N	206.6711	1	206.6711	5.481006	0.04
G*G	857.2606	1	857.2606	22.73492	0.0008
C*C	125.7022	1	125.7022	3.333676	0.097
Residual	377.0678	10	37.70678		
Lack of Fit	243.2444	5	48.64887	1.817651	0.26
Pure Error	133.8235	5	26.7647		
Total	45672.13	19			

Table 4.7 shows the regression coefficients of the model and equation (4) shows the second order polynomial model consisting of all the coefficients of the significant and insignificant terms.

$$\sigma_{UTS} = 16.176 + 32.46^{*} N - 1.51^{*}G + 0.17^{*}O + 0.013^{*}N^{*}G - 0.048^{*}N^{*}O - 0.006^{*}G^{*}O - 8.67^{*}N^{2} + 0.16^{*}G^{2} + 0.013^{*}O^{2} \quad \ldots\ldots\ldots (4)$$

Table 4.7 Regression coefficients obtained in the first step of analysis of σ_{UTS}

Coefficient	b_0	b_1	b_2	b_3	b_{11}	b_{22}	b_{33}	b_{12}
value	16.176	32.46	-1.51	0.17	-8.67	0.16	0.013	0.136
Coefficient	b_{13}	b_{23}	R^2 %					
value	-0.048	-0.0062	99.17					

The ineffective terms were eliminated and the ANOVA analysis was repeated for the remaining terms and the results are given in table 4.8. It is observed from this table is that the P-value for the G*G term decreased after excluding insignificant terms and p-value for the term N*N increased. The ANOVA analysis was repeated for the third time after excluding the term N*N and the new ANOVA table can be seen in table 4.9. This time p-value for the term N increased from 0.0087 to 0.012 and remaining factors shown no change in p-values.

Table 4.8 ANOVA table obtained for σ_{UTS} in the second step of analysis

Source	Seq SS	DF	Adj MS	F-Value	p-value
Model	45125.76	5	9025.152	231.2571	< 0.0001
N	362.5244	1	362.5244	9.289189	0.0087
G	27451.31	1	27451.31	703.4021	< 0.0001
O	15828.46	1	15828.46	405.5826	< 0.0001
N*N	120.3932	1	120.3932	3.084911	0.1
G*G	1304.597	1	1304.597	33.42851	< 0.0001
Residual	546.3708	14	39.02648		
Lack of Fit	412.5473	9	45.83859	1.712651	0.28
Pure Error	133.8235	5	26.7647		
Total	45672.13	19			

Table 4.10 gives the regression coefficients obtained after the third step of analysis and equation (5) is a reduced second order polynomial comprising of the final coefficients of the significant terms.

Table 4.9 ANOVA table obtained for σ_{UTS} in the third step of analysis

Source	Seq SS	DF	Adj MS	F-Value	p-value
Model	45005.36	4	11251.34	253.1182	< 0.0001
N	362.5244	1	362.5244	8.155608	0.012
G	27451.31	1	27451.31	617.5643	< 0.0001
O	15828.46	1	15828.46	356.0884	< 0.0001
G*G	1363.066	1	1363.066	30.6645	< 0.0001
Residual	666.764	15	44.45094		
Lack of Fit	532.9405	10	53.29405	1.991207	0.23
Pure Error	133.8235	5	26.7647		
Total	45672.13	19			

Table 4.10 Regression coefficients obtained for σ_{UTS} in the third step of analysis

Coefficient	b_0	b_1	b_2	b_3	b_{11}	b_{22}	R^2 %
value	-18.42	24.42	-2.7	1.768	-6.133	0.183	98.8

$$\sigma_{UTS} = -18.42 + 24.42* N - 2.7* G + 1.768* O + 0.183* G^2 \quad \text{……..(5)}$$

It should be noticed that squares of the factors N and O were not effective on σ_{UTS}. Moreover, the coefficient of determination (R^2) for both steps of analysis of the response is shown in table 4.6 and table 4.9. Here, R^2 is the measure of the strength of fit of the model or the measure of nearness of the fitted values to the experimentally obtained values. In tables 4.7 & 4.10, the R^2 values are 99.17% and 98.8% for a fitted model in the first and final step of analysis, respectively. These high values of R^2 also indicate that the regressor terms in the model not only explain the total variability of the response but also give a good estimation of response at the desired levels of parameters.

Main effect plots

Figs. 4.7(a) - 4.7(c) display the main effect plots of factors N, G, and O. Fig. 4.7(a) shows that the magnitude of σ_{UTS} has undergone small change with an increase in nanoclay wt%. Fig. 4.7(b) shows that the σ_{UTS} increased as the magnitude of fiber volume increased. However, it is evident that the rate of increase in σ_{UTS} due to G is more compared to the rate of increase in σ_{UTS} due to N. the rate of increase in σ_{UTS} observed in Fig. 4.7(c) is at intermediate levels compared to the rate observed in Figs 4.7(a) &(b).

The main effect plots and the p-values of first-order terms from ANOVA results were in good agreement with each other. The sign of the regression coefficients also agrees with the trend of the σ_{UTS} for each parameter. It was also confirmed from the ANOVA analysis that the rate of change in σ_{UTS} is more due to G compared to the change due to other parameters.

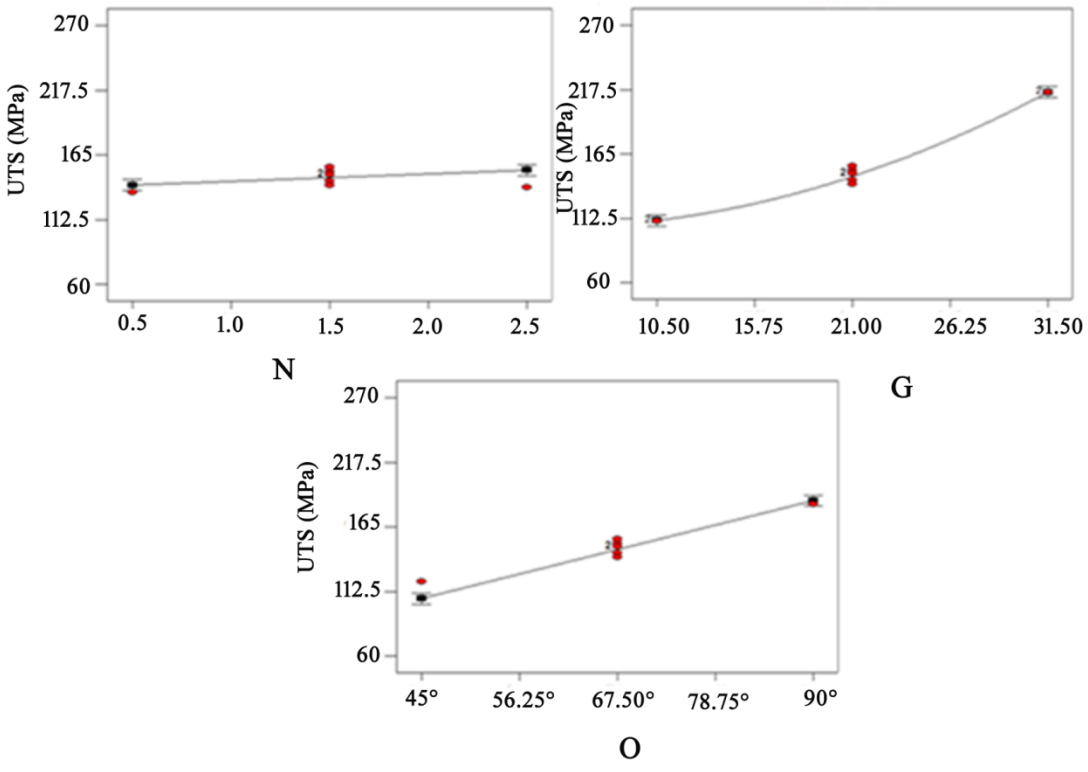

Figure 4.7 Main effect plots for factor (a) N, (b) G, and (c) O on σ_{UTS}

Normal Probability plots

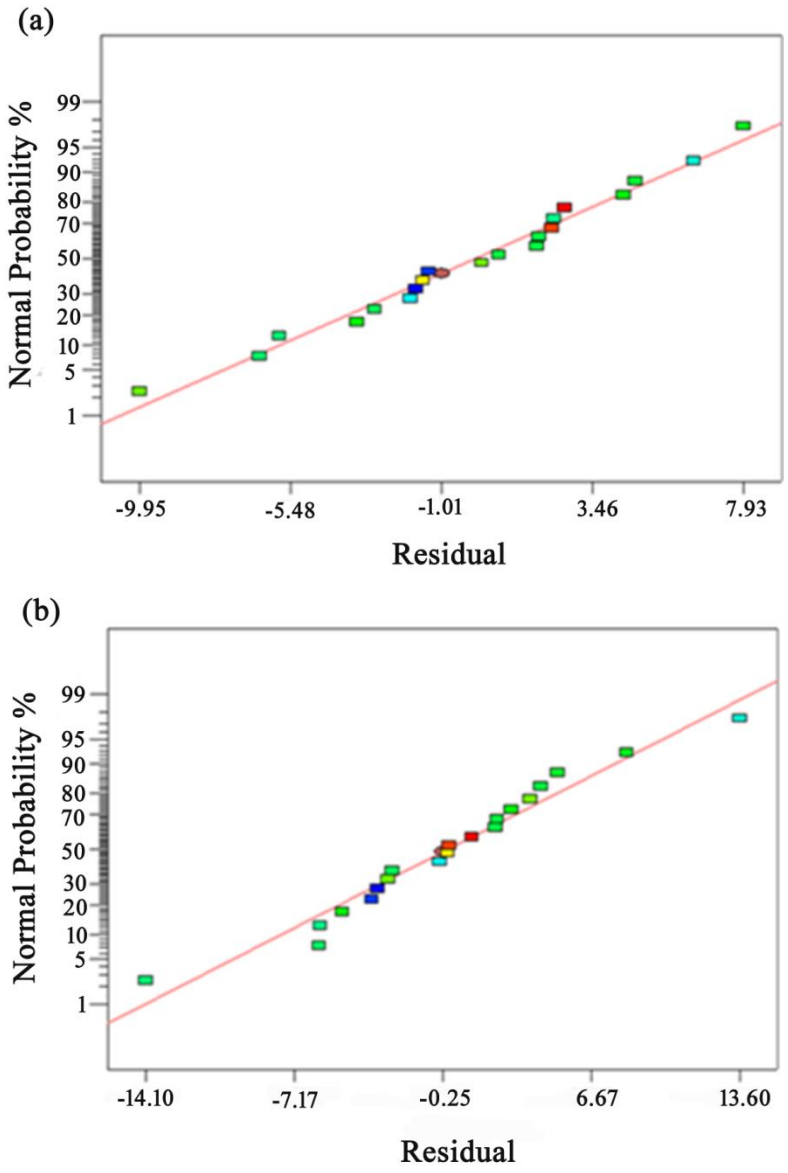

Figure 4.8 Normal probability plots of residuals from (a) initial and (b) final analysis of σ_{UTS}

Fig. 4.8(a) shows the plot between normal probability% and residuals generated in the first step of the ANOVA analysis. This plot shows whether the residuals are normally distributed or not. The condition for regression analysis is that the residuals should be normally distributed. If the residuals are not normally distributed, then the fitted regression model is invalid. In Fig.

4.8(a) the all the points are falling closer to the normal distribution line; therefore, the condition for regression analysis is satisfied. Fig. 4.8(b) shows the plot between normal probability and residuals for the final analysis. From Fig. 4.8(b) it is observed that the points fell slightly away from the normal distribution line. However, the condition that the residuals should be normally distributed is unaltered.

Plots of Residuals vs. predicted values

Figs. 4.9(a) & 4.9(b) show the plots between residuals and fitted values of σ_{UTS} obtained in the first and second step of ANOVA analysis. From these two figures, it can be observed that the residuals for σ_{UTS} in both first and third step of analysis were scattered randomly and elimination of the insignificant terms did not affect the random distribution of residuals. Therefore it can be concluded that the fitted model is adequate and there was no proof to suspect that the residuals are dependent.

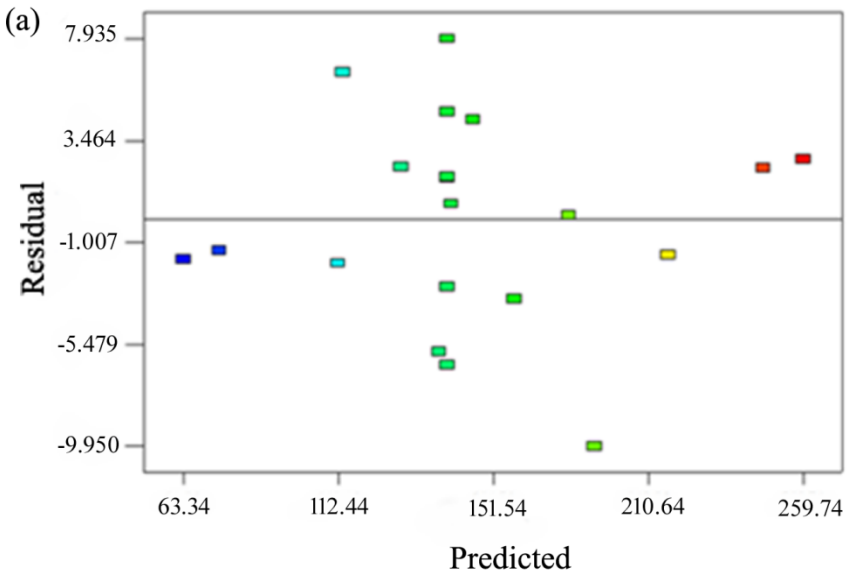

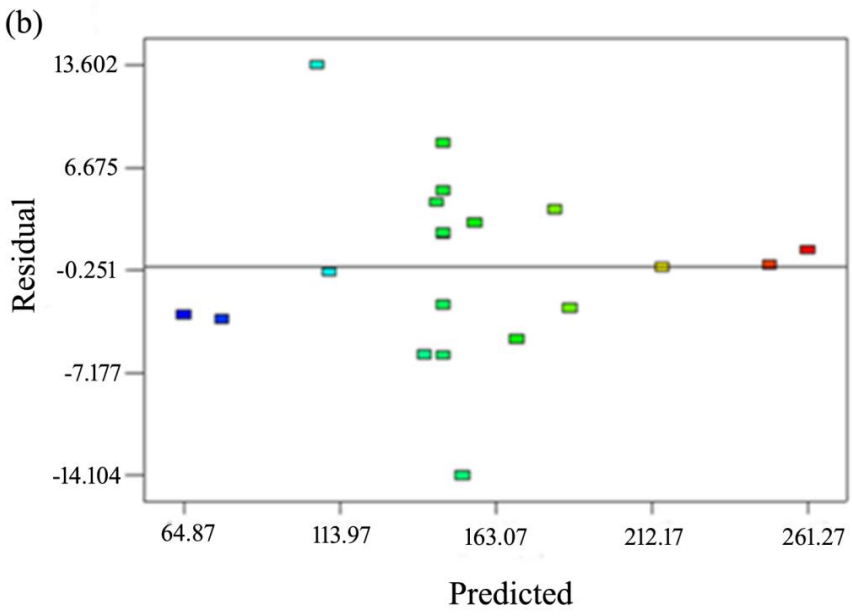

Figure 4.9 Residuals versus predicted values plots for (a) initial analysis of σ_{UTS}, (b) final analysis of σ_{UTS}

Plots of predicted values vs. actual values

Figs. 4.10(a) & 4.10(b) show the plots between predicted σ_{UTS} values and actual values of σ_{UTS}. From these graphs, it can be seen that the predicted σ_{UTS} values are in good agreement with the actual σ_{UTS} values; hence, the correlation between σ_{UTS} and parameters is satisfactory.

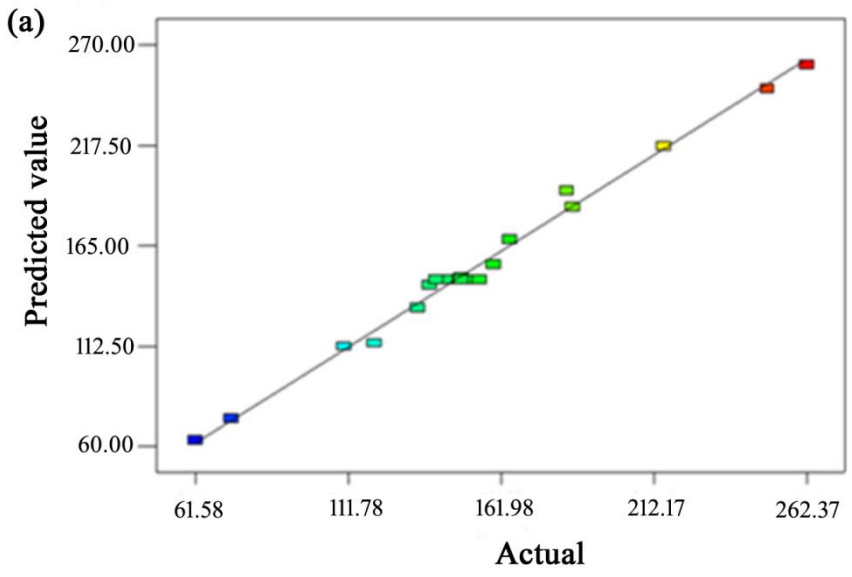

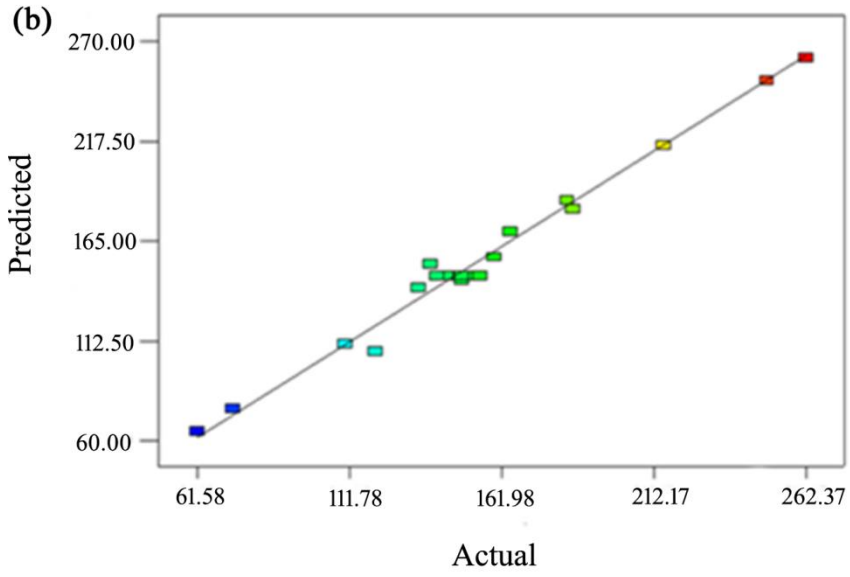

Figure 4.10 Plot of predicted versus observed for σ_{UTS} from (a) initial and (b) final analysis

3D Surface plots for σ_{UTS}

RSM method generates surface plots to demonstrate the main effects, quadratic effects and interactions between independent parameters. These surface plots are also called as 3D plots and are plotted as two parameters in x and y directions and the response on z-axis while the third parameter is kept constant.

Effect of nanoclay on σ_{UTS}

Fig. 4.11(a) displays a response surface plot consisting of two factors N and G on x and y axes while factor O was fixed at 67.5° and σ_{UTS} is shown on z-axis. Here, σ_{UTS} increases slowly with increase in N but increases at a faster rate with increase in G. Fig. 4.11(b) displays response surface plot consisting of two factors G and O on x and y axes while factor N was fixed at 1.5 wt% and σ_{UTS} is shown on z-axis. Here, σ_{UTS} increases at an intermediate rate with increase in O compared to the rate of increase in σ_{UTS} due to the other two parameters. Fig. 4.11(c) display response surface plot consisting of two factors N and O on x and y axes while factor G was fixed 21 vol. %.

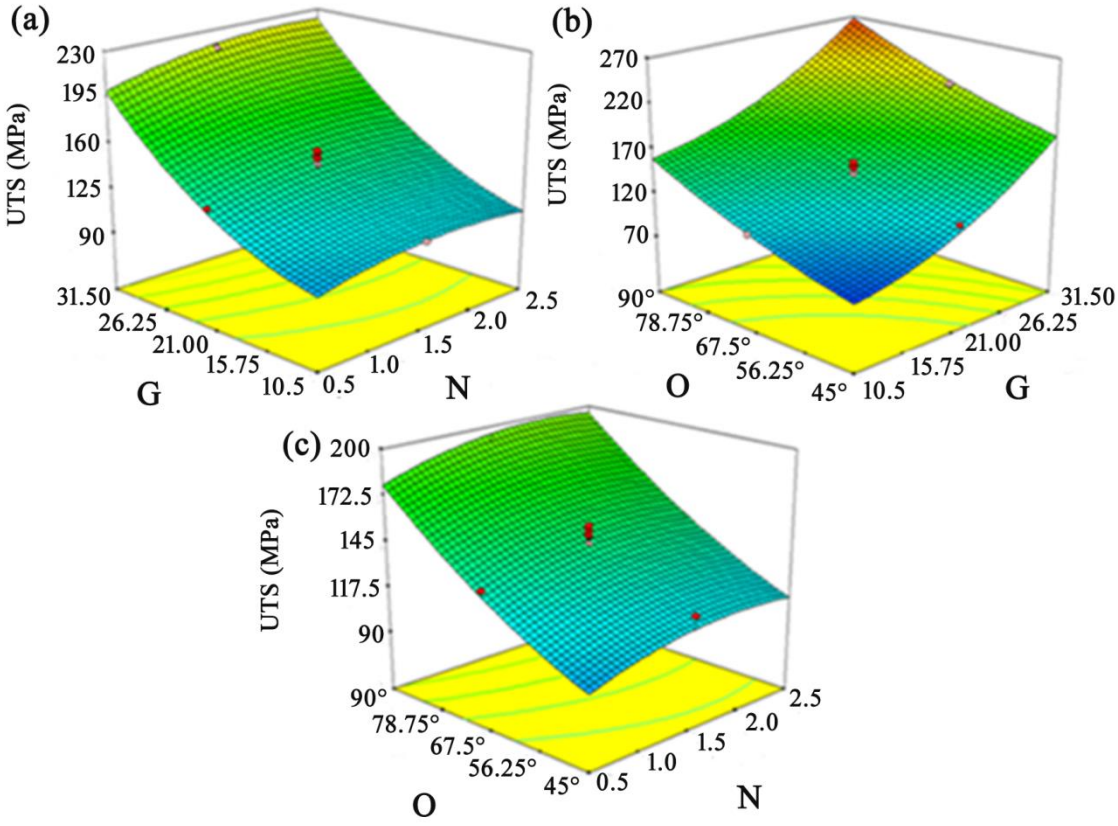

Figure 4.11 3D surface plots for effect of N, G, and O on σ_{UTS}

Maximum value of σ_{UTS} obtained in this study is 262.37 MPa which was observed at parameter levels of N = 2.5 wt%, G = 31.5 vol% and O = 0°/90° and the corresponding levels in coded form are N = +1, G = +1 and O = +1 respectively.

4.2.4 Scanning electron microscopy

The fracture surfaces of EGCN samples are shown in Fig. 4.12(a) & 4.12(b) which prove that the debonding between fibers and matrix is difficult due to the presence of clay platelets at the interface, whereas at 4 wt% of nanoclay, the fibers were well separated because of the poor bonding between fibers which might have resulted due to poor distribution of nanoclay platelets

at high volume of nanoparticles. The poor distribution of particles at high contents was also reported by other researchers [60, 131]. Less energy is required to fail the specimen when a poor distribution is obtained in the composite and the same type of fracture was observed when the clay is not added in the composite, which is shown in Fig. 4.13(d) and Fig. 4.14(b). The fracture surface of well dispersed nanoclay composite resembles a ductile failure because the epoxy molecules in the matrix were well bonded. When cracks generate in the matrix they propagate in a critical manner because of the resistance offered by nanoclay platelets; hence, more energy is

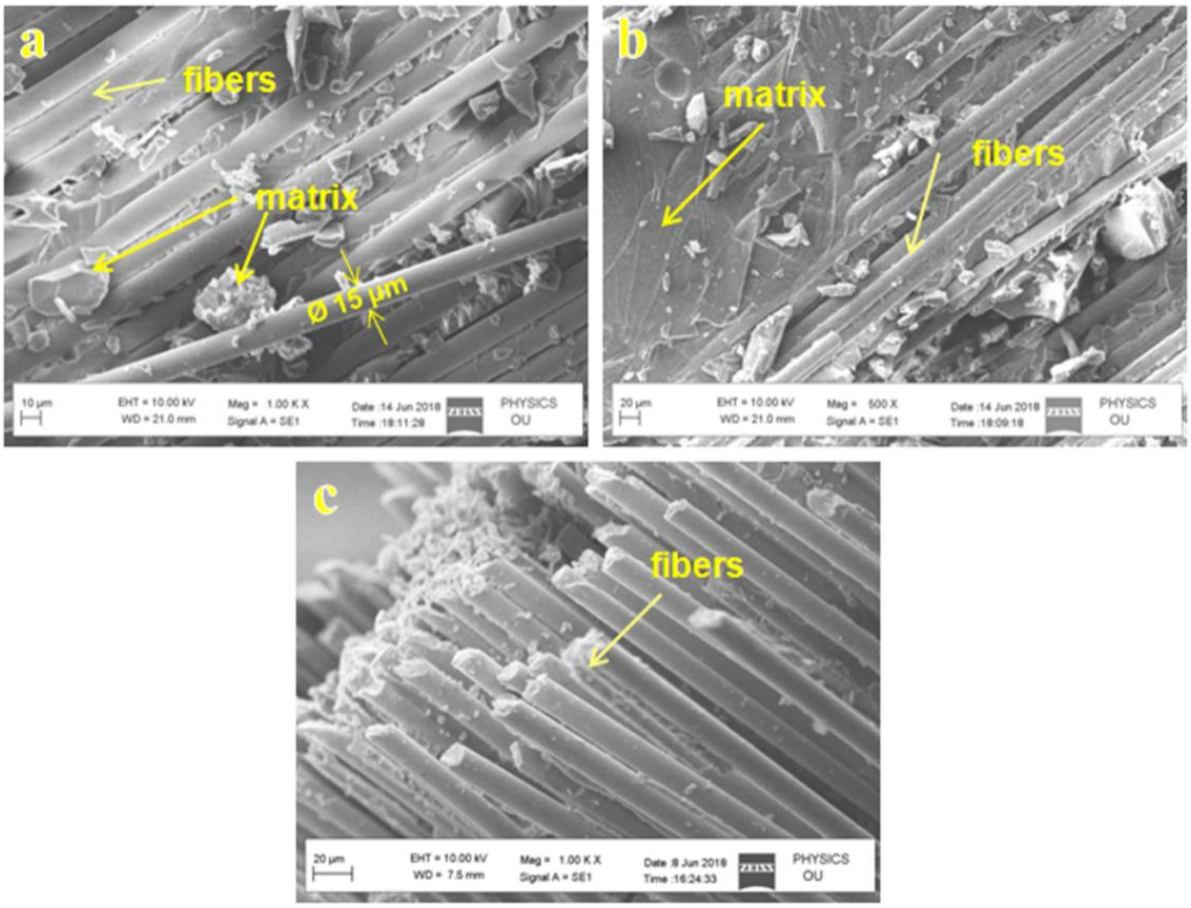

Figure 4.12 Fracture surfaces of EGCNs with nanoclay (a) 0.5 wt% (b) 2.5 wt% (d) 4 wt%

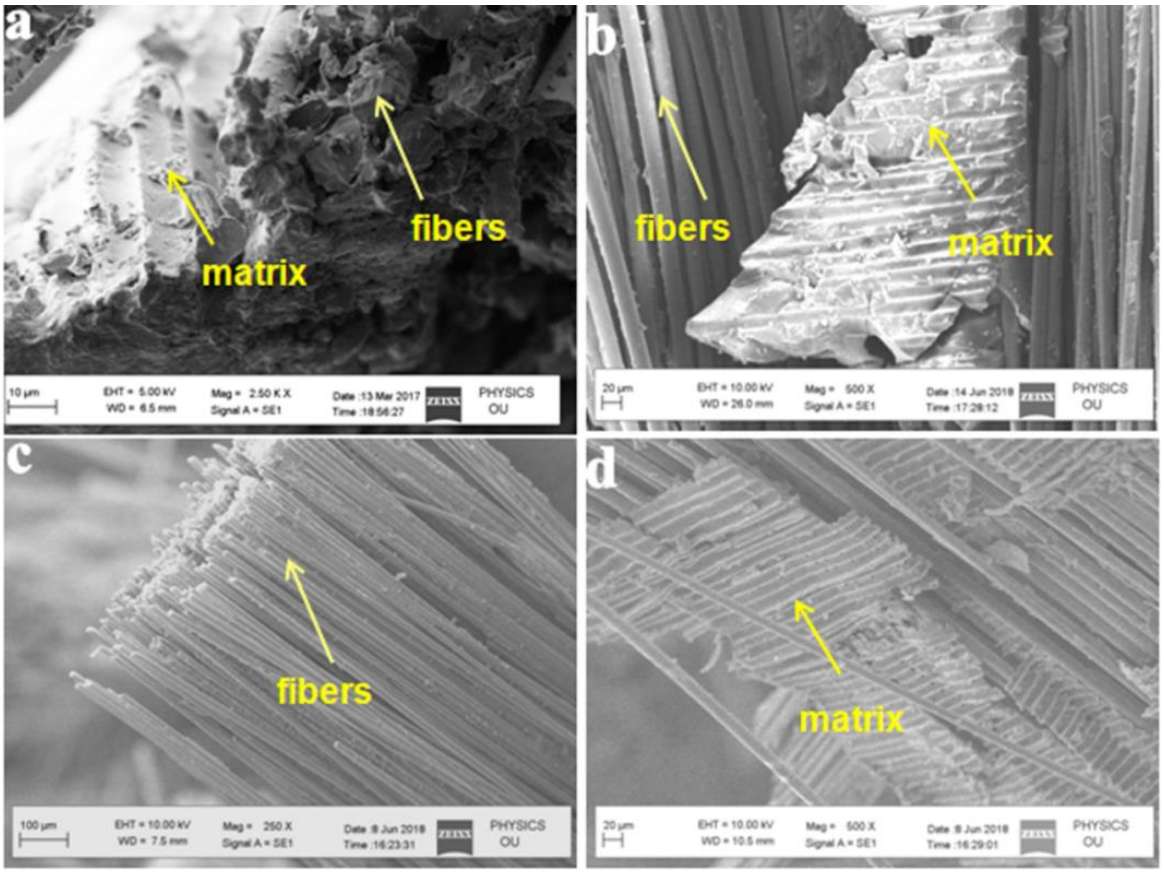

Figure 4.13 EGCNs at 2.5 wt% of nanoclay and glass fiber volume at (a) 10.5 vol % (b) 21 vol% (c) 35 vol% (d) Epoxy-31.5% glass fiber

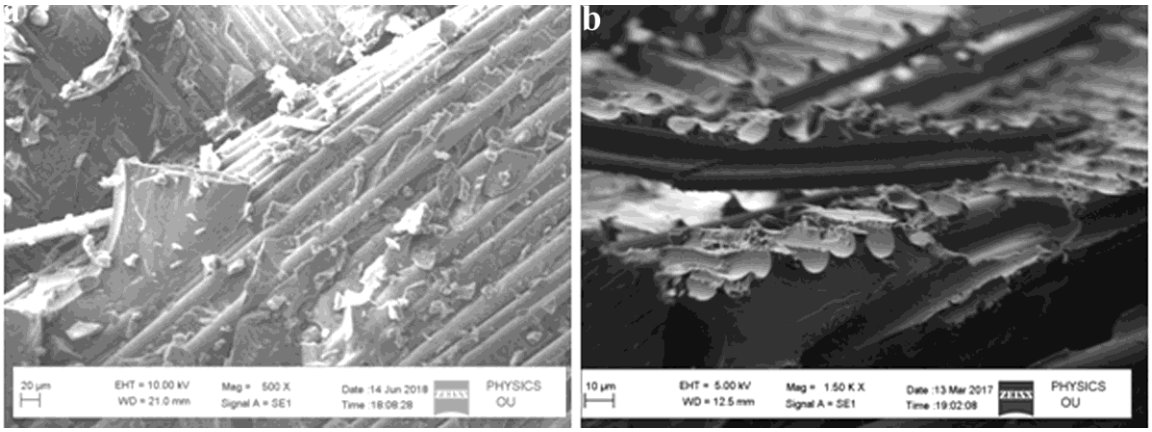

Figure 4.14 Fracture surface morphology of (a) EGCN at 2.5 wt% nanoclay, 31.5 vol% glass fibers, 0°/90° fiber angle (b) Epoxy-31.5 vol% glass fiber

required to fail the specimen. The fractured specimen shows less fiber pullout because of simultaneous failure of matrix and fibers with matrix still present on the fibers after failure as shown in Figs. 4.13(a) & (b) and Fig. 4.14(a). This phenomenon was also reported in the literature [99]. In contrast, in neat GRE, the cracks can easily progress without hindrance. Hence, failure of GRE is easy and fiber pullout also is more in GRE which can be observed in Fig. 4.14(b). This phenomenon was also reported by Zulfli et al. [99]. At a high fiber volume, there is an insufficient matrix to wet all the fibers and the failure of the specimen occurred is shown in Fig. 4.13(c) which is in a similar fashion to failure of the specimen, occurred in Fig. 4.13 (d) [61, 75, 76].

4.2.5 Density and void content

Table 4.11 shows the theoretical density, experimental density, and void content of all the EGCNs. The vol.% of voids in the composites ranged in between 2.37 to 3.42. The void content increased with increase in nanoclay content and glass fiber volume. The increase in void content is attributed to the air bubbles introduced during mechanical stirring and the air gaps created in between plies during hand-layup method.

Table 4.11 Density and void contents of the composites

Sl. No	Nanoclay wt% (N)	Glass Fiber vol % (G)	Angle (O)	Theoretical density (T_d)	Experimental Density (M_d)	Void content (vol. %)
1.	0.5	10.5	45°	1.767	1.725	2.37
2.	0.5	21	67.5°	1.82	1.775	2.47
3.	0.5	31.5	90°	1.872	1.822	2.64
4.	1.5	10.5	67.5°	1.785	1.736	2.73
5.	1.5	21	90°	1.838	1.785	2.88
6.	1.5	31.5	45°	1.89	1.833	2.97
7.	2.5	10.5	90°	1.803	1.746	3.13
8.	2.5	21	45°	1.856	1.795	3.25
9.	2.5	31.5	67.5°	1.908	1.842	3.42

4.2.6 Summary

In the present study, σ_{UTS} of the nanocomposites have been investigated. Glass fiber and nanoclay were reinforced in various proportions and fibers oriented at various angles. Taguchi and RSM methods were used to analyze the data and present the fitted quadratic model for predicting the σ_{UTS}. ANOVA analysis done using both methods showed that all three parameters were effectively influencing the σ_{UTS}. While only glass fiber volume has shown the quadratic effect and the remaining two parameters shown only linear effect and there are no significant interactions present between parameters. The optimized result obtained indicated that the best σ_{UTS} obtained was 270 MPa and occurred at 2.5 wt% of nanoclay, 31.5 vol% of fiber, and 0°/90° of fibers orientation. The result is confirmed by preparing and testing five samples and the average value of σ_{UTS} obtained was 262 MPa. The fracture morphology had shown the strong bond between fiber and matrix when nanoclay was added and rough matrix morphology compared neat glass-epoxy because of the restricted cracks propagation in the matrix by the clay platelets.

4.3 Optimization of Flexural Strength (σ_f)

The standard testing method for finding flexural properties is ASTM D 790. The dimensions of the specimen are 128 mm x 20 mm x 4 mm. The flexural test is performed in universal testing machine WDW-100S. The tests were performed at a crosshead speed of 10 mm/min. For each test five samples were tested and the average value was taken for analysis. For Taguchi method L9 array is selected and central composite design is selected for RSM. Pilot experiments were conducted to identify the effective ranges of parameters. After these ranges are fixed, the experiments were conducted according to Taguchi and RSM designs. The effect of each parameter is quantified using ANOVA and significance of parameter effect is evaluated. A linear model is fitted in Taguchi method and quadratic model is fitted in RSM. The R^2 value quantifies the strength of fit of the regression model, respectively. The fracture surface is studied with SEM micrography.

4.3.1 Taguchi Design

Flexural strength (σ_f) of the composites is evaluated for the same L9 orthogonal array selected in section 4.2 and given in Table 4.12. Fig. 4.15 shows the flexural stress-strain plots obtained after three-point bending tests of specimens. It is evident from Fig. 4.15 that EGCNs in which fibers oriented at 0°/90° with corresponding serial numbers 3, 5, 7 in table 4.12 are showing high σ_f. When fibers are oriented at 22.5°/67.5° with corresponding serial numbers 2, 4, 9 of EGCNs in table 4.12 are showing intermediate σ_f values. When fibers oriented at 45°/-45° with corresponding serial numbers 1, 6, 8 in table 4.12 are showing low σ_f values. The slopes of the curves are also following the same trend. The effect of nanoclay wt% and glass fiber vol% are not much evident in Fig. 4.15 as it is evident for fibers orientation. In case of high fiber content, the increase in σ_f is evident even when the fibers oriented at 45°/-45° and 22.5°/67.5° which can be seen for EGCNs with serial numbers 6 and 9.

Table 4.12. Experimental design using L9 orthogonal array for σ_f

Sl. No	Nanoclay wt% (N)	Glass Fiber vol % (N)	Angle (O)	σ_f (MPa)	S/N Ratio
1.	0.5	10.5	45°	65.06	36.26
2.	0.5	21	67.5°	128.24	42.16
3.	0.5	31.5	90°	194.93	45.79
4.	1.5	10.5	67.5°	98.66	39.88
5.	1.5	21	90°	166.59	44.43
6.	1.5	31.5	45°	161.45	44.16
7.	2.5	10.5	90°	132.3	42.43
8.	2.5	21	45°	127.6	42.11
9.	2.5	31.5	67.5°	190.29	45.58

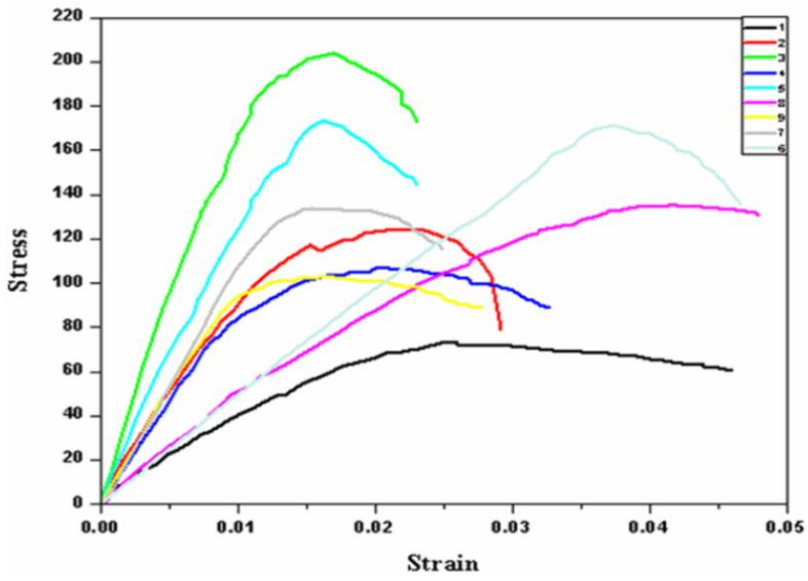

Figure 4.15 Stress-strain graph for the σ_f of epoxy-clay-glass nanocomposites

The experimental outcomes are transformed into the signal to noise ratio (S/N ratio). Signal means the desired output characteristic, whereas noise means the undesired output characteristic. The S/N ratio indicates the quality characteristic, which implies whether the output desired is maximum or minimum or intermediate. In Taguchi method, there are three quality characteristics which were defined as higher-the-better, lower-the-better, and nominal-the-better. The S/N ratio indicates the variation in the output due to an error where the smaller the variation due to error, the better the output is [129]. As the outcome is flexural strength for which the higher the better quality characteristic suits better, and hence, S/N ratio characteristic should be selected such that the larger the S/N ratio, the better the strength, calculated by equation (1):

Mean σ_f values and corresponding S/N ratios are depicted graphically in Figs. 4.16 & 4.17. These figures show the trend of each parameter's effect on σ_f and Fig. 4.18 shows the residual plots of S/N ratios. The residual plots indicate that the residuals are closer to the normal distribution line which means that the assumption of a normal distribution of residuals is satisfied [130].

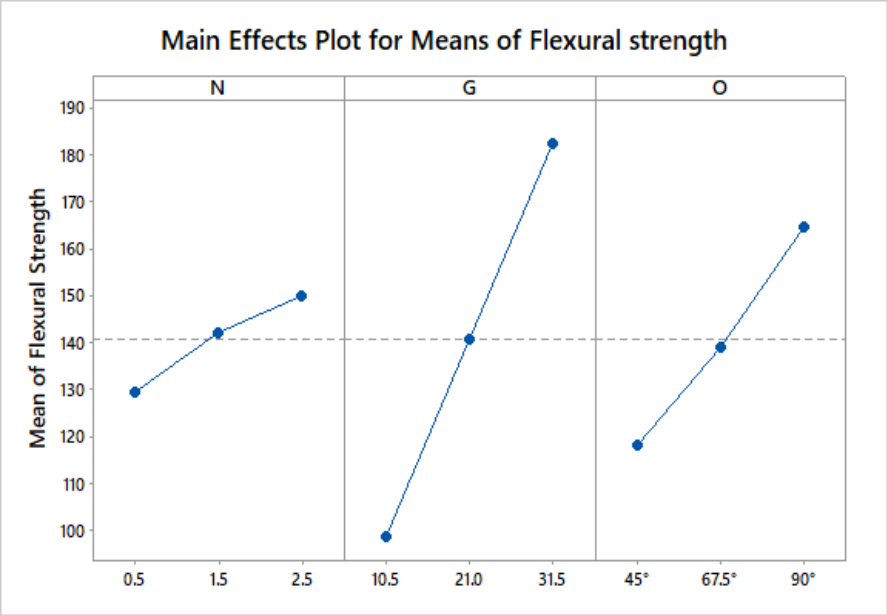

Figure 4.16 Main effect plot for σ_f

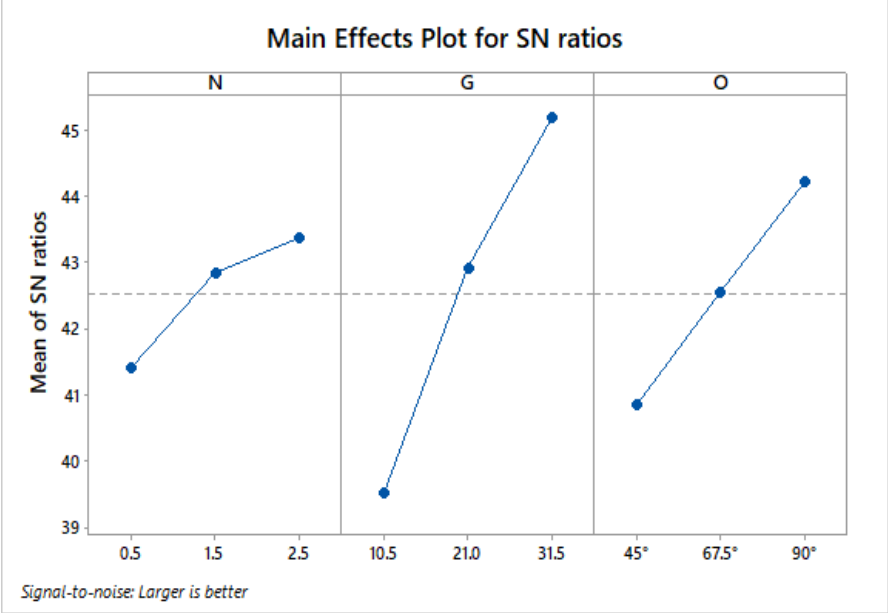

Figure 4.17 S/N ratio plot for σ_f

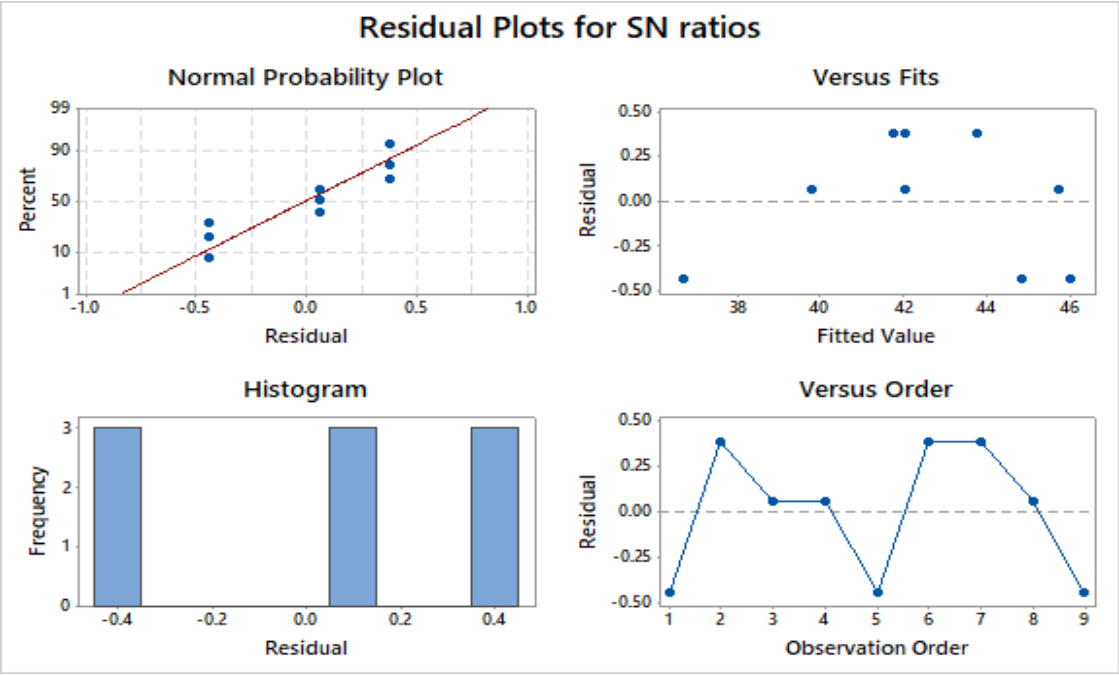

Figure 4.18 Residual Plots for S/N ratio's of σ_f

ANOVA for σ_f

Table 4.13 is the ANOVA table for S/N ratios of σ_f which is produced using Minitab 17 software. The p-value here indicates whether the parameter is significant in influencing the σ_f. If the P-value is less than 0.05, it indicates that the null hypothesis is false because the probability that the null hypothesis is true is very low, i.e., <5%. F-value in table 4.13 indicates the ratio between variance due to parameter to variance due to error, and there is an inverse relation between F-value and p-value which can be observed from table 4.13. The p-values for N, G, and O are 0.142, 0.021, and 0.057 respectively which means the probability that the parameters N, G, and O do not influence the σ_f is 14.2%, 2.1%, and 5.7% respectively. Therefore there is 85.8%, 97.9%, and 94.3% probability that the parameters N, G, and O influence the σ_f. The percentages of contributions are also significant. Hence, it can be said that all three parameters are showing a significant effect.

Table 4.13 ANOVA table for S/N ratio's of σ_f.

Source	DF	Seq SS	Contribution	Adj SS	Adj MS	F-Value	P-Value
N (wt %)	2	6.198	8.51%	6.198	3.0992	6.02	0.142
G (vol %)	2	48.577	66.66%	48.577	24.2883	47.18	0.021
O (deg)	2	17.062	23.42%	17.062	8.5312	16.57	0.057
Error	2	1.03	1.41%	1.03	0.5148		
Total	8	72.867	100.00%				

Optimal design for σ_f

The optimal setting of parameters is selected based on the trend observed in Fig. 4.16 or Fig. 4.17. In both figures, the set N3, G3, and O3 has the maximum S/N ratio or mean value. Hence, this set of variables is the optimum setting for the maximum σ_f. At this set of variables, the optimum values of S/N ratio and σ_f were predicted using the equations (6) and (7).

S/N Ratio = 42.538 - 1.129 N1 + 0.288 N2 + 0.841 N3 - 3.011 G1 + 0.366 G2 + 2.645 G3 - 1.689 O1 + 0.006 O2 + 1.683 O3 ……..(6)

= 42.538+ 0.841 + 2.645 + 1.683

= 47.70

σ_f = 140.569 - 11.158 N1 + 1.664 N2 + 9.494 N3 - 41.895 G1 + 0.241 G2 + 41.654 G3 - 22.532 O1 - 1.506 O2 + 24.037 O3 ……. (7)

= 140.569+ 9.494 + 41.654 + 24.037

= 215.75

Confirmation tests for σ_f

The predicted value of σ_f at optimal conditions is confirmed by performing experiments at those conditions. Five samples were tested, the average σ_f obtained and it's corresponding S/N ratio are 208.43 N/mm^2 and 45.65. The obtained values fall within ±5% of the predicted σ_f value and the S/N ratio. Hence, the fitted model validates the experimental value.

4.3.2 Response surface methodology

Table 4.14. Experimental design according to CCD and corresponding response

Run	Nanoclay wt% (N)	Glass Fiber Volume % (G)	Angle (O)	σ_f (MPa)
1	1.5	31.5	67.5°	65.58
2	1.5	21	45°	140.61
3	2.5	31.5	45°	214.76
4	1.5	21	67.5°	193.23
5	0.5	31.5	45°	119.65
6	2.5	10.5	45°	133.43
7	0.5	21	67.5°	136.77
8	2.5	31.5	90°	168.64
9	1.5	21	67.5°	128.87
10	0.5	31.5	90°	132.89
11	1.5	21	67.5°	148.57
12	0.5	10.5	45°	110.78
13	2.5	21	67.5°	181.77
14	1.5	21	90°	147.32
15	1.5	21	67.5°	144.42
16	1.5	21	67.5°	141.76
17	1.5	21	67.5°	98.55
18	2.5	10.5	90°	134.98
19	0.5	10.5	90°	85.79
20	1.5	10.5	67.5°	166.98

Table 4.14 shows the generated experimental design according to central composite design and the corresponding σ_f for each EGCN. The input parameters are nanoclay wt%, glass fiber vol%, and fibers orientation which are indicated in ANOVA tables, 2D, and 3D plots as N, G and O respectively. To evaluate the effect of parameters, ANOVA analysis was performed and the confidence level selected is 95%. Based on the p-value, whether the particular parameter is significant or insignificant is evaluated. If the p-value is less than 0.05, it indicates that there is greater than 95% probability that the input parameter affects the σ_f. If the p-value is greater than 0.05, it indicates that there is less than 95% probability that the input parameter affect the σ_f. If

any of the parameters are insignificant, then those parameters should be eliminated and analysis should be repeated with the remaining ones.

ANOVA and regression model for σ_f

Tables 4.15 & 4.16 show the ANOVA tables; the first one is obtained after the initial analysis and the second table is obtained by repeating the analysis by removing the insignificant terms observed in the first table. It can be noticed from table 4.15 that the probability values for terms N, G, and O were more than 99%. The terms N*G, N*O, G*O, N*N, G*G, and O*O, are ineffective with p-values greater than 0.05. Moreover, "Lack-of-Fit" of the quadratic model was insignificant as the P-value is 0.97.

Table 4.15. ANOVA table obtained for σ_f in the first step of analysis

Source	Seq SS	DF	Adj MS	F-Value	p-value
Model	23476.32	9	2608.48	249.98	< 0.0001
N	1099.772	1	1099.77	105.39	< 0.0001
G	16985.11	1	16985.11	1627.77	< 0.0001
O	5366.636	1	5366.63	514.31	< 0.0001
NG	0.035113	1	0.035	0.003	0.9549
GO	0.556513	1	0.55	0.053	0.822
NO	0.009112	1	0.009	0.00087	0.977
N*N	8.51	1	8.51	0.815	0.3877
G*G	0.280002	1	0.28	0.027	0.8731
C*C	22.11655	1	22.11	2.12	0.1761
Residual	104	10	10.4		
Lack of Fit	13.28796	5	2.657592	0.145929	0.9727
Pure Error	91.05748	5	18.2115		
Total	23580.67	19			

Table 4.16 shows the regression coefficients of the model and equation (8) shows the second order polynomial model consisting of all the coefficients of the significant and insignificant terms.

$$\sigma_f = -6.79387 + 14.84*A + 4.04678*B + 0.26*C + 0.006*A*B + 0.01*A*C - 0.0001*B*C - 1.76*A^2 - 0.003*B^2 + 0.005*C^2 \quad \text{……. (8)}$$

Table 4.16 Regression coefficients obtained for σ_f after second step of analysis

Coefficient	b_0	b_1	b_2	b_3	b_{11}	b_{22}	b_{33}
value	-6.79387	14.84	4.04678	0.26	- 1.76	-0.003	0.005
Coefficient	b_{12}	b_{13}	b_{23}	R^2 %			
value	0.006	0.01	- 0.0001	99.56			

The ineffective terms were eliminated and ANOVA analysis was repeated for the remaining terms and the obtained results are given in table 4.17.

Table 4.17. ANOVA table obtained for σ_f in the second step of analysis

Source	Seq SS	DF	Adj MS	F-Value	p-value
Model	23451.52	3	7817.174	968.4771	< 0.0001
N	1099.772	1	1099.772	136.2518	< 0.0001
G	16985.11	1	16985.11	2104.302	< 0.0001
O	5366.636	1	5366.636	664.8776	< 0.0001
Residual	129.1458	16	8.071615		
Lack of Fit	38.08835	11	3.462577	0.190131	0.9896
Pure Error	91.05748	5	18.2115		
Total	23580.67	19			

$$\sigma_f = -27.887 + 10.487*A + 3.925*B + 1.0296*C \quad \text{……. (9)}$$

Table 4.18 shows regression coefficients obtained after doing the third step of ANOVA analysis and equation (9) is a reduced second order polynomial comprising of coefficients of the significant terms.

Table 4.18. Regression coefficients obtained for σ_f in the third step of analysis

Coefficient	b_0	b_1	b_2	b_3	R^2 %
value	-27.887	10.487	3.925	1.0296	99.45

It should be noticed that the squared terms of the factors N, G, and O were not effective on σ_f and there are no significant interactions. Moreover, the coefficient of determination (R^2) for both steps of analysis of the response is shown in table 4.16 and table 4.18. R^2 is the strength of fit of the model or the nearness of the fitted values and experimentally obtained values. In tables 4.16 & 4.18, the R^2 values are 99.56% and 99.45% for the fitted model in the first and final step of analysis respectively. These high values for R^2 also indicate that the regressor terms in the model not only explain the total variability of the response but also give a good estimation of response in the ranges of parameters selected.

Main effect plots

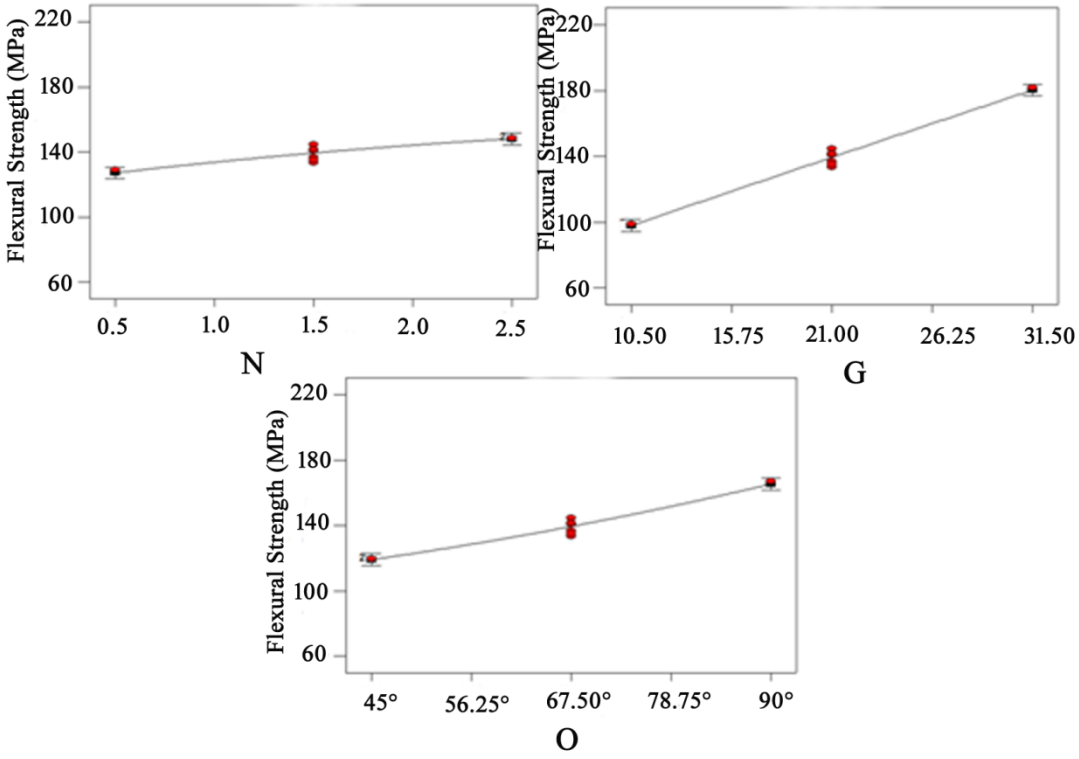

Figure 4.19 Main effect plots of factor (a) N, (b) G, and (c) O on σ_f

Figs. 4.19(a)-4.19(c) display the main effect plots of factors N, G, and O on σ_f. Fig. 4.19(a) shows that the magnitude of σ_f undergone small change with increase in nanoclay wt%. Fig. 4.19(b) shows that the σ_f increases substantially as the magnitude of fiber volume increases. However, it is evident that the rate of increase in σ_f due to glass fiber addition is more compared to the rate of increase in σ_f due to nanoclay addition. Fig. 4.19(c) gives the main effect plot between fibers orientation and σ_f. It can be seen that the increase in σ_f due to fibers orientation is in between the increase due to other parameters.

The trend of curves observed in main effect plots and the p-values of N, G, and O terms from ANOVA analysis were in good agreement. The sign of the regression coefficients of the terms N, G, and O also agree with the trend of the σ_f for each parameter. It was also confirmed that the rate of change of σ_f is more due to change in G compared to the change due to other two parameters.

Normal Probability plots

Fig. 4.20(a) shows the plot between normal probability% and residuals generated in the initial ANOVA analysis. This plot determines whether the residuals are normally distributed or not. The condition for regression analysis is that the residuals should be normally distributed. If the residuals are not normally distributed, then the fitted regression model is invalid. In Fig. 4.20(a), it is observed that all the points are falling close to the normal distribution line; therefore, the condition for regression analysis is satisfied. Fig. 4.20(b) shows the plot between normal probability and residuals for the final ANOVA analysis. It can be observed from Fig. 4.20(b) that the points fell slightly away from the normal distribution line. However, the condition that the residuals should be normally distributed is unaltered.

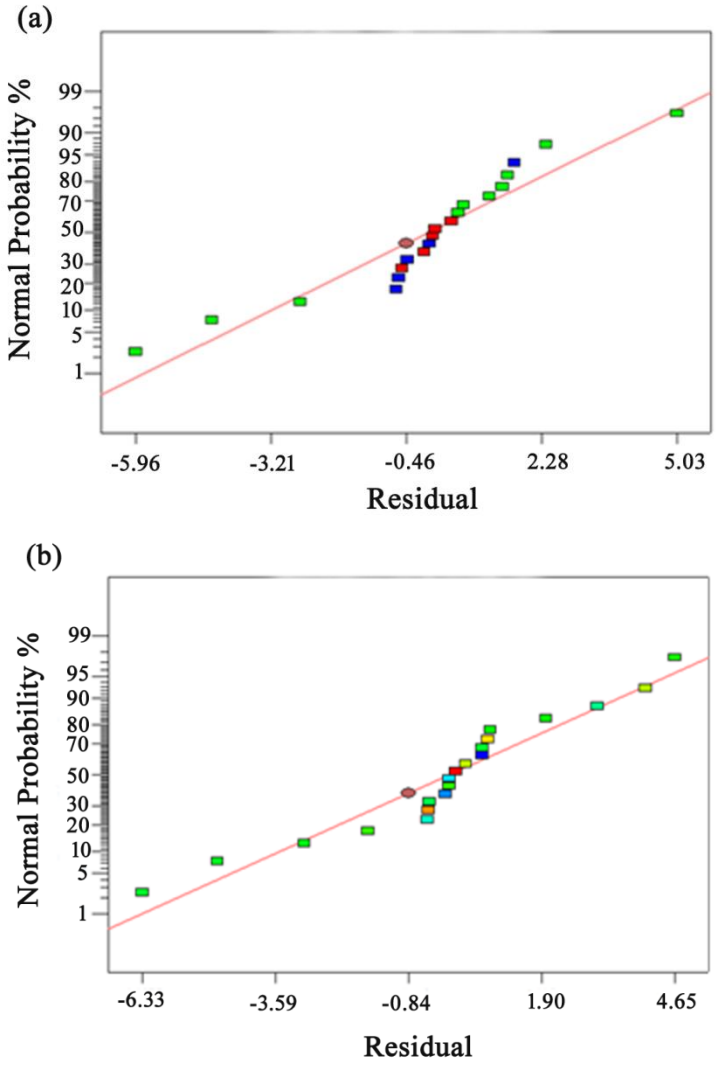

Figure 4.20 Normal probability plots of residuals from (a) initial and (b) final analysis of σ_f

Plots of Residuals vs. predicted values

Figs. 4.21(a) & 4.21(b) show the plots between residuals and fitted σ_f values for the initial and second time repeated ANOVA analyses. From these two figures, it can be observed that the residuals for σ_f in both initial and third time repeated ANOVA analyses are scattered randomly and elimination of the insignificant terms did not affect the random distribution of residuals. Therefore it can be concluded that the fitted model is adequate and there was no proof to suspect that the residuals are dependent.

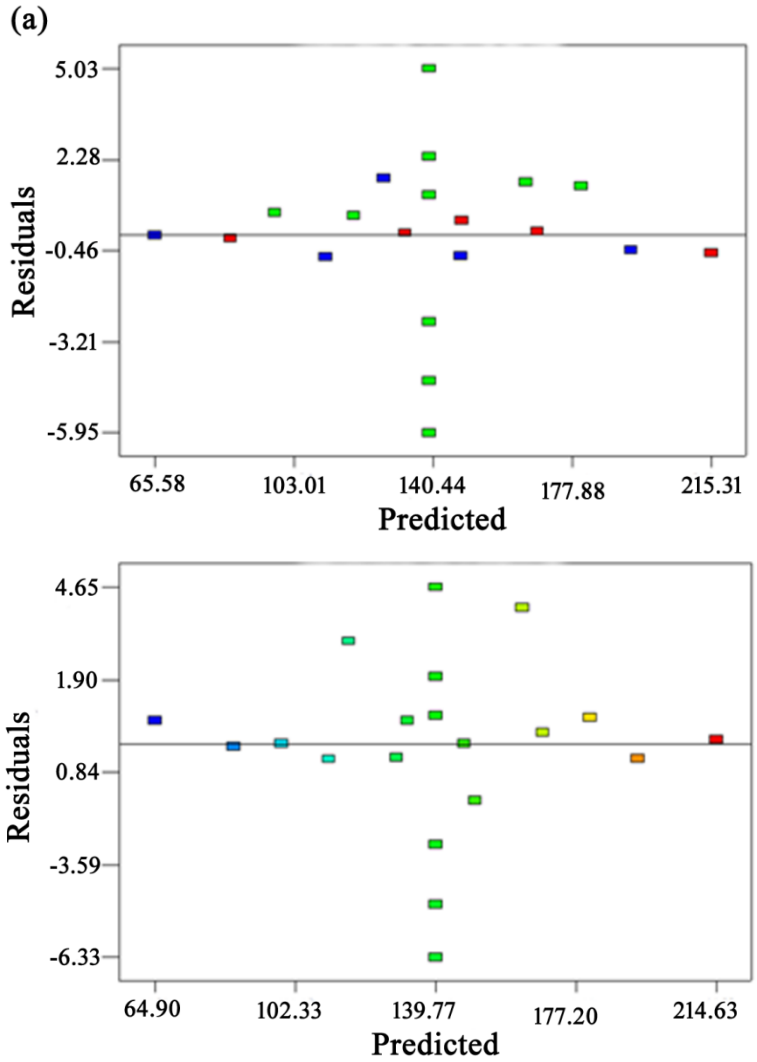

Figure 4.21 Residuals versus predicted values plots for (a) initial analysis of σ_f, (b) final analysis of σ_f

Plots of predicted values vs. actual values

Figs. 4.22(a) & 4.22(b) show the plots between predicted σ_f values and actual values of σ_f. From these graphs, it can be observed that the predicted σ_f values are in good agreement with the actual σ_f values; hence the correlation between σ_f and parameters is satisfactory.

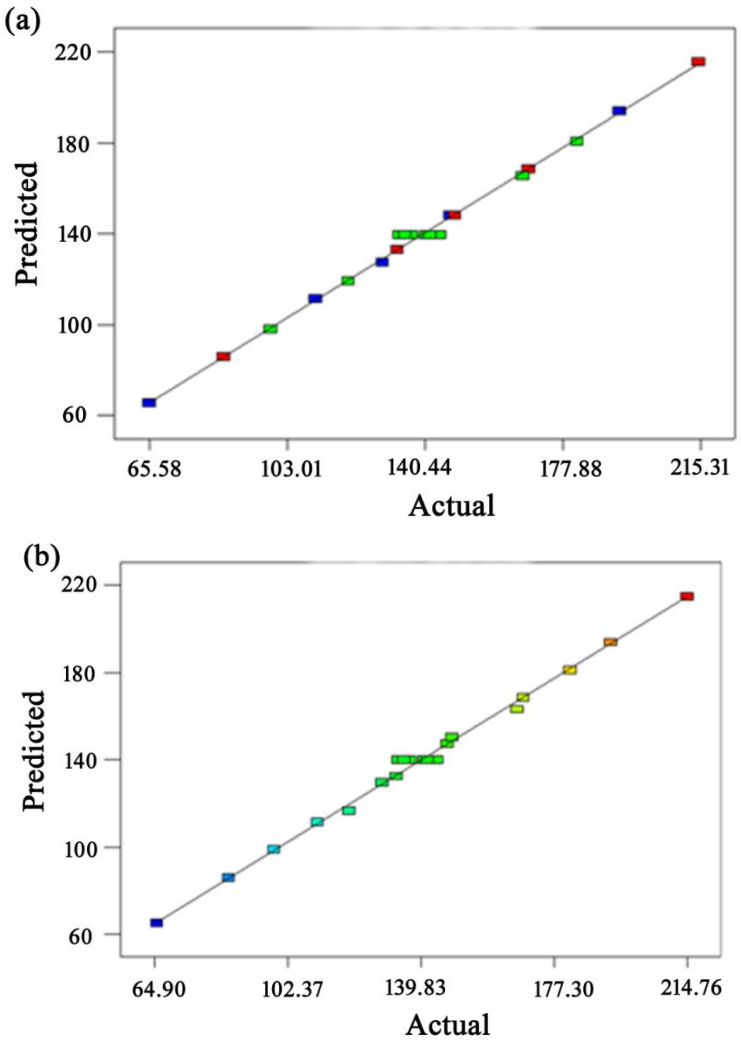

Figure 4.22 Plot of predicted versus observed for σ_f from (a) initial and (b) final analysis

3D Surface plots for σ_f

RSM method generates surface plots to demonstrate the main effects, quadratic effects and interactions between independent parameters. These surface plots are also called as 3D plots and consist of two parameters drawn on x and y directions and the response is drawn on z-axis while the third parameters kept constant.

Effect of nanoclay on σ_f

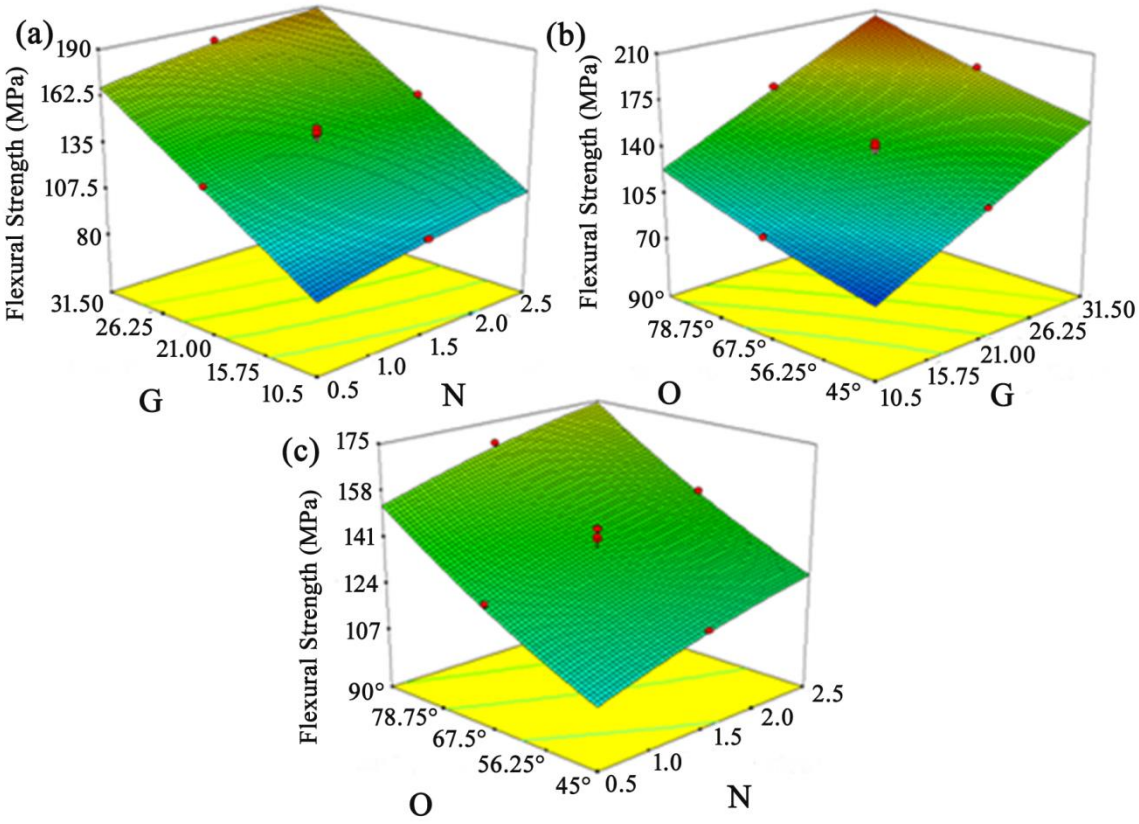

Figure 4.23 3D surface plots for effect of N, G, and O on σ_f

Fig. 4.23(a) displays response surface consisting of two factors N and G on x and y axes while factor O was fixed at 67.5° and σ_f is shown on the z-axis. It can be observed from Fig. 4.23(a) that the σ_f increases slowly with increase in N and increases at a faster rate with increase in G. Fig. 4.23(b) displays a response surface plot consisting of two factors G and O on x and y-axis while factor N was fixed at 1.5 wt% and σ_f is shown on z-axis. It can be observed that σ_f increases at an intermediate rate with increase in O compared to the increase in σ_f due to increase in G and N. Fig. 4.23(c) display response surface plot with two factors N and O on x and y axes while factor G was fixed 21 vol. %.

The maximum value of σ_f obtained in this study is 214.76 MPa which was observed at experiment number 3 in table 4.20 with parameter levels N= 2.5%, G=31.5% and O=0°/90° and the corresponding coded levels are N=+1, G=+1 and O=+1 respectively.

4.3.3 Scanning electron microscopy

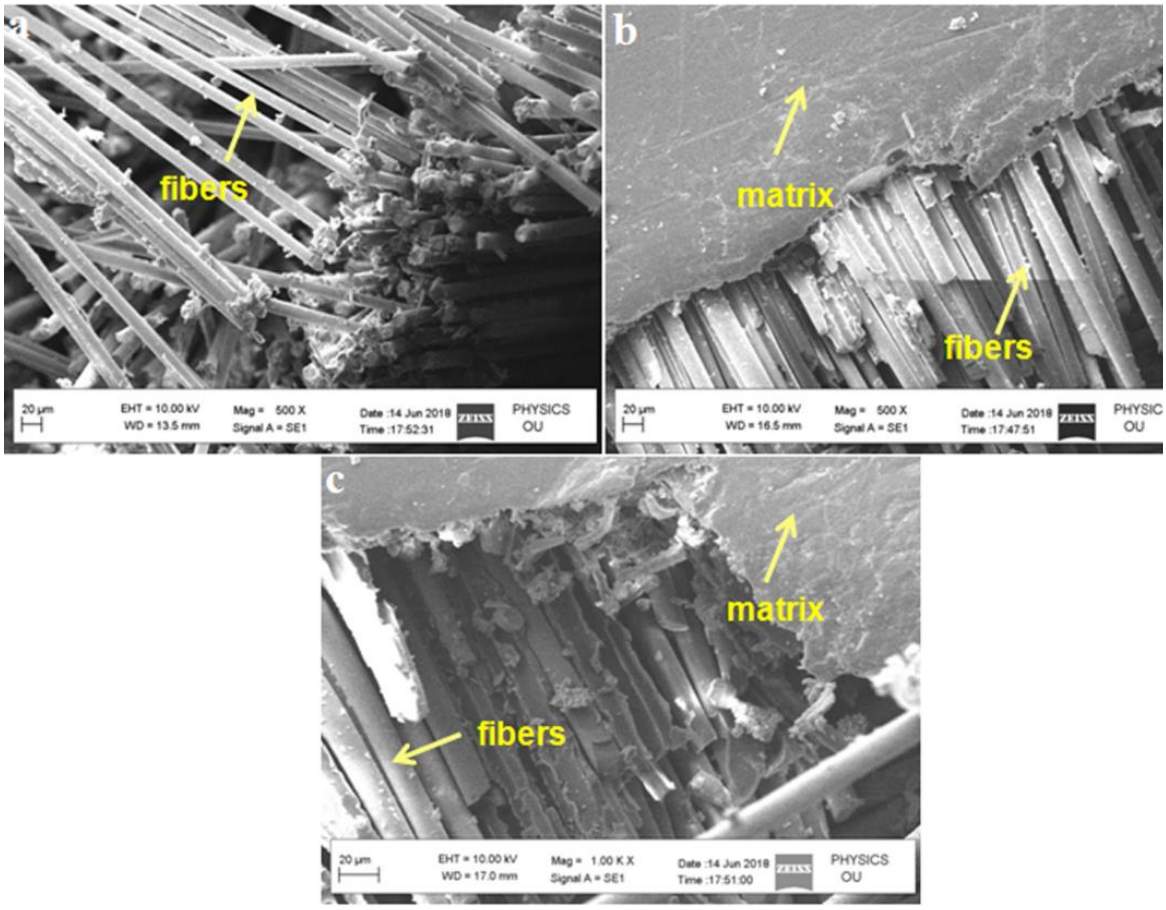

Figure 4.24 Fracture surfaces of EGCN's with nanoclay (a) 0.5 wt%, 10.5 vol%, 45° (b) 1.5 wt% , 21 vol%, 67.5 (d) 2.5 wt%, 31.5 vol%, 90°

The fracture surfaces of EGCN samples shown in Fig. 4.24(b) & 4.24(c) proves that the debonding between fibers and matrix is difficult due to the presence of clay platelets at the interface resisting the movement of epoxy molecules, whereas at 0.5 wt% nanoclay the fibers were well separated which might have resulted due to low content of nanoclay platelets as shown in Fig. 4.24(a). Less energy is required to fail the specimen when a poor distribution of nanoclay is obtained in the composite. The fracture surface of well dispersed nanoclay composites

resembles a ductile failure because in the matrix the crosslinks between epoxy molecules were increased and epoxy molecules hold the fibers firmly at the interface and cracks generated in matrix propagate in a critical manner hence more energy is required to fail the specimen. The fractured specimen shows less fiber pullout because the failure of matrix and fibers occur simultaneously with matrix still present on the fibers after failure as shown in Fig. 4.24(b) &4.24(c).

4.3.4 Summary

In the present study, σ_f of the nanocomposites has been investigated. Glass fiber and nanoclay were reinforced in various proportions and fibers oriented at various angles. Taguchi and RSM methods were used to analyze the data and present the fitted quadratic model for predicting the σ_f. ANOVA analysis done using both methods showed that all three parameters were effectively influencing the σ_f. There are no significant quadratic effects and interaction effects of parameters are identified. The optimized result obtained indicated that the best σ_f obtained was 215.75 MPa and occurred at 2.5 wt% of nanoclay, 31.5 vol% of fiber, and 0°/90° of fibers orientation. The result is confirmed by preparing and testing five samples and the average value of σ_f obtained was 208.43 MPa. The fracture morphology had shown the strong bond between fiber and matrix when nanoclay was added and rough matrix morphology compared neat glass-epoxy because of the restricted cracks propagation in the matrix by the clay platelets.

4.4 Optimization of Plane strain Fracture toughness (K_{IC})

The standard test method for finding flexural properties is ASTM D 5045. The dimensions of the specimen are 70 mm x 16 mm x 4 mm. The test is performed in universal testing machine WDW-100S. The tests were performed with a cross head speed of 10 mm/min. For each test five samples were tested and the average value is taken. For Taguchi method L9 array is selected and central composite design is selected for RSM. Pilot experiments were conducted to identify the effective ranges of parameters. After these ranges are fixed, the experiments were conducted according to Taguchi and RSM designs. The effect of each parameter is quantified using ANOVA and significance of parameter effect is evaluated. A linear model is fitted in Taguchi

method and a quadratic model is fitted in RSM. The R^2 value quantifies the strength of fit each model, respectively. The fracture surface is studied using SEM micrography.

4.4.1 Taguchi Design

K_{IC} of the composites is evaluated for the same L9 orthogonal array selected in section 4.2 and given in table 4.19. The experimental outcomes are transformed into the signal to noise ratio (S/N ratio). Signal means the desired output characteristic, whereas noise means the undesired output characteristic. The S/N ratio indicates the quality characteristic, which implies whether the output desired is maximum or minimum or intermediate. In Taguchi method, three quality characteristics were defined, they are, higher-the-better, lower-the-better, and nominal-the-better. The S/N ratio indicates the variation in the output due to an error where the smaller the variation due to error, the better the output is [129]. As the outcome is flexural strength for which higher the better quality characteristic suits better; hence, S/N ratio characteristic should be selected such that the larger the S/N ratio the better the strength which is calculated using equation (1).

Table 4.19 Experimental design using L9 orthogonal array for K_{IC}

Sl. No	Nanoclay wt.% (N)	Glass Fiber vol. % (G)	Angle (O)	K_{IC} (Mpa-$m^{1/2}$)	S/N Ratio
1.	0.5	10.5	45°	4.47	13.00
2.	0.5	21	67.5°	8.83	18.92
3.	0.5	31.5	90°	11.64	21.32
4.	1.5	10.5	67.5°	7.79	17.83
5.	1.5	21	90°	11.84	21.47
6.	1.5	31.5	45°	9.47	19.53
7.	2.5	10.5	90°	10.05	20.04
8.	2.5	21	45°	9.96	19.96
9.	2.5	31.5	67.5°	13.57	22.65

Mean fracture toughness values and corresponding S/N ratios at each level of each parameter are depicted graphically in Figs. 4.25 & 4.26. These figures show the trend of each

parameter's effect on fracture toughness and Fig. 4.27 shows the residual plots of S/N ratios. The residual plots

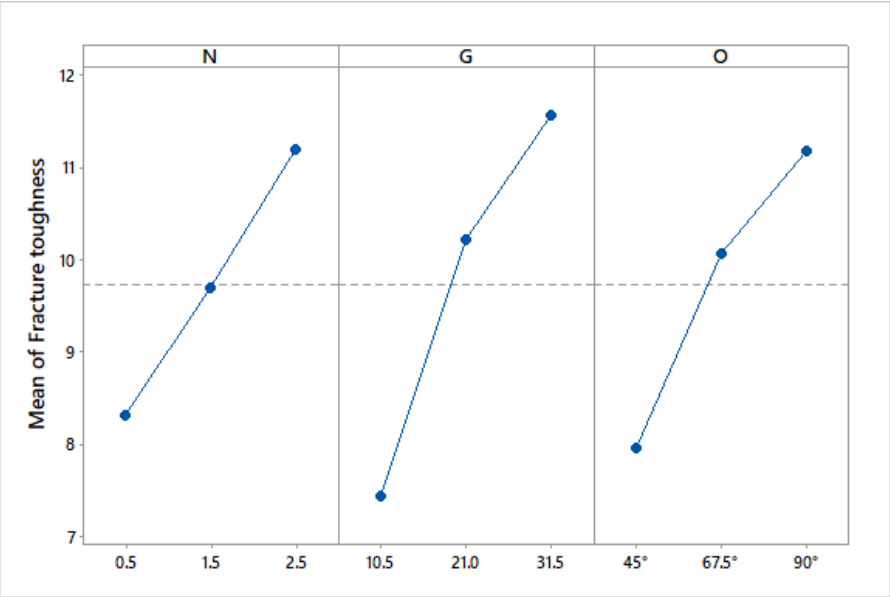

Figure 4.25 Main effect plot for fracture toughness K_{IC}

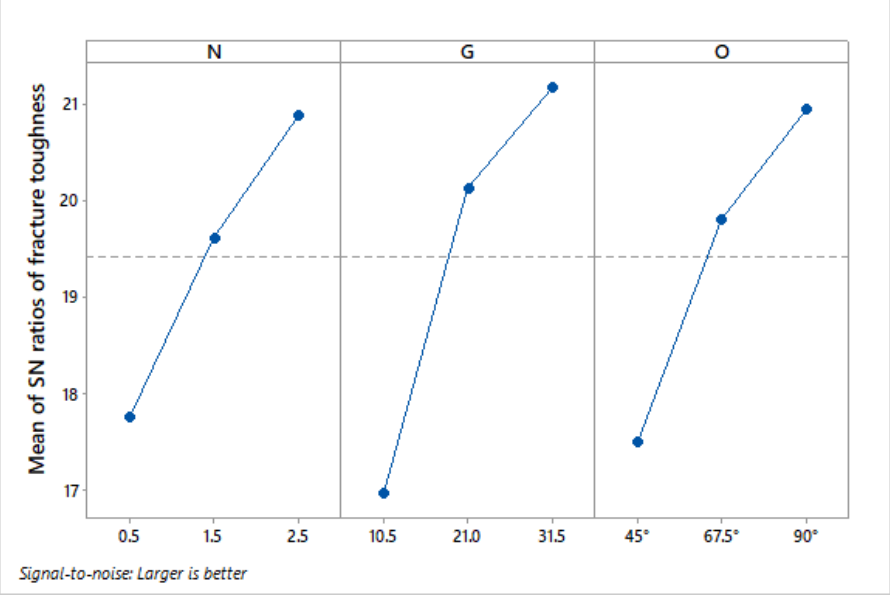

Fig. 4.26 S/N ratio plot for K_{IC}

indicate that the residuals are closer to the normal distribution line, which means the assumption of a normal distribution of residuals is satisfied. Besides, the residual plots also reveal that the residuals are randomly distributed [130].

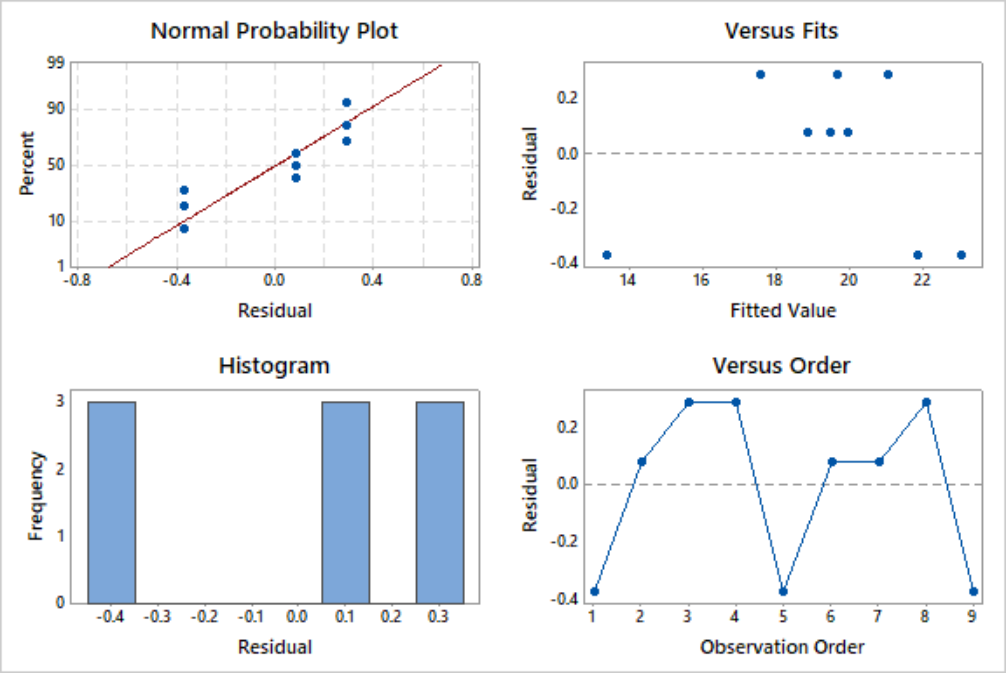

Figure 4.27 Residual Plots for S/N ratios of K_{IC}

ANOVA for Fracture toughness

Table 4.20 is the ANOVA table for S/N ratios of K_{IC} which is produced using Minitab 17 software. The p-value here indicates whether the parameter is significant in influencing the fracture toughness. If the P-value is less than 0.05, it indicates that the null hypothesis is false because the probability that the null hypothesis is true is very low, i.e., <5%. F-value in table 4.20 indicates the ratio between variance due to parameter to variance due to error, and there is an inverse relation between F-value and p-value, which can be observed from table 4.20. The p-values for N, G, and O are 0.044, 0.023, and 0.036 respectively which means the probability that the parameters N, G, and O do not influence the K_{IC} is 4.4%, 2.3%, and 3.6% respectively.

Therefore there is 95.6%, 97.7%, and 96.4% probability that the parameters N, G, and O influence the fracture toughness, respectively. The percentage of contribution values are also significant; hence, all three parameters are showing a significant effect.

Table 4.20. ANOVA table for S/N ratios of K_{IC}.

Source	DF	Seq SS	Contribution	Adj SS	Adj MS	F-Value	P-Value
N (wt %)	2	14.9586	23.78%	14.9586	7.4793	21.81	0.044
G (vol %)	2	28.8045	45.80%	28.8045	14.4022	41.99	0.023
O (deg)	2	18.4447	29.33%	18.4447	9.2223	26.89	0.036
Error	2	0.686	1.09%	0.686	0.343		
Total	8	62.8937	100.00%				

Optimal design for K_{IC}

The optimal setting of parameters is selected based on the trend observed in Fig. 4.25 or Fig. 4.26. In both figures, the set N3, G3, and O3 has the maximum S/N ratio or mean value. Hence, this set of variables is the optimum setting for the maximum fracture toughness. At this set of variables, the optimum values of S/N ratio and K_{IC} were predicted using the equations (10) and (11).

S/N Ratio = 19.416 - 1.668 N1 + 0.196 N2 + 1.472 N3 - 2.456 G1+ 0.704 G2 + 1.753 G3 - 1.914 O1 + 0.386 O2 + 1.528 O3 …….. (10)

= 19.416+ 1.472 + 1.753 + 1.528

= 24.169

Fracture toughness = 9.738 - 1.424 N1 - 0.033 N2+ 1.457 N3 - 2.302 G1+ 0.475 G2 + 1.826 G3- 1.768 O1 + 0.327 O2+ 1.441 O3 ...……. (11)

= 9.738+ 1.457 + 1.826 + 1.441

= 14.462

Confirmation tests for K_{IC}

The predicted value of fracture toughness at optimal conditions is confirmed by performing experiments at those conditions. Five samples were tested and the average K_{IC} and corresponding S/N ratio obtained are 14.28 N/mm^2 and 23.1. The obtained values fall within ±5% of the predicted fracture toughness value and S/N ratio. Hence, the fitted model validates the experimental value.

4.4.2 Response surface methodology

Table 4.21. Experimental design according to CCD and corresponding K_{IC}

Run	Nanoclay wt% (N)	Glass Fiber Volume % (G)	Angle (O)	K_{IC} (MPa-m$^{1/2}$)
1	1.5	31.5	67.5°	11.85
2	1.5	21	45°	8.41
3	2.5	31.5	45°	11.25
4	1.5	21	67.5°	10.29
5	0.5	31.5	45°	8.37
6	2.5	10.5	45°	7.12
7	0.5	21	67.5°	9.06
8	2.5	31.5	90°	14.46
9	1.5	21	67.5°	10.24
10	0.5	31.5	90°	11.87
11	1.5	21	67.5°	10.73
12	0.5	10.5	45°	4.7
13	2.5	21	67.5°	11.99
14	1.5	21	90°	12.07
15	1.5	21	67.5°	10.46
16	1.5	21	67.5°	10.60
17	1.5	21	67.5°	10.5
18	2.5	10.5	90°	10.28
19	0.5	10.5	90°	7.45
20	1.5	10.5	67.5°	8.02

Table 4.21 shows the generated experimental design according to central composite design and the corresponding K_{IC} for each EGCN. The input parameters are nanoclay wt%, glass fiber vol%, and fibers orientation which are indicated in ANOVA tables, 2D, and 3D plots as N, G and O respectively. To evaluate the effect of parameters ANOVA analysis was performed and the confidence level selected is 95%. Based on the p-value, whether the particular parameter is significant or insignificant is evaluated. If the p-value is less than 0.05, it indicates that there is greater than 95% probability that the input parameter affects the K_{IC}. If the p-value is greater than 0.05, it indicates that there is less than 95% probability that the input parameter affect the K_{IC}. If any of the parameters are insignificant, then those parameters should be eliminated and analysis should be repeated with the remaining ones.

ANOVA and regression model for K_{IC}

Tables 4.22 & 4.24 show the ANOVA tables obtained after the first and second step of analysis. Table 4.24 is obtained by eliminating terms that were not effective on K_{IC} after first step. It can be noticed from table 4.22 that the probability values for terms N, G, and O were more than 99%. The terms N*G, N*O, G*O, N*N, G*G, and O*O, are ineffective with P-values greater than 0.05. Moreover, “Lack-of-Fit” of the quadratic model was insignificant as the P-value is 0.97.

Table 4.23 shows the regression coefficients of the model and equation (12) shows the second order polynomial model consisting of all the coefficients of the significant and insignificant terms.

Table 4.22. ANOVA table obtained for K_{IC} in the first step of analysis

Source	Seq SS	DF	Adj MS	F-Value	p-value
Model	90.63148	9	10.07016	232.243	< 0.0001
N	18.63225	1	18.63225	429.7061	< 0.0001
G	40.92529	1	40.92529	943.839	< 0.0001
O	26.50384	1	26.50384	611.2445	< 0.0001
NG	0.00605	1	0.00605	0.139528	0.7165
GO	0.0018	1	0.0018	0.041512	0.8426
NO	0.08	1	0.08	1.844999	0.2042
N*N	0.010664	1	0.010664	0.245943	0.6307
G*G	1.170014	1	1.170014	26.98344	0.0004
C*C	0.331645	1	0.331645	7.64857	0.0199
Residual	0.433605	10	0.04336		
Lack of Fit	0.262805	5	0.052561	1.538668	0.3239
Pure Error	0.1708	5	0.03416		
Total	91.06508	19			

$$\text{Fracture toughness} = -0.58 + 1.45*N + 0.41*G + 0.15*O + 0.00262*N*G + 0.0066*N*O + 0.00042*G*O - 0.062*N^2 - 0.0059*G^2 - 0.00068*O^2 \quad \ldots\ldots\ldots (12)$$

Table 4.23 Regression coefficients of fitted model for fracture toughness in the first step of analysis

Coefficient	b_0	b_1	b_2	b_3	b_{11}	b_{22}	b_{33}	b_{12}
value	-0.58	1.45	0.41	0.15	-0.062	-0.0059	-0.00068	0.00262
Coefficient	b_{13}	b_{23}	R^2 %					
value	0.0066	0.00042	99.52					

The ineffective terms were eliminated and ANOVA analysis was repeated for the remaining terms and the results are given in table 4.24.

Table 4.24. ANOVA table obtained for fracture toughness in the second step of analysis

Source	Seq SS	DF	Adj MS	F-Value	p-value
Model	90.53296	5	18.10659	476.3829	< 0.0001
N	18.63225	1	18.63225	490.2129	< 0.0001
G	40.92529	1	40.92529	1076.741	< 0.0001
O	26.50384	1	26.50384	697.3138	< 0.0001
G*G	1.460701	1	1.460701	38.43093	< 0.0001
O*O	0.439561	1	0.439561	11.56482	0.0043
Residual	0.532119	14	0.038008		
Lack of Fit	0.361319	9	0.040147	1.17525	0.4525
Pure Error	0.1708	5	0.03416		
Total	91.06508	19			

$$\text{Fracture toughness} = -6.5 + 1.365*N + 0.45*G + 0.17*O - 0.006*G^2 - 0.0007*O^2 \quad \ldots\ldots\ldots \quad (13)$$

Equation (13) is a reduced second order polynomial comprising of the final coefficients of the significant terms and table 4.25 shows regression coefficients obtained after the second step of analysis.

Table 4.25. Regression coefficients of fitted model for fracture toughness obtained after second step

Coefficient	b_0	b_1	b_2	b_3	b_{22}	b_{33}	R^2 %
Fracture toughness	-6.5	1.365	0.45	0.17	-0.006	-0.0007	99.42

It should be noticed that the square term of the factor N is not effective and there are no significant interactions. Moreover, the coefficient of determination (R^2) for first and second steps of analysis is shown in table 4.23 and table 4.25, respectively. R^2 is the strength of fit of the model or the nearness of the fitted values to the experimentally obtained values. R^2 values are 99.52% and 99.42% for fitted models in the first and final step of analysis respectively. These high values of R^2 also indicate that the regressor terms in the model not only explain the total

variability of the response but also give the good estimation of response in the ranges of parameters selected.

Main effect plots

Figs. 4.28(a)-4.28(c) display the main effect plot of factors N, G, and O. These plots show the effect of first-order terms N, G, and O on the response. Fig. 4.28(a) shows that the magnitude of K_{IC} undergoes obvious change with increase in nanoclay wt%. Fig. 4.28(b) shows that the K_{IC}

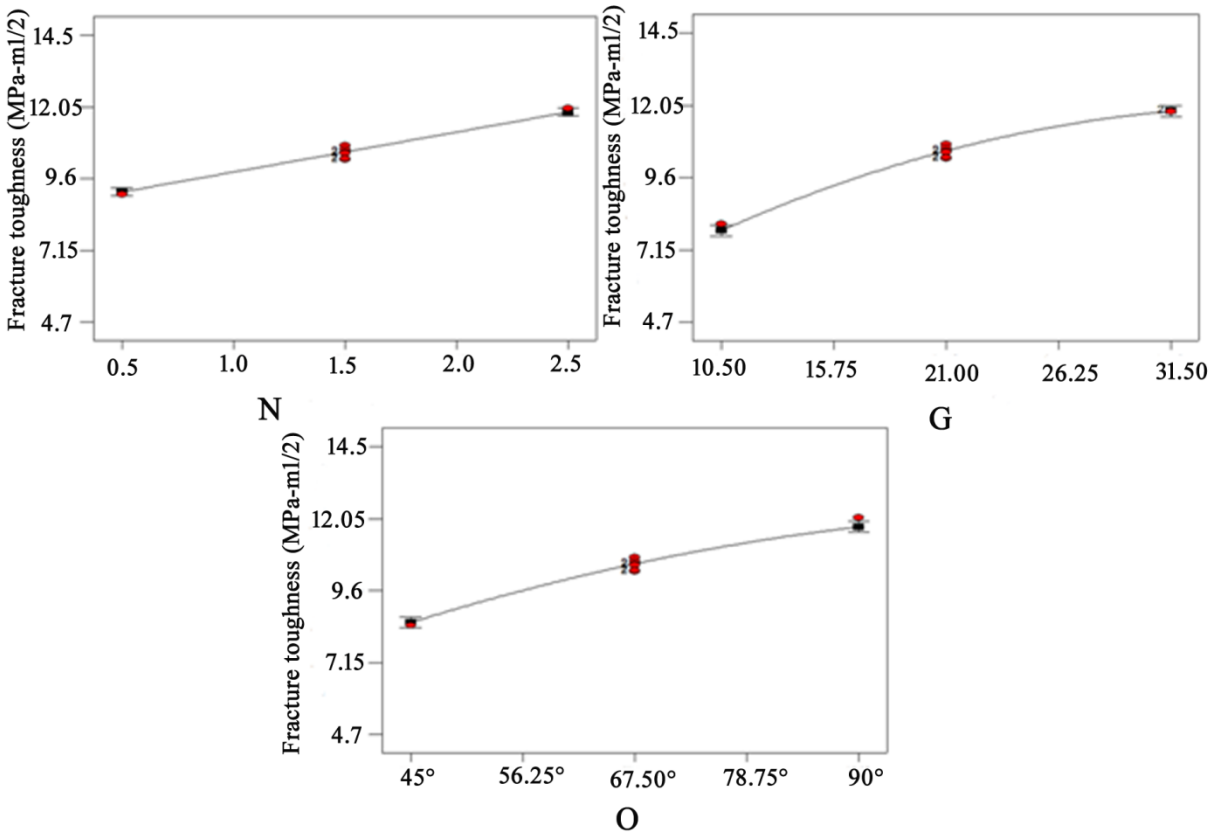

Figure 4.28 Main effect plots of factors (a) N, (b) G, and (c) O on fracture toughness

increases substantially with increase in magnitude of fiber volume. It is also evident that the rate of increase in K_{IC} due to fiber volume is more compared to the rate of increase due to nanoclay wt%. Fig. 4.28(c) gives the main effect plot between O and fracture toughness. It can be noticed that the K_{IC} increases while the angle of fibers changes from 45° to 90° and this rate of increase is similar compared to the rate of increase due to and glass fiber volume.

The trend of curves in the main effect plots and the p-values of first order terms in the ANOVA table are in good agreement with each other. The sign of the regression coefficients also agrees with the trend of the fracture toughness for each parameter. It was also confirmed that the rate of change of fracture toughness is more due to change G compared to the other two parameters.

Normal Probability plots

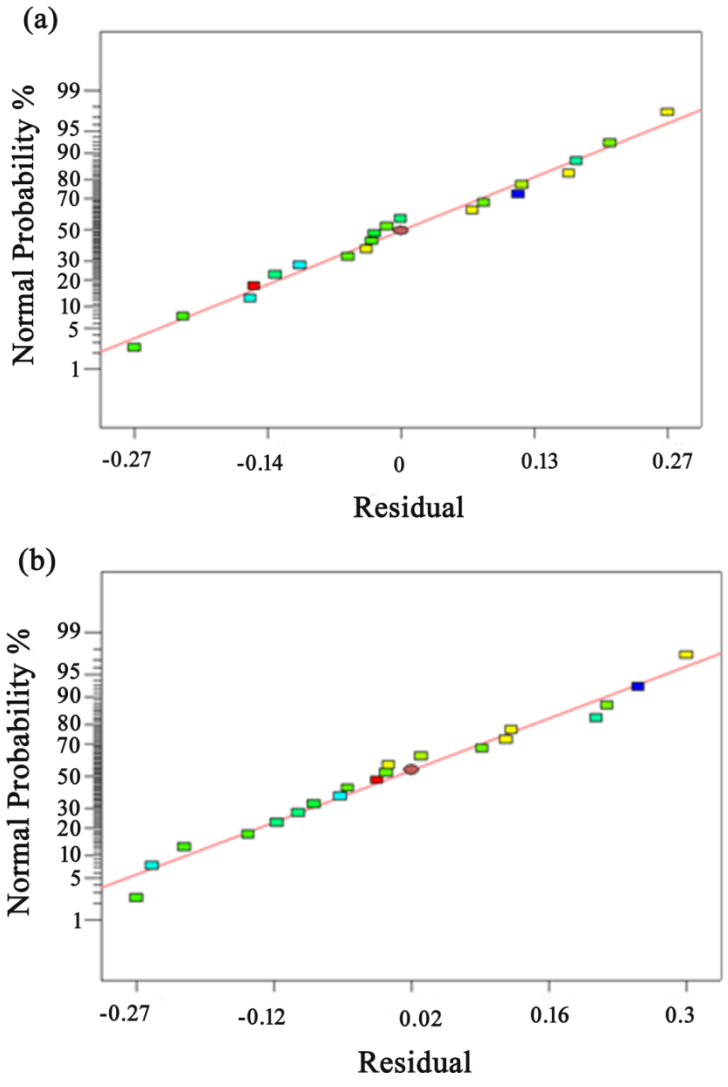

Figure 4.29 Normal probability plots of residuals from (a) initial and (b) final analysis of fracture toughness

Fig. 4.29(a) shows the plot between normal probability and residuals generated in the first step of the ANOVA analysis. This plot determines whether the residuals are normally distributed or not. The condition for regression analysis is that the residuals should be normally distributed. If the residuals are not normally distributed, then the fitted regression model is invalid. In Fig. 4.29(a) all the points are falling closer to the normal distribution line; therefore, the condition for regression analysis is satisfied. Fig. 4.29(b) shows the plot between normal probability and residuals for the final analysis and it can be observed that the points fell slightly closer to the normal distribution line. Therefore, the condition that the residuals should be normally distributed is satisfied.

Plots of Residuals vs. predicted values

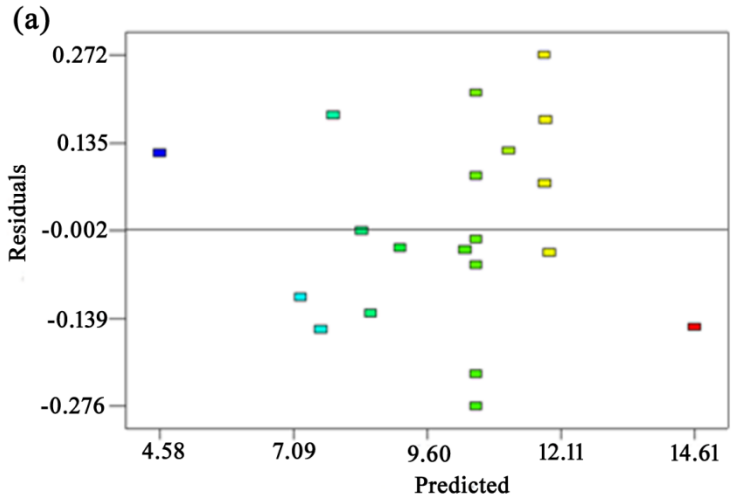

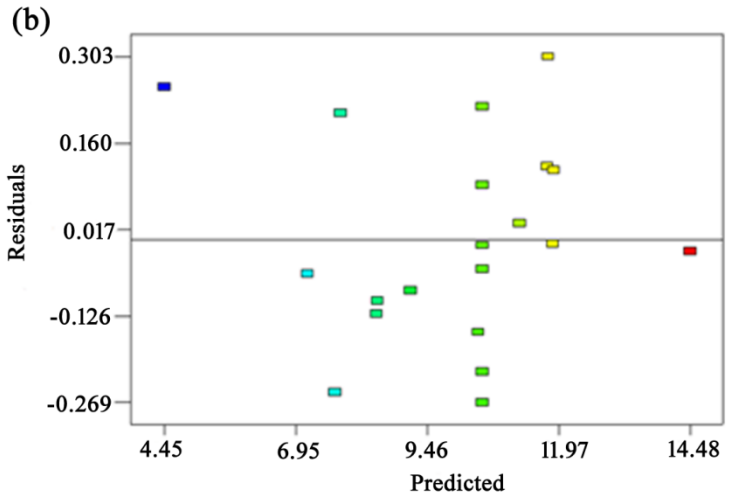

Figure 4.30 Residuals versus predicted values plots for (a) initial analysis of fracture toughness, (b) final analysis of fracture toughness

Figs. 4.30(a) & 4.30(b) show the plots between residuals and fitted fracture toughness values for the first and second step of ANOVA analysis. From these two figures, it can be observed that the residuals for fracture toughness in both first and third step of analysis were scattered randomly and elimination of the insignificant terms did not affect the random distribution of residuals because both figures show the random distribution of residuals. Therefore it can be concluded that the fitted model is adequate and there was no proof to suspect that the residuals are dependent.

Plots of predicted values vs. actual values

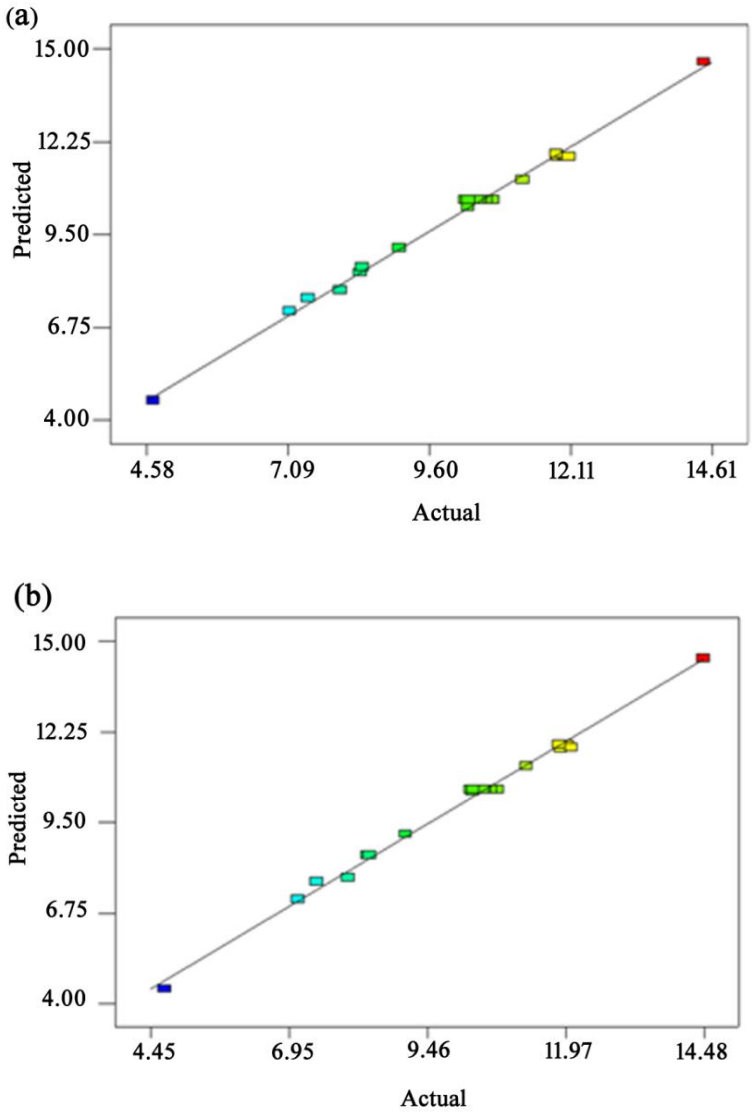

Figure 4.31 Plot of predicted versus observed for fracture toughness from (a) initial and (b) final analysis

Figs. 4.31(a) & 4.31(b) show the plots between predicted fracture toughness values and actual values of fracture toughness. From these graphs, it can be seen that the predicted fracture toughness values are in good agreement with the actual fracture toughness values, hence the correlation between fracture toughness and parameters is satisfactory.

3D Surface plots for fracture toughness

RSM method generates surface plots to demonstrate the main effects, quadratic effects and interactions between independent parameters. These surface plots also called as 3D plots and these plots consist of two parameters drawn on x and y directions and the response on z-axis while the third parameters kept constant.

Effect of nanoclay on fracture toughness

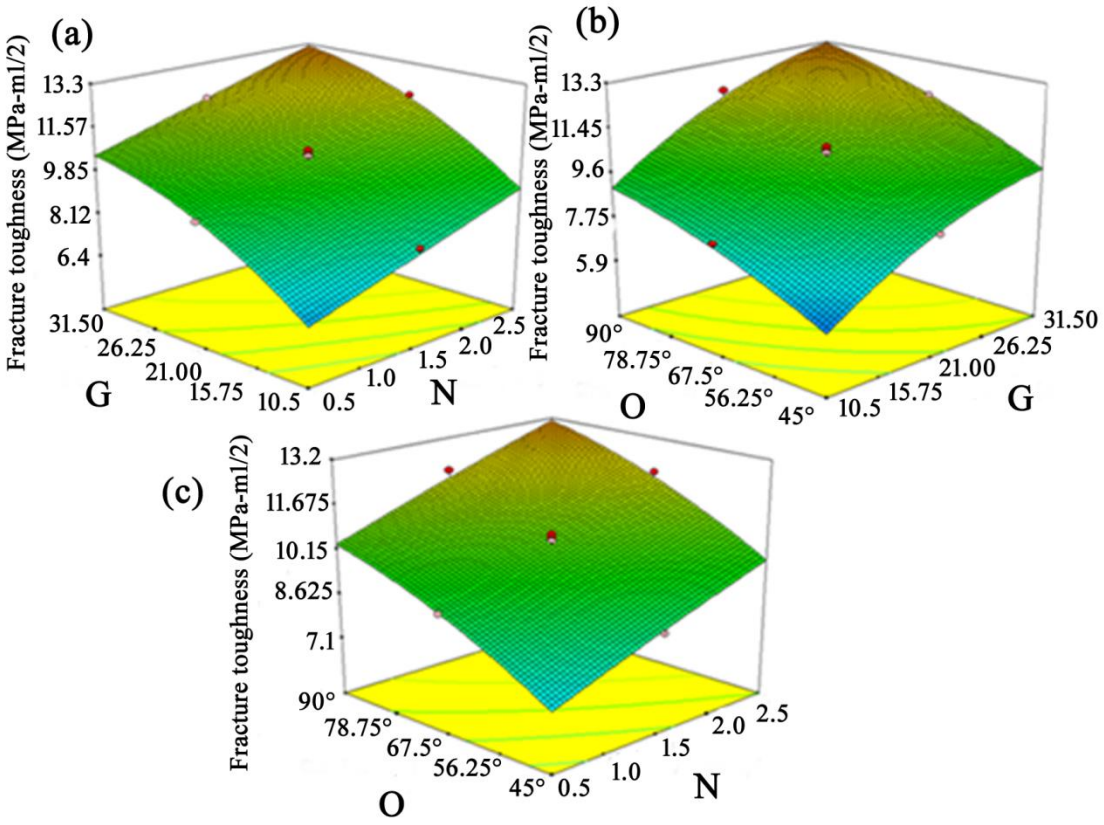

Figure 4.32 3D surface plots for effect of N, G, and O on fracture toughness

Fig. 4.32(a) displays response surface consisting of two factors N and G on x and y axes while factor O was fixed at 67.5° and K_{IC} is shown on z-axis. It can be observed that K_{IC} increases slowly with increase in N and increases at a faster rate with increase in G. Fig. 4.32(b) displays a response surface plot consisting of two factors G and O on x and y axes while factor N

was fixed at 1.5 wt% and K_{IC} is shown on the z-axis. It can be observed that K_{IC} increases at an intermediate rate with increase in O compared to the rate of increase in plane strain fracture toughness due to G and N. Fig. 4.32(c) display response surface plot consisting of two factors N and O on x and y axes while factor G was fixed 21 vol. %.

Maximum value of K_{IC} obtained in this study is 14.46 MPa-$m^{1/2}$ which was observed at parameter levels N= 2.5%, G=31.5% and O=0°/90° and the corresponding coded levels are N=+1, G=+1 and O=+1 respectively.

4.4.3 Scanning electron microscopy

The fracture surfaces of EGCN samples shown in Fig. 4.33(b) & 4.33(c) proves that the debonding between fibers and matrix is difficult due to the presence of clay platelets at the interface resisting the matrix-fiber debonding. Fig. 4.33(a) shows EGCN at 0.5 wt% addition of nanoclay, the fibers are slightly separated which might have resulted due to the low content of nanoclay platelets resulting in the poor crosslinked matrix thereby nonuniform load distribution between fibers. Less energy is required to fail the specimen when a poor distribution is obtained in the composite. The fracture surface of EGCNs in which nanoclay is well dispersed resembles a ductile failure because within the matrix the epoxy molecules were well bonded and hold the fibers firmly in place; hence, increased load distribution between fibers and the cracks generated in the matrix propagate in a critical manner due to nanoclay. Therfore, more energy is required to fail the specimen. The fractured specimen shows less fiber pullout because the failure of matrix and fibers occur simultaneously with the matrix still present on the fibers after failure as shown in Fig. 4.33(b) & 4.33(c).

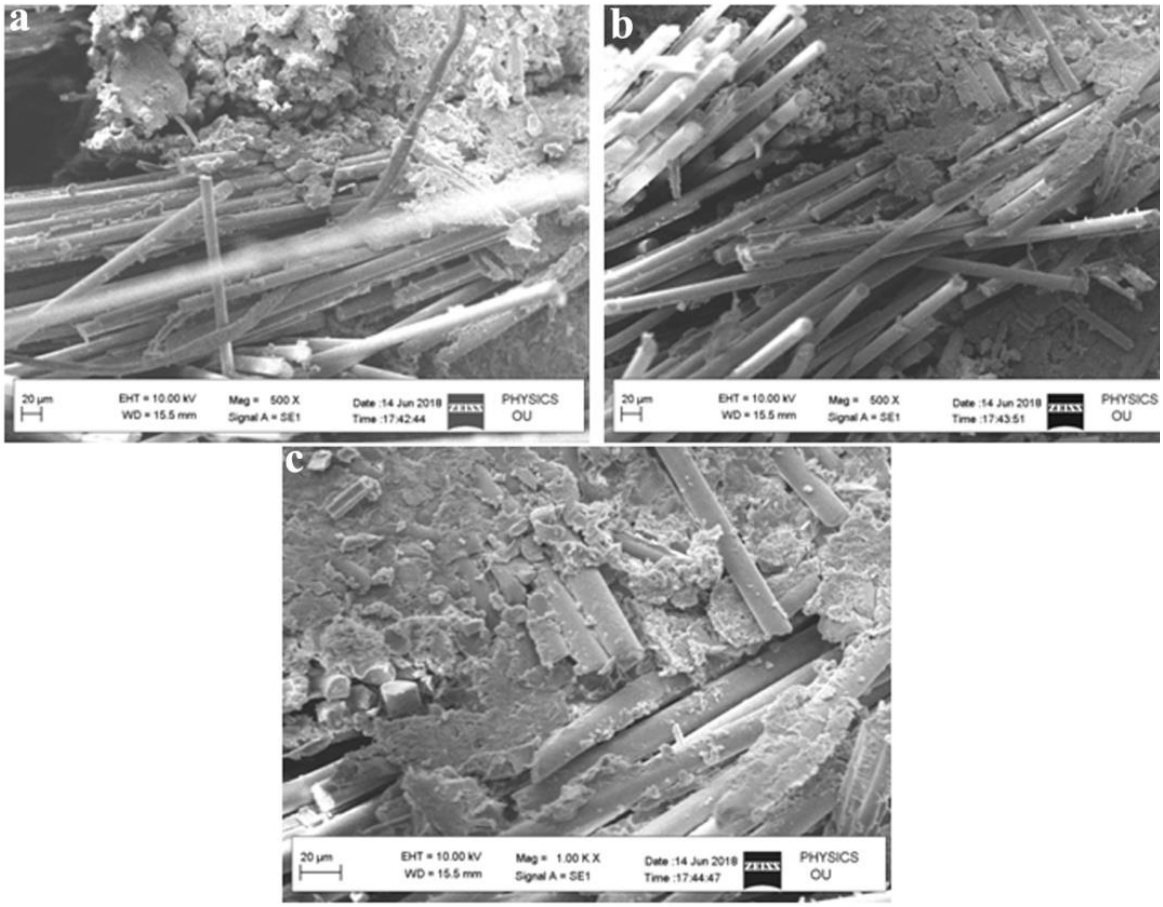

Figure 4.33 Fracture surfaces of EGCN's with nanoclay (a) 0.5 wt%, 10.5 vol%, 45° (b) 1.5 wt% , 21 vol%, 67.5 (d) 2.5 wt%, 31.5 vol%, 90°

4.4.4 Summary

In the present study, K_{IC} of the nanocomposites has been investigated. Glass fiber and nanoclay were reinforced in various proportions and fibers oriented at various angles. Taguchi and RSM methods were used to analyze the data and present the fitted quadratic model for predicting the K_{IC}. ANOVA analysis done using both methods showed that all three parameters were effectively influencing the K_{IC}. Glass fiber volume and fiber orientation have shown quadratic effect and nanoclay content did not have quadratic effect. There are no interactions of parameters were observed. The optimized result obtained indicated that the best K_{IC} was 14.48 MPa-$m^{1/2}$ and occurred at 2.5 wt% of nanoclay, 31.5 vol% of fiber, and 0°/90° of fibers orientation. The result is confirmed by preparing and testing five samples and the average value

of σ_f obtained was 14.26 MPa-$m^{1/2}$. The fracture morphology had shown the strong bond between fiber and matrix when nanoclay was added. The matrix morphology of EGCN is rough because of the restricted crack propagations in the matrix by the clay platelets, whereas GRE has shown smooth morphology.

4.5 Optimization of Microhardness

The standard test method for finding microhardness is ASTM E 384. The dimensions of the specimen are 5 mm x 5 mm x 4 mm. The hardness test is performed using Shimadzu HMV-G20ST instrument. A diamond indenter of a pyramid shape with a square base consisting of 136° between opposite faces is pressed into the material surface under a load of 500 gms. For Taguchi method L9 array is selected and a central composite design is selected from RSM. The experiments were conducted according to Taguchi and RSM designs. The effect of each parameter is quantified using ANOVA. A linear model is fitted in Taguchi method and a quadratic model is fitted in RSM method. The R^2 value quantifies the strength of fit.

4.5.1 Taguchi Design

Taguchi method transforms the responses into the S/N ratios, which are classified into three types, namely, higher-the-better, lower-the-better, and nominal-the-better. In the present study, for optimizing microhardness, higher-the-better S/N ratio suits well as the desired hardness should be as high as possible. Increase in S/N ratio implies the response also has increased. S/N ratio for the selected quality characteristic is calculated using equation (1).

From Table 4.1, for given three parameters and each with three levels, the suitable orthogonal array available in the Taguchi method is L9. The L9 experimental design is shown in Table 4.26 with obtained microhardness values and S/N ratios.

Table 4.26 L9 experimental design for microhardness

Expt. No.	Nanoclay wt.% (N)	Glass Fiber vol. % (G)	Angle (O)	Microhardness (HV)	S/N ratio
1.	0.5	10.50	45°	16.9	24.56
2.	0.5	21	67.5°	18.8	25.48
3.	0.5	31.50	90°	20.1	26.06
4.	1.5	10.50	67.5°	20.7	26.32
5.	1.5	21	90°	20.8	26.36
6.	1.5	31.50	45°	21.3	26.56
7.	2.5	10.50	90°	22.0	26.85
8.	2.5	21	45°	23.0	27.23
9.	2.5	31.50	67.5°	26.7	28.53

Figure 4.34 & Table 4.27 demonstrate the S/N ratio plots and ANOVA results of S/N ratios. The parameters N, G had a significant effect on microhardness, and parameter O is insignificant. The maximum hardness is observed at a set of parameters N3G3O1 from the S/N ratio plot. Since the orientation *C* did not affect, 0˚ is chosen arbitrarily for the prediction of the optimum value of hardness. Equation. (2) is used to calculate the estimated optimum S/N ratio.

From Figure 4.34 it can be observed that with an increase in nanoclay content (N) and glass fiber content (G) the hardness is increased, whereas the orientation of the fibers in the composite (O) shows negligible effect. ANOVA Table 4.27 corroborates the results observed from S/N ratio plot. When the indenter is pressed on the composite surface, it exerts compressive stress resulting in compaction of clay particles and glass fiber to the epoxy. Thus, the load is transferred effectively below the specimen surface resulting in enhancement in hardness of the composite [132]. The effect of fiber content on hardness may be described as follows: increase in fiber volume decreases the volume of matrix correspondingly and fiber-matrix interface become close to the indenter, whereby the hardness is increased. The same phenomenon was reported by Mahapatra et al. [133]. The negligible effect of fibers orientation is attributed to the fact that increase or decrease in hardness is based on the load transferred by the matrix which is applied by the indenter and the orientation of fibers does not affect this phenomenon. If the fibers orientation

is causing changes in hardness, it can only be imputed to the discontinuity of fibers on the surface making the interface of fiber-matrix located at uneven depths from the surface and the load applied by the indenter has also become uneven. The same phenomenon was reported by Alomayri et al. [134].

Table 4.27 ANOVA table for S/N ratios of microhardness

Source	**DF**	**Seq SS**	**Percentage Contribution**	**Adj SS**	**Adj MS**	**F-Value**	**P-Value**
N	2	7.062	72.04%	7.0626	3.531	75	0.013
G	2	1.997	20.37%	1.997	0.998	21.21	0.045
O	2	0.649	6.63%	0.649	0.3249	6.9	0.127
Error	2	0.094	0.96%	0.094	0.047		
Total	8	9.804	100.00%				

Microhardness = 21.144- 2.544N1- 0.211N2+ 2.756 N3 - 1.278 G1 - 0.278 G2 + 1.556 G3
- 0.744 O1 + 0.922 O2 - 0.178 O3 ……..(14)

= 21.144+ 2.756 + 1.556 + 0.922

= 26.38 HV

S/N Ratio = 26.4407 - 1.072 A1 - 0.025 A2 + 1.097 A3 - 0.532 B1- 0.081 B2
+ 0.613 B3 - 0.321 C1 + 0.337 C2 - 0.016 C3 …….. (15)

= 26.4407+ 1.097 + 0.613 + 0.337

= 28.48 HV

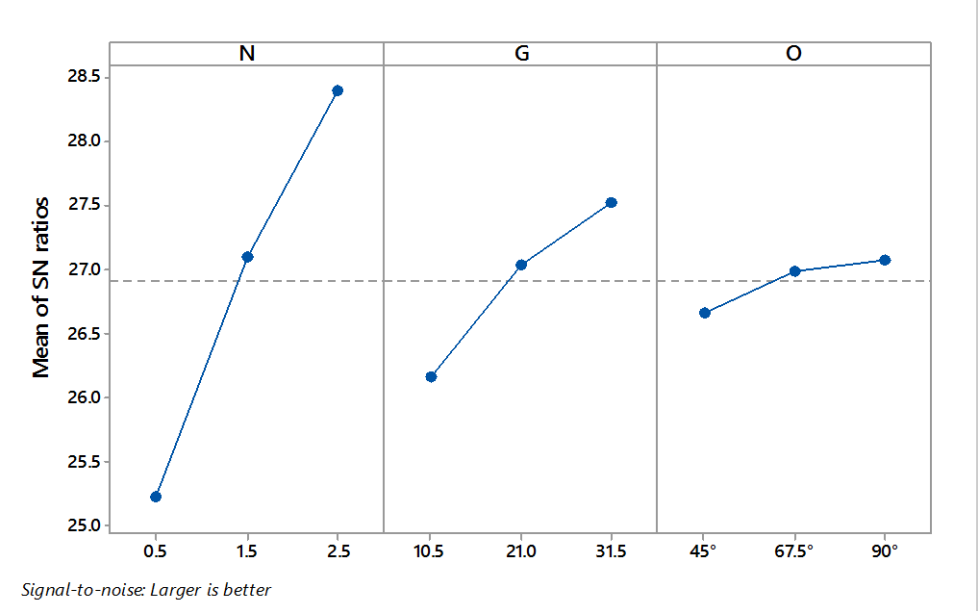

Figure 4.34 Plots of control factors vs. mean S/N ratios of microhardness

Equations (14) and (15) are the general linear models, generated by doing ANOVA analysis using MINITAB software. The optimized value of hardness is 26.38 HV and corresponding experimental value is 27.23 HV, shown in table 4.28. A comparison was made among the optimum value of hardness obtained for EGCN, hardness of neat epoxy, and also the hardness of GRE. The microhardness numbers at the conditions mentioned above were evaluated experimentally and obtained as 12 HV and 17.4 HV. The improvement in hardness at N3G3O1 is 127%, 56%.

Table 4.28 Results at the optimum conditions

	Optimal Control factors	
	Predicted	**Experimental**
Level	N3G3O1	N3G3O1
S/N ratio	28.48	28.69 ± 0.2
Microhardness (HV)	26.38	27.23 ± 0.63

4.5.2 Response surface methodology

Table 4.29 Experimental design according to CCD for microhardness

Run	Nanoclay wt% (N)	Glass Fiber Volume % (G)	Angle (O)	Microhardness (HV)
1	2.5	31.5	45°	24.7
2	1.5	21	45°	19.9
3	1.5	21	67.5°	21.1
4	1.5	21	67.5°	20.9
5	2.5	31.5	90°	25.2
6	1.5	21	67.5°	21.5
7	2.5	10.5	90°	22
8	1.5	31.5	67.5°	23.4
9	1.5	21	67.5°	21
10	1.5	21	90°	20.8
11	1.5	10.5	67.5°	20.7
12	0.5	31.5	45°	19.4
13	2.5	10.5	45°	21.8
14	0.5	10.5	45°	16.9
15	0.5	21	67.5°	18.8
16	1.5	21	67.5°	21.2
17	2.5	21	67.5°	24.5
18	1.5	21	67.5°	21.8
19	0.5	10.5	90°	17
20	0.5	31.5	90°	20.1

Table 4.29 gives the generated experimental design according to central composite design and the corresponding microhardness for each test. To evaluate the effect of the input parameters N, G, and O on microhardness ANOVA analysis was performed and confidence level is selected as 95%. Based on the p-value, it is evaluated whether the parameter is significant or insignificant. If the p-value is less than 0.05, it indicates greater than 95% probability that the input parameter has an effect on microhardness. If the p-value is greater than 0.05, it indicates less than 95% probability that the input parameter affects microhardness. If the parameters are insignificant, then those parameters or terms should be eliminated and analysis should be repeated.

ANOVA and regression model for microhardness

Tables 4.30 & 4.32 show the ANOVA tables obtained after the initial and second step of analysis. Table 4.32 is obtained by eliminating terms that were not effective after the first step. It can be noticed from table 4.30 that the probability values for terms N, G, and O were more than 99%. The terms N*G, N*O, G*O, and N*N, are ineffective with P-values greater than 0.05, whereas, G*G and O*O are effective. Moreover, "Lack-of-Fit" of the quadratic model was insignificant as the P-value is 0.56.

Table 4.30 ANOVA table obtained for microhardness after the first step of analysis

Source	Seq SS	DF	Adj MS	F-Value	p-value
Model	92.86098	9	10.31789	96.925	< 0.0001
N	67.6	1	67.6	635.0264	< 0.0001
G	20.736	1	20.736	194.7915	< 0.0001
O	0.576	1	0.576	5.410876	0.0423
NG	0.03125	1	0.03125	0.293559	0.5998
GO	0.00125	1	0.00125	0.011742	0.9159
NO	0.10125	1	0.10125	0.95113	0.3524
N*N	0.069602	1	0.069602	0.653835	0.4376
G*G	0.859602	1	0.859602	8.075002	0.0175
O*O	3.579602	1	3.579602	33.62636	0.0002
Residual	1.064523	10	0.106452		
Lack of Fit	0.489523	5	0.097905	0.851344	0.5679
Pure Error	0.575	5	0.115		
Total	93.9255	19			

Table 4.31 shows the regression coefficients of the model and equation (16) shows the second order polynomial model consisting of all the coefficients of the significant and insignificant terms.

Microhardness = 6.97 + 2.035*N - 0.117*G + 0.3*O + 0.006*N*G - 0.00055*N*O + 0.000476*G*O + 0.159*N* N + 0.0051*G* G - 0.0022*O* O ..... (16)

Table 4.31 Regression coefficient of fitted model for microhardness obtained after first step of analysis

Coefficient	b_0	b_1	b_2	b_3	b_{11}	b_{22}	b_{33}	b_{12}
Microhardness	6.97	2.035	-0.117	0.3	0.159	0.0051	-0.0022	0.006
Coefficient	b_{13}	b_{23}	R^2 %					
Microhardness	0.00055	0.000476	98.87					

The ineffective terms were eliminated and ANOVA analysis was repeated for the remaining terms and the results are given in table 4.32. The fitness of the model was slightly decreased because there was a slight decrease in a p-value for the term "Lack- of- Fit" but still indicates an insignificant effect.

Table 4.32 ANOVA table obtained for microhardness after second step of analysis

Source	Seq SS	DF	Adj MS	F-Value	p-value
Model	92.66	5	18.53	204.63	< 0.0001
N	67.6	1	67.6	746.45	< 0.0001
G	20.74	1	20.74	228.97	< 0.0001
O	0.58	1	0.58	6.36	0.0244
G* G	1.23	1	1.23	13.53	0.0025
O* O	3.74	1	3.74	41.31	< 0.0001
Residual	1.27	14	0.091		
Lack of Fit	0.69	9	0.077	0.67	0.7172
Pure Error	0.58	5	0.12		
Total	93.93	19			

$$\text{Microhardness} = 6.61 + 2.6*N - 0.098*G + 0.299*O + 0.0056* G^2 - 0.0021* O^2 \quad \ldots\ldots (17)$$

Table 4.33 shows regression coefficients obtained after the third step of analysis and equation (17) is a reduced second order polynomial comprising of the final coefficients of the significant terms. It should be noticed that squares of the factors N, G, and O are not effective on microhardness and there are no significant interactions. Moreover, the coefficient of determination (R^2) obtained in both steps of ANOVA analysis are given in table 4.31 and table

Table 4.33 Regression coefficients of fitted model obtained after third step of analysis

Coefficient	b_0	b_1	b_2	b_3	b_{22}	b_{33}	R^2 %
Microhardness	6.61	2.6	-0.098	0.299	0.0056	-0.0021	98.65

4.33. R^2 is the strength of fit of the model or the nearness of the fitted values to the experimentally obtained values. In tables 4.31 & 4.33, the R^2 values are given as 98.87% and 98.65% for fitted models in the first and final step of analysis respectively. These high values for R^2 also indicate that the regressor term in the model not only explains the total variability of the response but also give a good estimation of response in the ranges of parameters selected.

Main effect plots

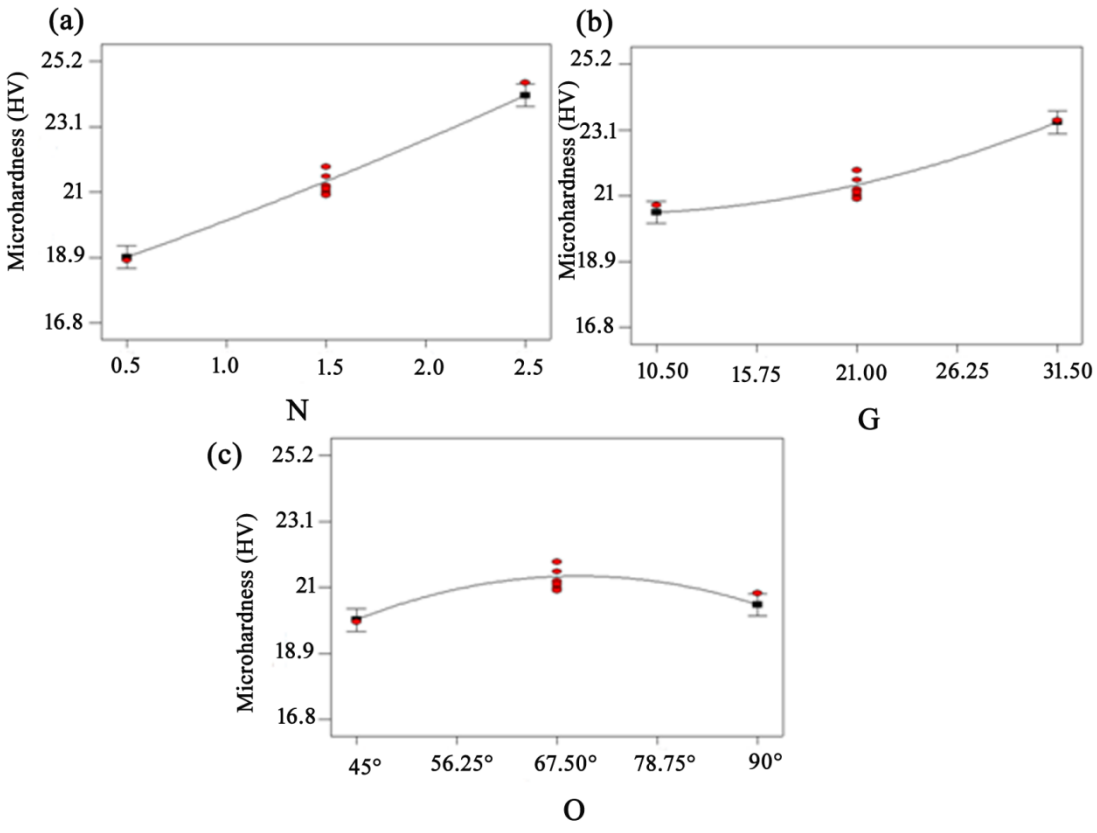

Figure 4.35 Main effect plots of factor (a) N, (b) G, and (c) O on microhardness

Figs. 4.35(a)-4.35(c) display the main effect plots of factors N, G, and O. These plots show the effect of first order terms N, G, and O on the response microhardness. Fig. 4.35(a) shows that the microhardness values of EGCNs undergo obvious change with increase in nanoclay content and glass fiber content. Fig. 4.35(b) shows that the microhardness increases substantially as the nanoclay content increases. However, it is evident that the rate of increase in microhardness due to nanoclay addition is more compared to the rate of increase microhardness due to glass fiber addition. Fig. 4.35(c) gives the main effect plot in between O and microhardness. It can be seen that the microhardness has slightly increased at 67.5° and remained same at 45° and 90°. This effect of fibers orientation on microhardness is imputed to the discontinuity of fibers on the surface making the interface of fiber-matrix located at uneven depths from the surface and the load applied by the indenter has also become uneven resulting in erroneous values. The same phenomenon was reported by Alomayri et al. [134]. The trend of curves in main effect plots and the p-values of first order terms from ANOVA results were in good agreement with each other. It was also confirmed that the rate of change of microhardness is more due to change in N compared to the change in the remaining two parameters.

Normal Probability plots

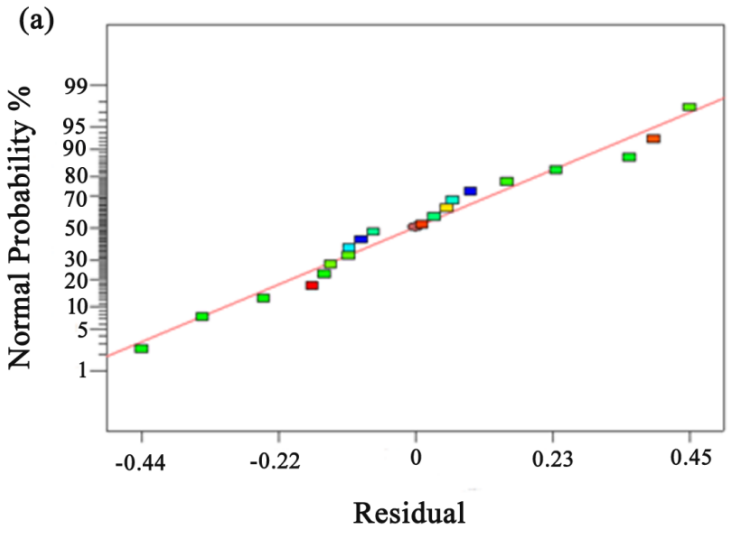

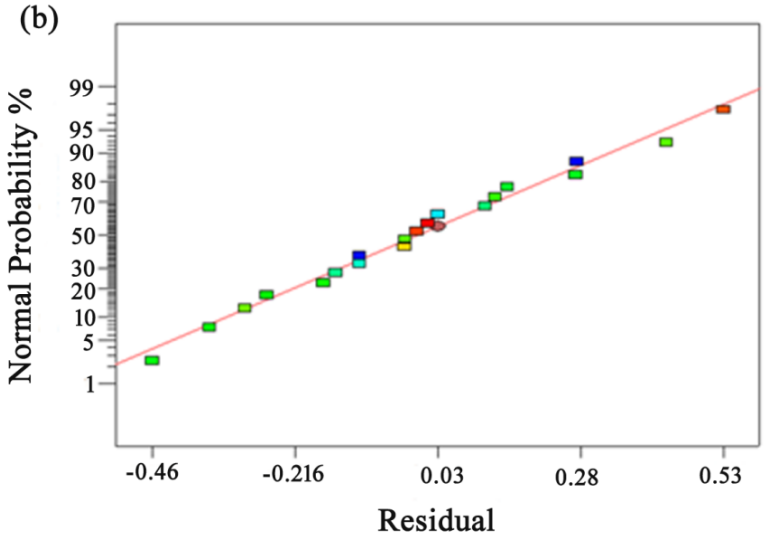

Figure 4.36 Normal probability plots of residuals from (a) initial and (b) final analysis of microhardness

Fig. 4.36(a) shows the plot between normal probability vs residuals generated in the first step of the ANOVA. This plot determines whether the residuals are normally distributed or not. The condition for regression analysis is that the residuals should be normally distributed. If the residuals are not normally distributed, then the fitted regression model is invalid. In Fig. 4.36(a) all the points are falling close to the normal distribution line, therefore, the condition for regression analysis is satisfied. Fig. 4.36(b) shows the plot between normal probability and residuals for the final analysis. It can be observed from Fig. 4.36(b) that the points fell slightly closer to the normal distribution line. Therefore, the condition that the residuals should be normally distributed is satisfied.

Plots of Residuals vs. predicted values

Figs. 4.37(a) & 4.37(b) show the plots between residuals and fitted microhardness values for the first and second step of ANOVA. From these two figures, it can be observed that the residuals for microhardness in both first and second step of analysis were scattered randomly and elimination of the insignificant terms did not affect the random distribution of residuals.

Therefore it can be concluded that the fitted model is adequate and there was no proof to suspect that the residuals are dependent.

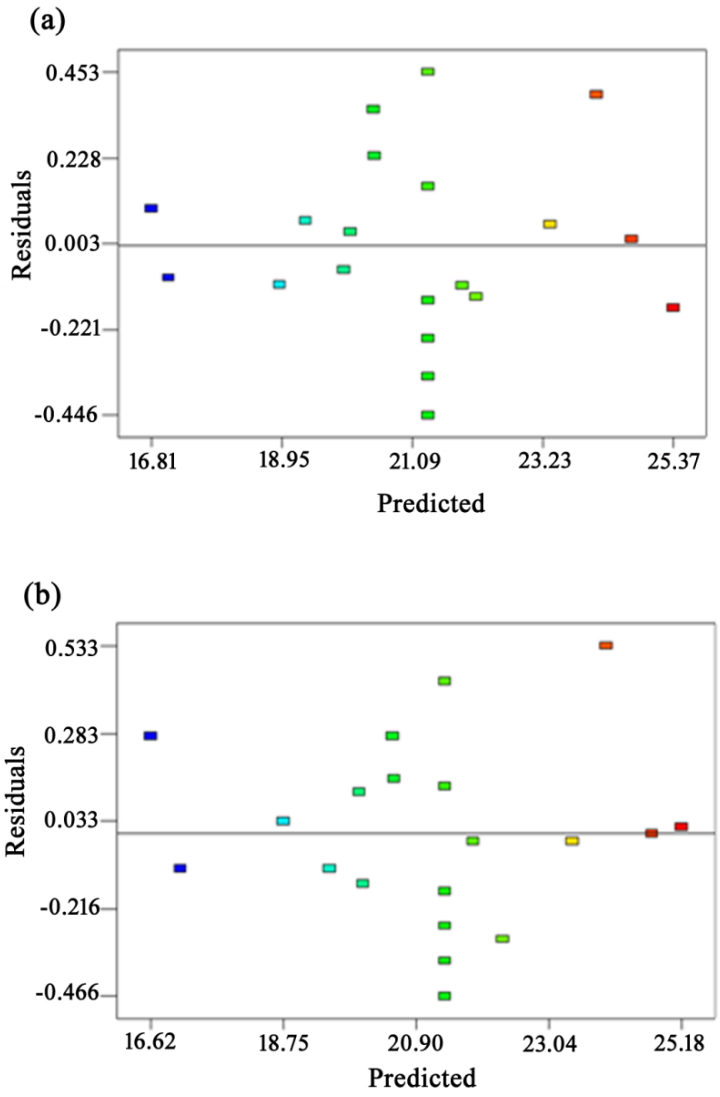

Figure 4.37 Residuals versus predicted values plots for (a) initial analysis of microhardness, (b) final analysis of microhardness

Plots of predicted values vs. actual values

Figs. 4.38(a) & 4.38(b) show the plots between predicted and actual values of microhardness. From these graphs, it can be seen that the predicted microhardness values are in good agreement with the actual microhardness values; hence, the correlation between microhardness and parameters is satisfactory.

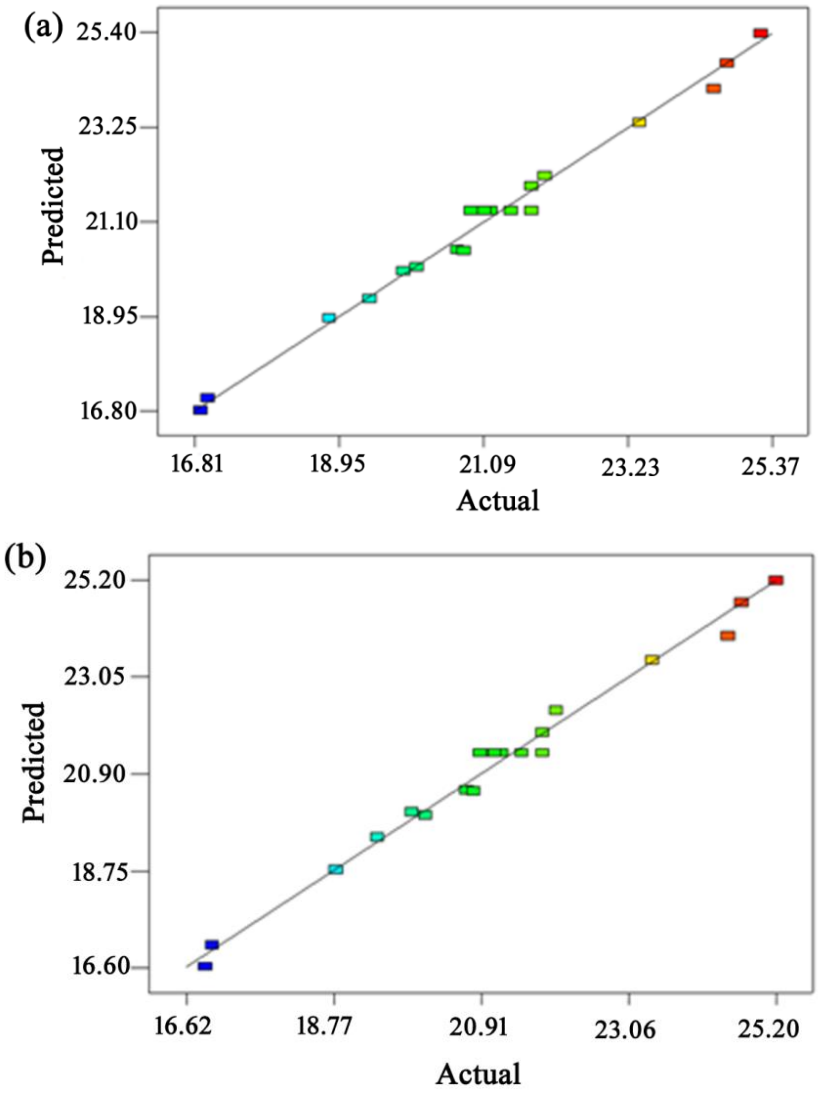

Figure 4.38 Plot of predicted versus observed for microhardness from (a) initial and (b) final analysis

3D Surface plots for microhardness

RSM method generates surface plots to demonstrate the main effects, quadratic effects and interactions between independent parameters. These surface plots are also called as 3D plots which consist of two parameters shown on x and y directions and the response on z-axis while the third parameter is kept constant.

Effect of nanoclay on microhardness

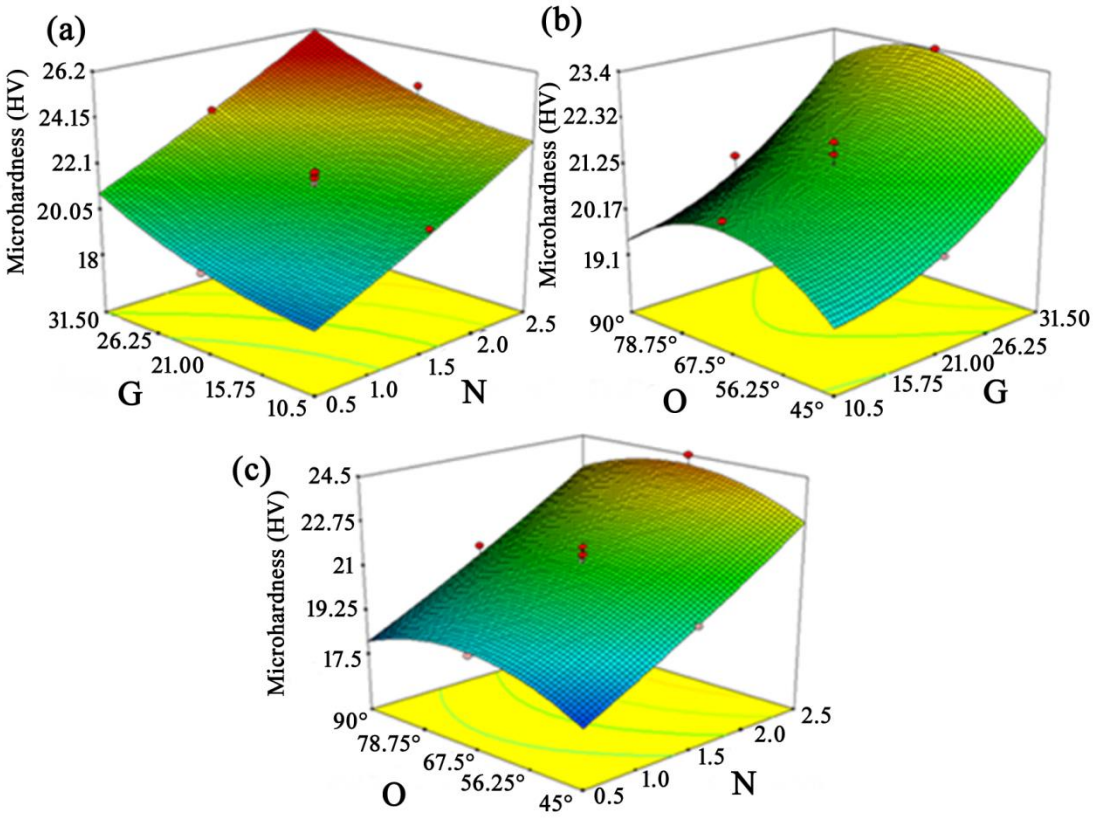

Figure 4.39 3D surface plots for effect of N, G, and O on microhardness

Fig. 4.39(a) displays response surface plot consisting of factors N and G on x and y axes while factor O was fixed at 67.5° and microhardness is shown on the z-axis. It can be observed that microhardness increases slowly with increase in G and increases at a faster rate with increase in N. Fig. 4.39(b) displays a response surface plot consisting of two factors G and O on x and y axes while factor N was fixed at 1.5 wt% and microhardness is shown on z-axis. Fig. 4.39(c)

display response surface plot for two factors N and O on x and y axes while factor G was fixed 21 vol. %.

Maximum value of microhardness obtained in this study is 25.2 HV which was observed at parameter levels N= 2.5%, G=31.5% and O=0°/90°.

4.5.3 Summary

The microhardness of the nanocomposites has been investigated. Glass fiber and nanoclay were reinforced in various proportions and fibers oriented at various angles. Taguchi and RSM methods were used to analyze the data and present the fitted regression models for predicting the microhardness. ANOVA analysis was done using both methods and showed that nanoclay content and glass fiber volume are effectively influencing the hardness. Glass fiber volume and fiber orientation have shown quadratic effects and nanoclay content did not have a quadratic effect. There are no interactions between parameters are observed. The optimized result indicated that the highest microhardness obtained was 27.44 HV which occurred at 2.5 wt% of nanoclay, 31.5 vol% of fiber, and 0°/90° of fibers orientation. The result is confirmed by preparing and testing five samples and the average value of microhardness obtained was 26.73 HV, whereas GRE composite with 31.5 vol% of glass fiber has shown 17.4 HV.

Chapter 5

Erosive Wear Characteristics of Epoxy/Glass/Clay Nanocomposites

5.1 Introduction

The present chapter gives the discussion on investigation of erosive wear, its optimization, and characterization of fracture surfaces of EGCNs. For optimization, Taguchi method and Response surface methodology were used by selecting suitable experimental designs available in Taguchi and RSM methods. The obtained results were analyzed using ANOVA analysis to identify the fact that whether the parameters have a significant effect on wear rate or not. The erosion test is performed to optimize composite composition followed by optimization of the erosion testing parameters. To optimize the composite composition, the parameters selected were nanoclay content, glass fiber volume, and glass fiber orientation. The testing parameters selected were sand flow rate, air stream pressure, impingement angle, stand-off distance, and holding time which were fixed at selected levels. The ranges of erosion testing parameters were selected based on pilot experiments conducted. For optimization of testing parameters, Taguchi L18 array was selected. The fracture surface is studied using SEM micrography.

5.2 Erosive wear: Optimization of composite parameters

The standard test method for finding E_r of polymer composites is ASTM G 76. The dimensions of specimen are 20 mm x 20 mm x 4 mm. The wear test is performed on Magnum TE-400-HMI instrument. For Taguchi method L9 array is selected and central composite design is selected for RSM method. The experiments were conducted according to Taguchi and RSM designs. The effect of each parameter is quantified using ANOVA analysis and the significance of each parameter's effect is also evaluated. Regression models are is fitted in Taguchi and RSM methods and the R^2 value gives the strength of fit of each model.

5.2.1 Taguchi Design

Erosive wear rate (E_r) of the composites is evaluated for the same L9 orthogonal array selected in section 4.2. Table 5.1 shows the E_r values and corresponding S/N ratios for the composites fabricated according to L9 orthogonal array design. Fig. 5.1 shows the effects of all three control factors on E_r. Three parameters selected were nanoclay weight percentage, glass fiber volume percentage, and angle of orientation of glass fibers. The nanoclay content is indicated in terms of weight percentages, and glass fiber content is indicated in terms of volume percentage. For this study lower-the-better S/N ratio was selected and the corresponding equation is shown in equation (1).

$$S/N_L = -10 \log[\frac{1}{R}\sum_{j=1}^{R}(y_j^2)] \quad \text{.....(1)}$$

Table 5.1. L9 Experimental design for erosion test of EGCN's

Sl. No	Nanoclay wt% (N)	Glass Fiber Volume % (G)	Angle (O)	E_r (mg/kg)	S/N ratio
1.	0.5	10.50	45°	2318.8	-67.30
2.	0.5	21	67.5°	2827.2	-69.03
3.	0.5	31.5	90°	3416.4	-70.67
4.	1.5	10.50	67.5°	2329.6	-67.34
5.	1.5	21	90°	2648.8	-68.46
6.	1.5	31.5	45°	2438	-67.74
7.	2.5	10.50	90°	2205.2	-66.87
8.	2.5	21	45°	1994.4	-65.99
9.	2.5	31.5	67.5°	2459.6	-67.82

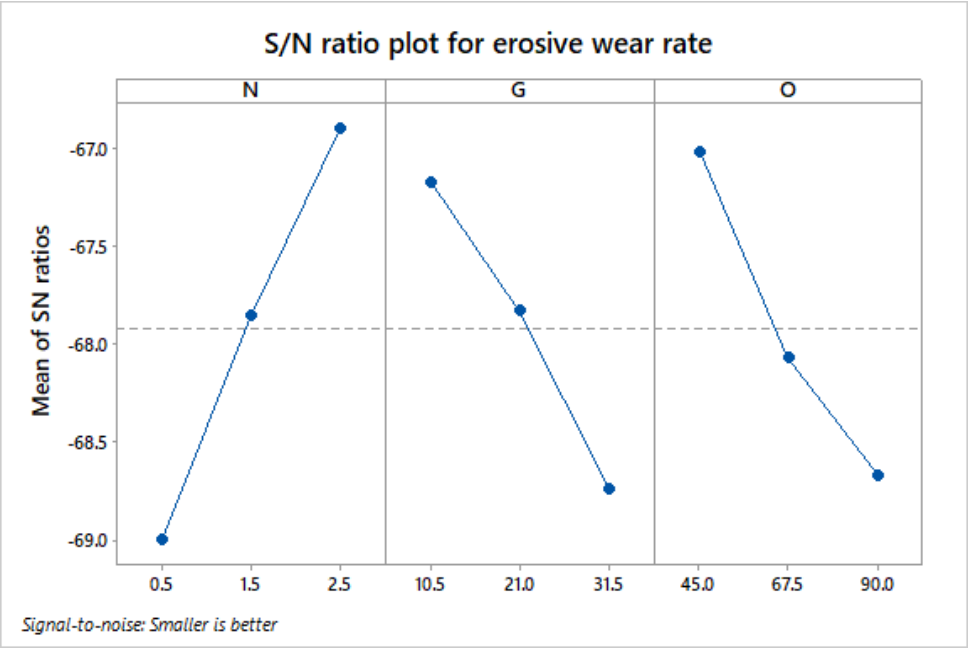

Figure 5.1 Plots between control factors and S/N ratios of E_r

From Figure 5.1 it is obvious that with an increase in clay content, E_r decreased, whereas, with increase in glass fiber volume, E_r increased, and with an increase in angle of fibers in the range 45˚/-45˚ to 90˚/0˚, E_r increased. ANOVA results displayed in Table 5.2 show that the parameters N, G, O have a significant effect on the erosion of EGCN. The lowest E_r is observed at the condition N3G1O1; under these parameters, the predicted value of S/N ratio is calculated using equation (3). The predicted and confirmation experiment results of E_r are given in Table 5.3.

E_r = 2515.3 + 338.8 N1 - 43.2 N2 - 295.6 N3 - 230.8 G1 - 25.2 G2 + 256.0 G3 - 264.9 O1 + 23.5 O2 + 241.5 O3 …….(2)

= 2515.3 - 295.6 - 230.8 - 264.9

= 1724 mg/kg

S/N Ratio = -67.9148 - 1.0864 N1 + 0.0657 N2 + 1.0207 N3 + 0.7416 G1 + 0.0867 G2 - 0.8283 G3 + 0.9008 O1 - 0.1485 O2 - 0.7523 O3 ...…….(3)

= -67.9148 + 1.0207 + 0.7416 + 0.9008

= -65.25

Equations (2) and (3) are the general linear models, generated by doing ANOVA analysis using MINITAB software. The optimized value of E_r is 1724 mg/kg, and the corresponding experimental value is 1865 mg/kg shown in Table 5.3. A comparison was made between E_r obtained under optimum conditions with E_r of neat epoxy and also with E_r of composite made without added nanoclay, while fixing the other two parameters at optimum conditions. The E_r of neat epoxy is 2519 mg/kg which is 26% higher and that of the composite without adding nanoclay is 2645 mg/kg which is 29.5% higher. The weight loss due to erosion increased with increase in glass fiber volume in the composite, due to the breaking of fibers by means of bending moment, because of the impinging sand particles. As the glass fibers are brittle they broke easily by the bending moment and were expelled from the zone by air [135].

The mechanism of erosion of matrix is in contrast to the erosion of the fibers in which the matrix cracks first and fractures into small fragments by the ploughing action of sand particles and hence this process is slow. Therefore, with an increase in fiber volume, the erosion rate is increased which can be observed in Fig. 5.1. The reduced wear rate with increase in nanoclay content is attributed to the increased hardness with addition of nanoclay. The specimens with 90˚/0˚ fiber direction exhibited higher E_r values and the specimens with 45˚/-45˚ fiber direction exhibited lower E_r values. When the particles were striking at othen than normal angle the composites with 0˚/90˚ fiber direction were subjected to pure bending moment. In case of the composites with 45˚/-45˚ fiber direction, the bending moment was in two directions, one normal to the fibers, and the other tangential to the fibers. Hence, the normal bending moment which causes failure is reduced, thereby reducing wear, a phenomenon observed previously by Bagci et al. [135].

Table 5.2. Anova table for S/N ratios of E_r

Source	DF	Seq SS	Percentage Contribution	Adj SS	Adj MS	F-Value	P-Value
N	2	6.679	45.61%	6.679	3.339	182.59	0.005
G	2	3.730	25.47%	3.73	1.865	101.98	0.01
O	2	4.198	28.67%	4.198	2.099	114.76	0.009
Error	2	0.036	0.25%	0.036	0.018		
Total	8	14.6442	100.00%				

Table 5.3. Results at the optimum conditions

	Optimal Control Parameters	
	Prediction	Experimental
Level	N3G1O1	N3G1O1
S/N ratio	-65.25	-65.4 ± 0.34
E_r (mg/kg)	1724	1865 ± 72

5.2.2 Response surface methodology

Table 5.4. Actual and coded levels of the design parameter

Factors	Levels			Axial points α = 1	
	Low (-1)	Central (0)	High (+1)	-α	+α
Nanoclay wt%	0.5	1.5	2.5	-1	+1
Glass fiber vol%	10.5	21	31.5	-1	+1
Fiber angle	+45˚/-45˚	67.5˚/22.5˚	0˚/90˚	-1	+1

Table 5.5. Experimental design according to CCD for E_r

Run	Nanoclay wt% (N)	Glass Fiber Volume % (G)	Angle (O)	E_r (mg/kg)
1	2.5	10.5	90°	2205.21
2	1.5	31.5	67.5°	2751.63
3	1.5	10.5	67.5°	2329.46
4	1.5	21	67.5°	2525.44
5	1.5	21	67.5°	2423.54
6	0.5	10.5	45°	2318.38
7	1.5	21	67.5°	2470.13
8	1.5	21	67.5°	2440.5
9	0.5	10.5	90°	2864.8
10	2.5	21	67.5°	2218
11	1.5	21	67.5°	2463.42
12	1.5	21	67.5°	2507.34
13	1.5	21	90°	2648.58
14	0.5	21	67.5°	2827.22
15	1.5	21	45°	2182
16	2.5	31.5	90°	2717.12
17	2.5	31.5	45°	2210.18
18	0.5	31.5	45°	2845.24
19	0.5	31.5	90°	3416.41
20	2.5	10.5	45°	1724

Table 5.5 shows the generated experimental design according to central composite design and the corresponding E_r for each test. The input parameters are nanoclay wt%, glass fiber vol%, and fibers orientation which are indicated in ANOVA, 2D, and 3D plots as N, G and O respectively. To evaluate the effect of parameters on E_r, ANOVA analysis was performed and the confidence level selected is 95%. Based on the p-value, whether the parameter is significant or insignificant is evaluated. If p-value is less than 0.05, it indicates that there is greater than 95% probability that the input parameter affects E_r. If p-value is greater than 0.05, it indicates that there is less than 95% probability that the input parameter affects E_r. If any parameters are insignificant, then those parameters terms should be eliminated and analysis should be repeated.

ANOVA and regression model for E_r

Tables 5.6 & 5.8 show the ANOVA tables obtained after the first and second step of analysis. It can be noticed from table 5.6 that the probability values for terms N, G, and O are more than 99%. The term N*N is effective with P-value 0.04 and the term G*G is effective with P-value 0.009 but the term O*O was significant because the p-value is 0.03. There are no significant interactions between variables because the corresponding p-values are >0.05.

Table 5.6. ANOVA table for E_r obtained in the first step of analysis

Source	Seq SS	DF	Adj MS	F-Value	p-value
Model	2346107	9	260678.6	196.1027	< 0.0001
N	1022426	1	1022426	769.1483	< 0.0001
G	624365.2	1	624365.2	469.6959	< 0.0001
O	661683	1	661683	497.7693	< 0.0001
NG	807.6181	1	807.6181	0.607553	0.4538
GO	2094.339	1	2094.339	1.575524	0.2379
NO	318.5288	1	318.5288	0.239622	0.635
N*N	7394.847	1	7394.847	5.562977	0.04
G*G	13394.62	1	13394.62	10.07647	0.0099
O*O	8459.73	1	8459.73	6.364065	0.0302
Residual	13292.97	10	1329.297		
Lack of Fit	5770.925	5	1154.185	0.767202	0.6109
Pure Error	7522.041	5	1504.408		
Total	2359400	19			

Table 5.7 shows the regression coefficients of the equation (4) which is a second order polynomial consisting of all the coefficients of the significant and insignificant terms.

$$E_r = 1511.1 - 406.68*N - 3.15*G + 26.74*O - 0.95*N*G - 0.72*N*O + 0.026*G*O + 51.85*N*N + 0.63*G*G - 0.11*O*O \quad \ldots\ldots\ldots (4)$$

Table 5.7 Regression coefficients of fitted model for E_r after first step of analysis

Coefficient	b_0	b_1	b_2	b_3	b_{11}	b_{22}	b_{33}	b_{12}
value	1511.1	- 406.68	- 3.15	26.74	51.85	0.63	- 0.11	- 0.95
Coefficient	b_{13}	b_{23}	R^2 %					
value	- 0.72	0.026	99.44					

The ineffective terms were eliminated and ANOVA analysis was repeated for the remaining terms and the results are given in table 5.8. It is observed from table 5.8 that the P-values of N*N, G*G, and O*O decreased after excluding insignificant terms. The ANOVA was repeated for the third time after excluding the term N*N and the new ANOVA table obtained is given as table 5.9. This time p-value for the term N increases from 0.0087 to 0.012 and all other factors show no change in p-values.

Table 5.8. ANOVA table obtained for E_r after second step of analysis

Source	Seq SS	DF	Adj MS	F-Value	p-value
Model	2342887	6	390481.2	307.4012	< 0.0001
N	1022426	1	1022426	804.8917	< 0.0001
G	624365.2	1	624365.2	491.5233	< 0.0001
O	661683	1	661683	520.9013	< 0.0001
N*N	7394.847	1	7394.847	5.821497	0.0313
G*G	13394.62	1	13394.62	10.54474	0.0064
O*O	8459.73	1	8459.73	6.659812	0.0228
Residual	16513.45	13	1270.266		
Lack of Fit	8991.411	8	1123.926	0.747089	0.6606
Pure Error	7522.041	5	1504.408		
Total	2359400	19			

Table 5.9 shows regression coefficients obtained after third step of analysis and equation (5) is a reduced second order polynomial comprising of the final coefficients of the significant terms.

Table 5.9. Regression coefficients and percentage of R^2 for both responses in first step of analysis of variance for fracture toughness

Coefficient	b_0	b_1	b_2	b_3	b_{11}	b_{22}	b_{33}	R^2 %
E_r	1576.19	- 475.32	- 2.79	26.22	51.85	0.63	- 0.11	99.3

$$E_r = 1576.19 - 475.32*N - 2.79*G + 26.22*O + 51.85*N* N + 0.63*G* G - 0.11*O* O \quad \text{…….(5)}$$

It should be noticed that squares of the factors N, G, and O are effective on E_r but there are no significant interactions. Moreover, the coefficient of determination (R^2) obtained after both steps of analysis is shown in table 5.7 and table 5.9. R^2 is the strength of fit of the model or the nearness of the fitted values to the experimentally obtained values. In tables 5.7 & 5.9, R^2 values are given as 99.44% and 99.3% for the fitted models in first and final step of analysis respectively. These high values of R^2 also indicate that the regressor terms in the model not only explain the total variability of the response but also give a good estimation of response in the ranges of parameters selected.

Main effect plots

Figs. 5.2(a) - 5.2(c) display the main effect plot of factors N, G, and O. These plots show the effect of first order terms N, G, and O on the response E_r. Fig. 5.2(a)-(c) shows that the magnitude of E_r undergoes obvious change with change N, G, and O. Fig. 5.2(a) shows that with increase in nanoclay content Er decreases. In Figs. 5.2(b)-(c) there is an increasing trend in E_r with increase in G and O.

The trend of curves in main effect plots and the p-values of first order terms from the ANOVA table are in good agreement. The sign of the regression coefficients also agrees with the trend of the E_r for each parameter.

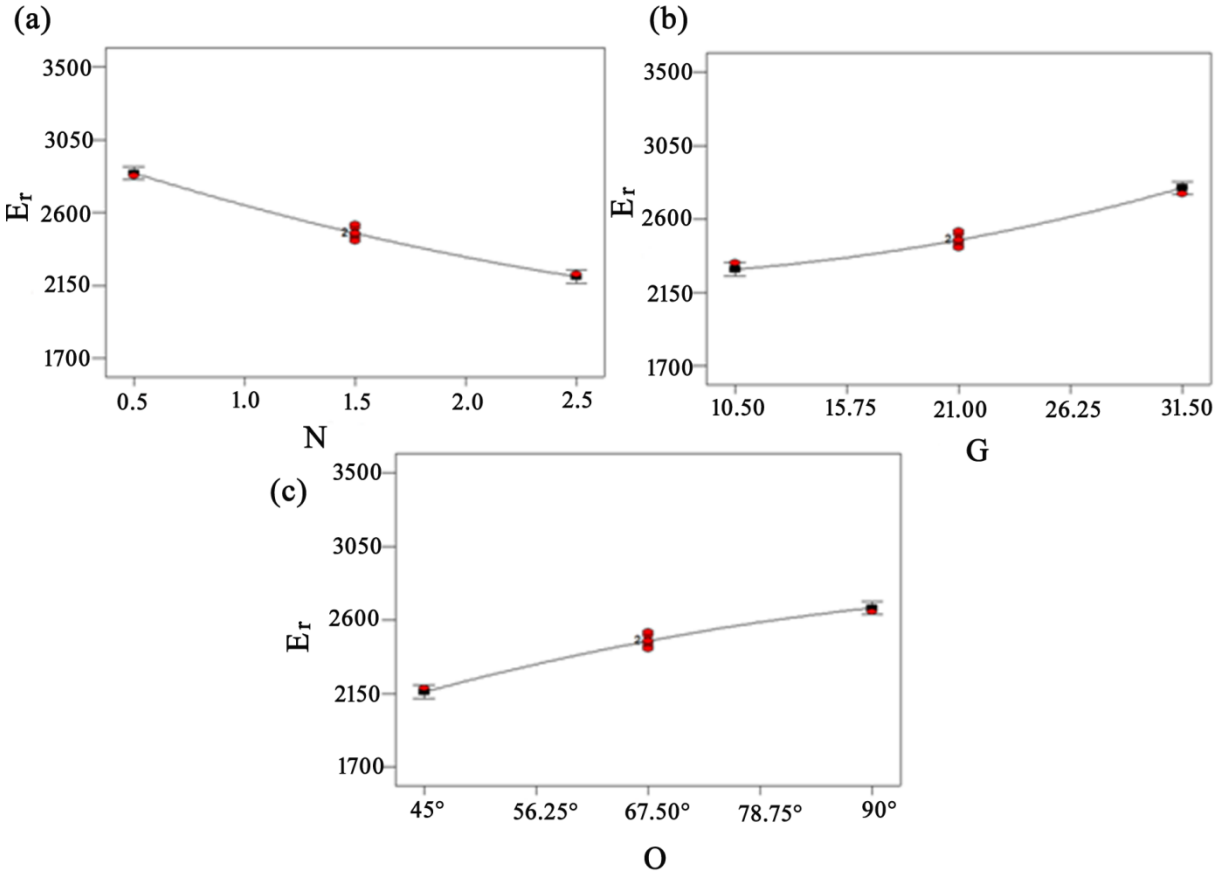

Figure 5.2 Main effect plots of factor (a) N, (b) G, and (c) O on E_r

Normal Probability plots

Fig. 5.3(a) shows the plot between normal probability and residuals generated in the first step of the ANOVA analysis. This plot determines whether the residuals are normally distributed or not. The condition for regression analysis is that the residuals should be normally distributed. If the residuals are not normally distributed, then the fitted regression model is invalid. In Fig. 5.3(a) the all the points are falling closer to the normal distribution line, therefore, the condition for regression analysis is satisfied. Fig. 5.3(b) shows the plot between normal probability and residuals for the final analysis. It can be observed from Fig. 5.3(b) that the points fell slightly away from the normal distribution line. However, the condition that the residuals should be normally distributed is unaltered.

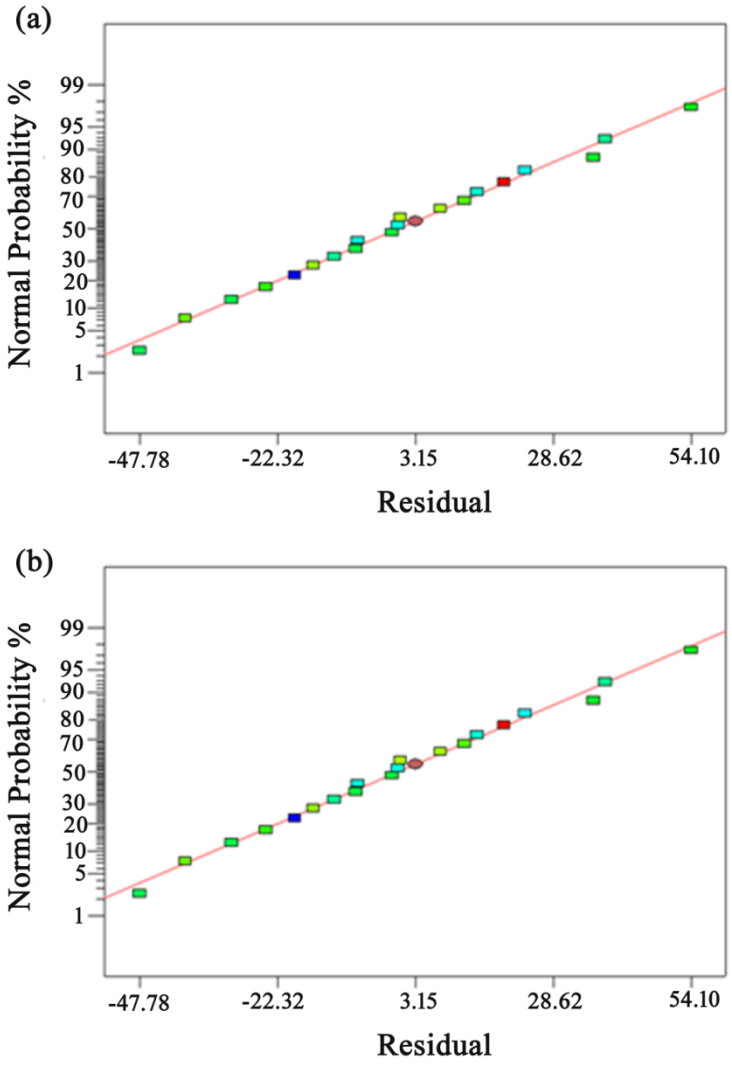

Figure 5.3 Normal probability plots of residuals from (a) initial and (b) final analysis of E_r

Plots of Residuals vs predicted values

Figs. 5.4(a) & 5.4(b) show the plots between residuals and fitted E_r values for the first and second step of ANOVA analysis. From these two figures, it can be observed that the residuals for E_r in both first and third step of analysis were scattered randomly and elimination of the insignificant terms did not affect the random distribution of residuals. Therefore it can be concluded that the fitted model is adequate and there is no proof to suspect that the residuals are dependent.

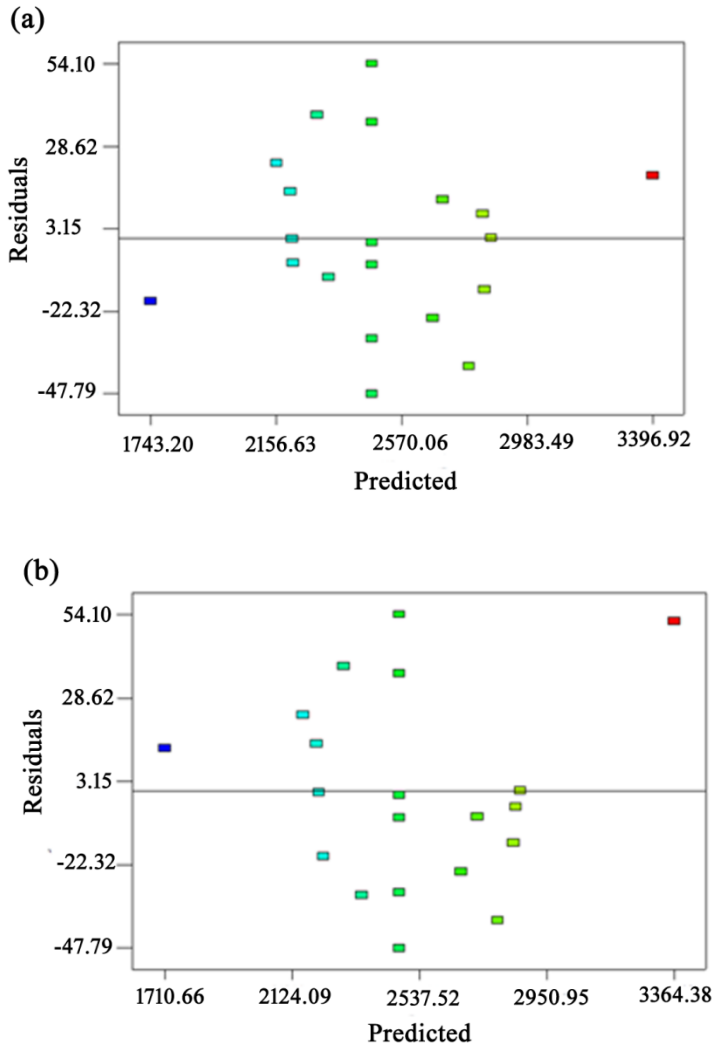

Figure 5.4 Residuals versus predicted values plots for (a) initial analysis of E_r, (b) final analysis of E_r

Plots of predicted values vs. actual values

Figs. 5.5(a) & 5.5(b) show the plots between predicted E_r values and actual values of E_r. From these graphs, it can be observed that the predicted E_r values are in good agreement with the actual E_r values; hence, the correlation between E_r and parameters is satisfactory.

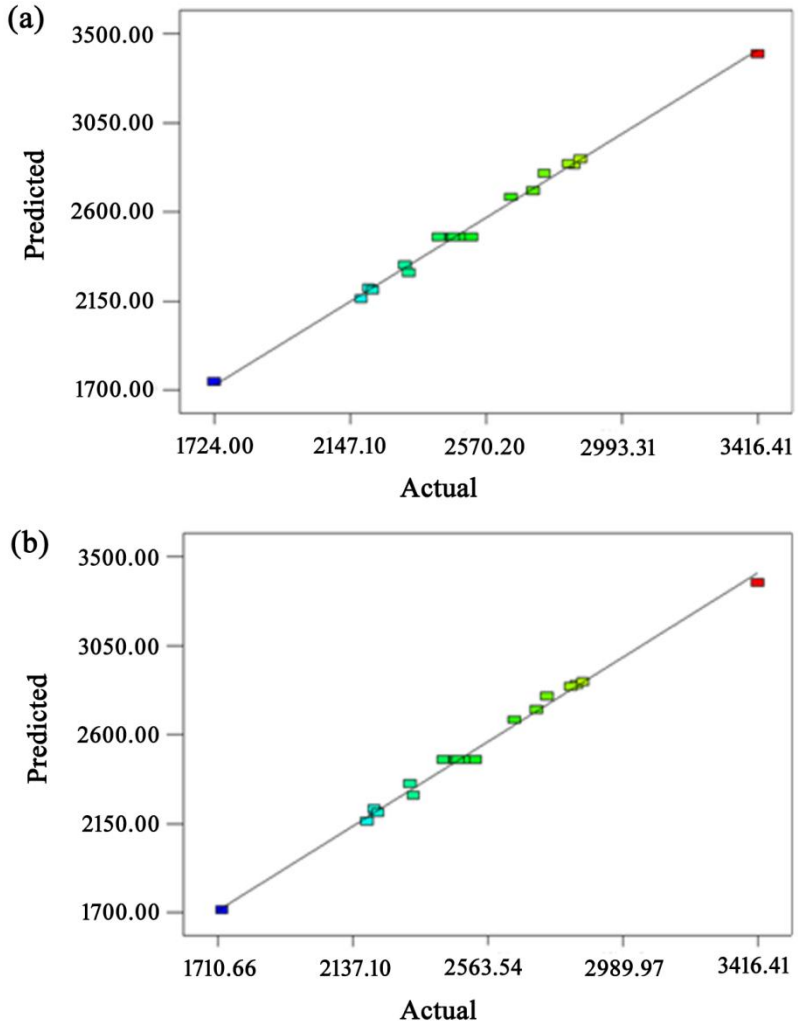

Figure 5.5 Plot of predicted versus observed for E_r from (a) initial and (b) final analysis

3D Surface plots for E_r

RSM method generates surface plots to demonstrate the main effects, quadratic effects and interactions between independent parameters. These surface plots are also called as 3D plots which consist of two parameters drawn on x and y directions and response on z-axis while the third parameters are kept constant.

Fig. 5.6(a) displays response surface consisting of two factors N and G on x and y axes while factor O was fixed at 67.5° and response E_r is on the z-axis. It can be observed that E_r decreases with increase in N and increases with increase in G and O. Fig. 5.6(b) displays a response surface plot consisting of two factors G and O on x and y axes while factor N was fixed at 1.5 wt% and the response E_r is shown on the z-axis. It can be observed that E_r increases with increase in O and G. Fig. 5.6(c) display response surface plot consisting of two factors N and O on x and y axes while factor G was fixed 21 vol. %.

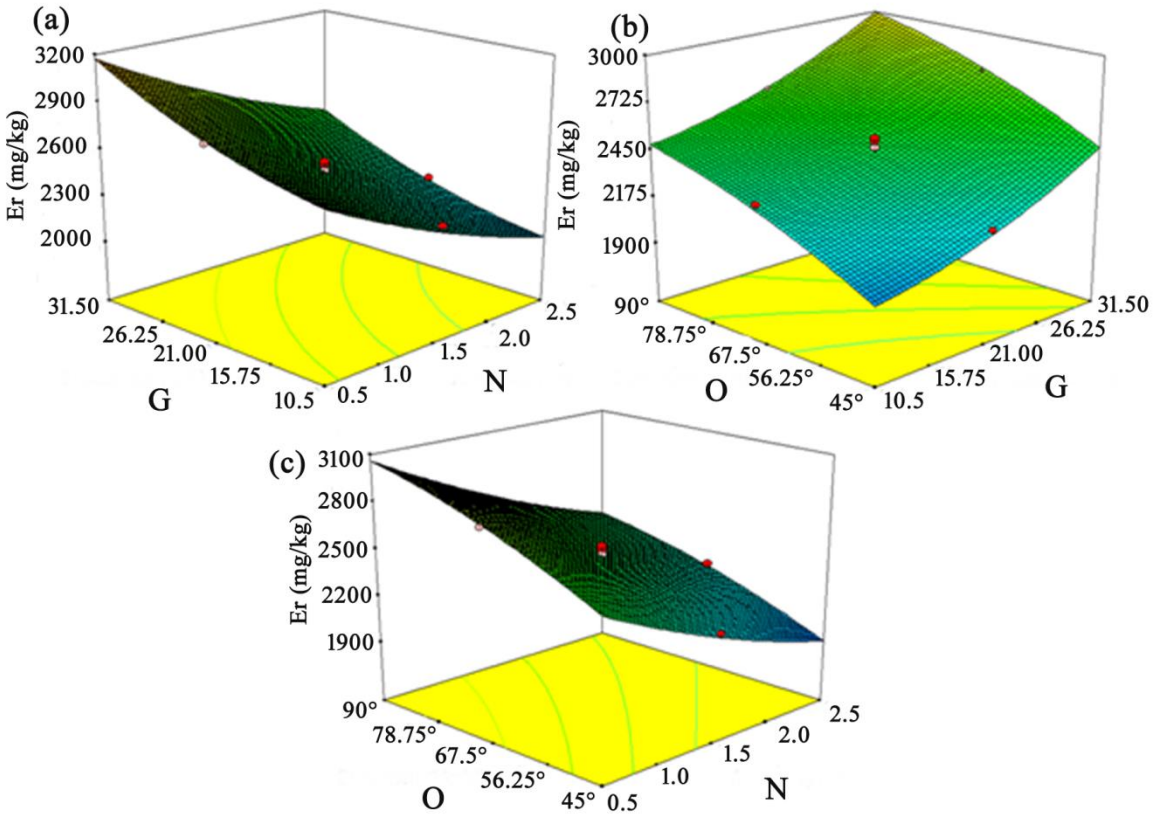

Figure 5.6 3D surface plots for effect of N, G, and O on E_r

Minimum value of E_r obtained in this study is 1724 MPa which was observed at parameter levels N = 2.5%, G = 10.5% and O = 45° and the corresponding coded levels are N=+1, G=-1 and O=-1 respectively.

5.2.3 Surface Morphology of tested specimens

Figure 5.7(a) is the SEM image of the tested neat GRE specimens and Figures 5.7(b)-40(c) are of EGCN are tested at the fixed erosion testing conditions as follows: 2gm/min, 30° impinging angle, 2 bar pressure, 1 min holding period, 30 mm stand-off distance. The mechanism of deformation of the FRPs subjected to erodent particles is as follows; the abrasive

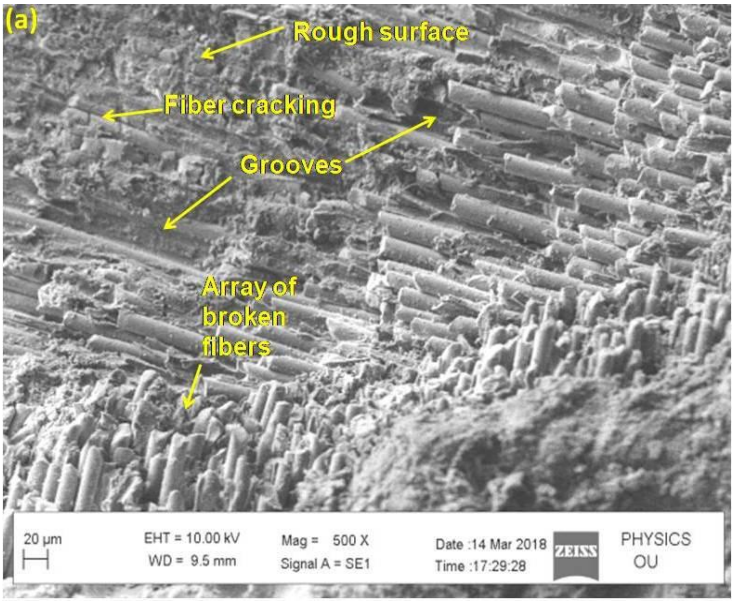

Figure 5.7(a). SEM image of specimen tested at 2gm/min, 30° impinging angle, 2 bar pressure, 1 min holding period, 30 mm stand-off distance for a composition of 0 wt.%, 10.5 vol.%, 0°/90°

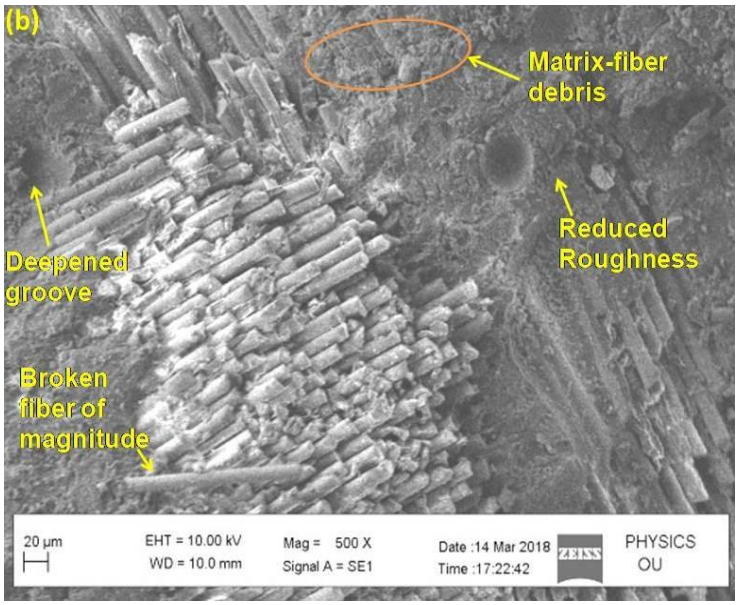

Figure 5.7(b). SEM image of specimen tested at 2gm/min, 30° impinging angle, 2 bar pressure, 1 min holding period, 30 mm stand-off distance for compositions 0.5 wt.%, 21 vol.%, 45°/-45°

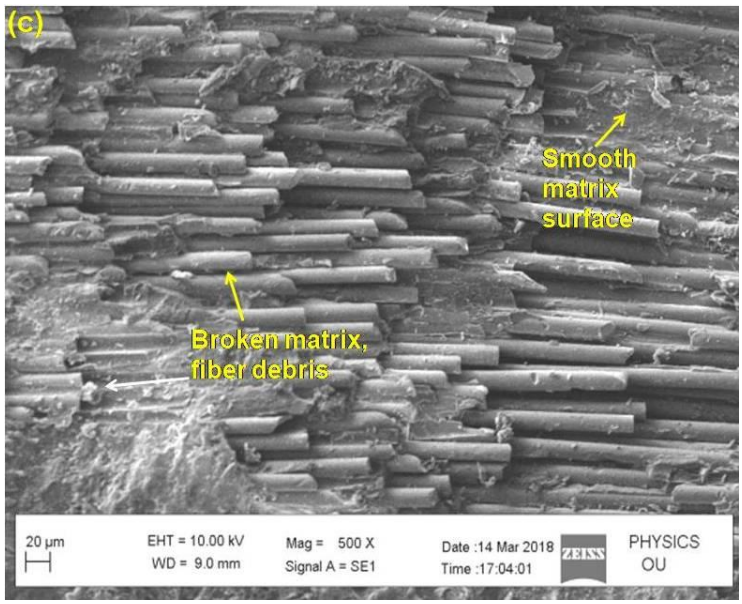

Figure 5.7(c) SEM image of specimen tested at 2gm/min, 30° impinging angle, 2 bar pressure, 1 min holding period, 30 mm stand-off distance for compositions 2.5 wt.%, 21%, 45°/-45°

particles striking the surface remove the matrix layer first and the fibers are exposed to airstream creating high bending moments on the fibers forming cracks resulting in fracture and ejection of broken fibers forming grooves. If the bombardment persists, it results in the formation of craters. The decreased surface roughness in Figs. 5.7(b)-5.7(c) indicates that the composites containing nanoclay demonstrated critical deformation, which means that the nanoclay has good compatibility with the epoxy resin and glass fiber, forming a strong bond between fiber and matrix thereby slowing down the erosion of EGCN. The neat GFRP in Fig. 5.7(a) shows the rough surface which is comparatively rougher than EGCNs shown in Figs. 5.7(b)-5.7(c). The size of the broken fiber in Fig. 5.7(b) indicates how fast the failure of the fibers occurred, unlike the matrix which takes more time since it breaks slowly into small debris.

5.2.4 Summary

In the present study, E_r of the nanocomposites has been investigated. Glass fiber and nanoclay were reinforced in various proportions and fibers were oriented at various angles. Taguchi and RSM methods were used to analyze the data and fit regression models for predicting the E_r. ANOVA analysis done using both methods showed that all three parameters were effectively influencing the E_r of EGCNs. All three parameters have quadratic effects but there were no interactions between parameters. The optimized result obtained indicated that the best E_r obtained was 1828 mg/kg which occurred at 2.5 wt% of nanoclay, 10.5 vol% of fiber, and 45°/-45° of fibers orientation. The result is confirmed by preparing and testing five samples and the average value of E_r obtained was 1865 mg/kg. The fracture morphology has shown strong bonding between fiber and matrix when nanoclay was added. SEM micrography has shown that with an increase in nanoclay content, the surface roughness of the eroded surface greatly reduced indicating slow erosion. Irrespective of increased hardness with addition of glass fiber, increase in fiber content increased the erosion rate because fibers broke into fragments of sizes much bigger than the matrix fragments and expelled easily from the zone.

5.3 Erosive wear: Optimization of testing parameters

The EGCN with 2.5 wt% of nanoclay, 10.5 vol% of glass fiber, and 45°/-45° of fibers orientation has exhibited least E_r in the previous section 5.2. In this section the same EGCN is selected to study the effect of various testing erosion parameters selected, namely, sand flow rate, air stream pressure, impingement angle, stand-off distance, and holding time. Taguchi L18 array is selected to optimize the selected testing parameters. Pilot experiments were conducted to select the ranges of each parameter. The effect of each parameter is quantified using ANOVA and significance of parameter effect is evaluated. A linear regression model is fitted for which the R^2 value gives the strength of fit.

5.3.1 Taguchi Design

From table 5.10, for the given five parameters, one with two levels and four with three levels, the suitable orthogonal array available in Taguchi method is L18. The L18 design with obtained E_r values is given in table 5.11. In this study, the aim is to find the lowest E_r. Therefore, the required quality characteristic that should be selected is lower-the-better. Eq. (4) is used to calculate the S/N ratios for the selected quality characteristic. Figure 5.8 shows the S/N ratio plot versus parameter levels. Table 5.12 demonstrates ANOVA results for S/N ratios. The significance of the effect of parameters is given in the order as follows: impingement angle, holding time, pressure, and stand-off distance.

Table 5.10 Erosion Testing Parameters for L18 Design

Test Parameters	Ranges
Sand Flow Rate (gm/min) , (f)	2 - 4
Impingement angle (deg), (θ)	15° - 60°
Air Stream Pressure (bar), (P)	2 - 6
Holding Period (min), (t)	1 - 3
Stand-off distance (mm), (d)	10 - 30

Table 5.11 L18 Experimental design for erosion test

Expt. No.	f (gm/min)	θ	P (bar)	t (min)	d (mm)	E_r (mg/kg)	S/N Ratio
1.	2	15˚	2	1	10	1819.85	-65.19
2.	2	15˚	4	2	20	2071.45	-66.32
3.	2	15˚	6	3	30	2288.81	-67.19
4.	2	30˚	2	1	20	1992.33	-65.98
5.	2	30˚	4	2	30	2207.35	-66.87
6.	2	30˚	6	3	10	2843.65	-69.07
7.	2	60˚	2	2	10	2536.18	-68.08
8.	2	60˚	4	3	20	2824.97	-69.02
9.	2	60˚	6	1	30	2555.21	-68.15
10.	4	15˚	2	3	30	2331.43	-67.35
11.	4	15˚	4	1	10	2590.54	-68.266
12.	4	15˚	6	2	20	2784.65	-68.89
13.	4	30˚	2	2	30	2491.78	-67.93
14.	4	30˚	4	3	10	3187.46	-70.06
15.	4	30˚	6	1	20	2942.53	-69.37
16.	4	60˚	2	3	20	3090.68	-69.79
17.	4	60˚	4	1	30	2893.87	-69.23
18.	4	60˚	6	2	10	3543.21	-70.98

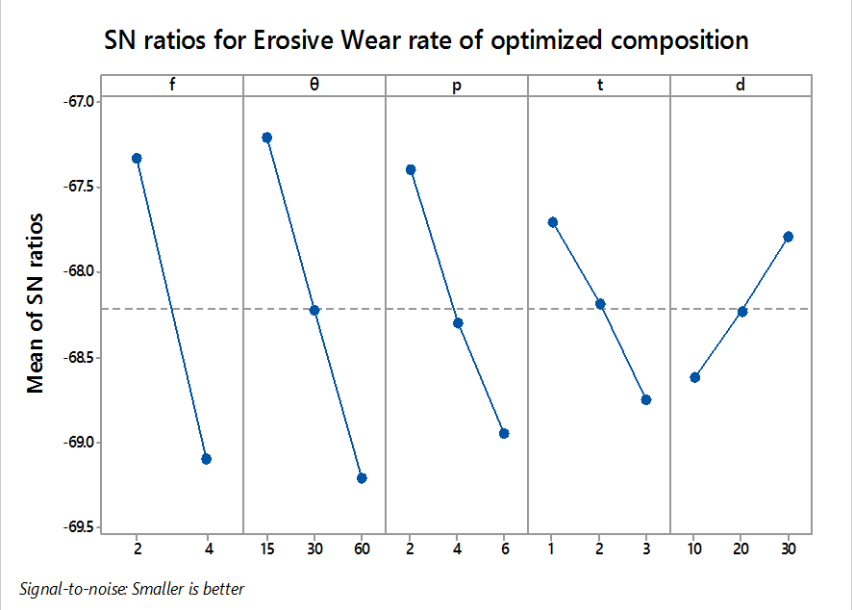

Figure 5.8 Plots between testing parameters and S/N ratios of E_r for EGCN with optimized composition

The effect of each control factor on E_r of EGCN can be observed in Fig. 5.8. The optimal level of each parameter corresponds to the higher value of S/N ratio, respectively. The optimum value of E_r will occur at the parameter level corresponding to the high S/N ratio value. Based on ANOVA analysis, it is noted that the airflow rate has a dominant effect over other factors. The other parameters in the order of dominance in effect on E_r are angle, pressure, holding period, and stand-off distance. The optimal conditions were identified from S/N ratio plot and given as f1θ1p1t1d3. The optimal E_r can be calculated using equation (6) and it is obtained as 1523.96 mg/kg. The value of predicted S/N_L proportion at the optimal conditions can be obtained using equation (7) and it is obtained as -64.56. The predicted and confirmation test values of E_r are given in Table 5.13.

$$E_r\ (mg/kg) = 2610.89 - 262.02\ f_1 + 262.02\ f_2 - 296.43\ \theta_1 - 0.04\ \theta_2 + 296.47\ \theta_3 - 233.84\ p_1 + 18.39\ p_2 + 215.46\ p_3 - 145.16\ t_1 - 5.12\ t_2 + 150.28\ t_3 + 142.60\ d_1 + 6.88\ d_2 - 149.48\ d_3 \quad \ldots\ldots\ldots(6)$$

$$= 2610.89 - 262.02 - 296.43 - 233.84 - 145.16 - 149.48$$

$$= 1523.96\ mg/kg$$

$$S/N\ Ratio = -68.2104 + 0.8887\ f_1 - 0.8887\ f_2 + 1.0071\ \theta_1 - 0.0072\ \theta_2 - 0.9999\ \theta_3 + 0.8199\ p_1 - 0.0859\ p_2 - 0.7340\ p_3 + 0.5110\ t_1 + 0.0285\ t_2 - 0.5396\ t_3 - 0.4023\ d_1 - 0.0216\ d_2 + 0.4240\ d_3 \quad \ldots\ldots\ldots\ldots(7)$$

$$= -68.2104 + 0.8887 + 1.0071 + 0.8199 + 0.5110 + 0.4240$$

$$= -64.56$$

Table 5.12 ANOVA table for S/N ratios of E_r

Source	DF	Seq SS	Percentage Contribution	Adj SS	Adj MS	F	P
f	1	14.2167	36.27%	14.2167	14.2167	539.75	0
θ	2	12.0847	30.83%	12.0847	6.0424	229.4	0
p	2	7.3099	18.65%	7.3099	3.655	138.76	0
t	2	3.3185	8.47%	3.3185	1.6593	63	0
d	2	2.0527	5.24%	2.0527	1.0263	38.97	0
Error	8	0.2107	0.54%	0.2107	0.0263		
Total	17	39.1933	100.00%				

A comparison was made between the E_r obtained for the EGCN at optimum levels of control factors with the E_r obtained for neat epoxy and also with the E_r of composite made without added nanoclay fixing the other two parameters at optimum conditions. The E_r of neat epoxy is 2013 mg/kg which is 21.2% higher and E_r of GRE without added nanoclay and with glass fiber volume of 10.5 vol%, and fiber oriented at 45°/-45° is 2261.4 mg/kg, which is 29.8% higher.

Table 5.13 Results at the optimum conditions

	Optimal Control Parameters	
	Prediction	Experimental
Level	*f1θ 1p1t1d3*	*f1θ 1p1t1d3*
S/N ratio	-64.56	-63.99±0.41
E_r (mg/kg)	1523.96	1586.41±76

Equation (8) is the general linear model generated for the erosion rate for the design shown in Table 5.11. It is generated by ANOVA analysis using MINITAB software. For validating the model, two composites were prepared under conditions not reported in Table 5.14.

Table 5.14 E_r at the optimum conditions

Expt. No.	f (gm/min)	θ	P (bar)	t (min)	d (mm)	Erosion Rate (mg/kg)	
						Predicted	Experimental
1.	2	30˚	6	2	20	2566.05	2620±82
2.	4	30˚	4	2	20	2893.02	2945±98

5.3.2 Surface Morphology of tested specimens

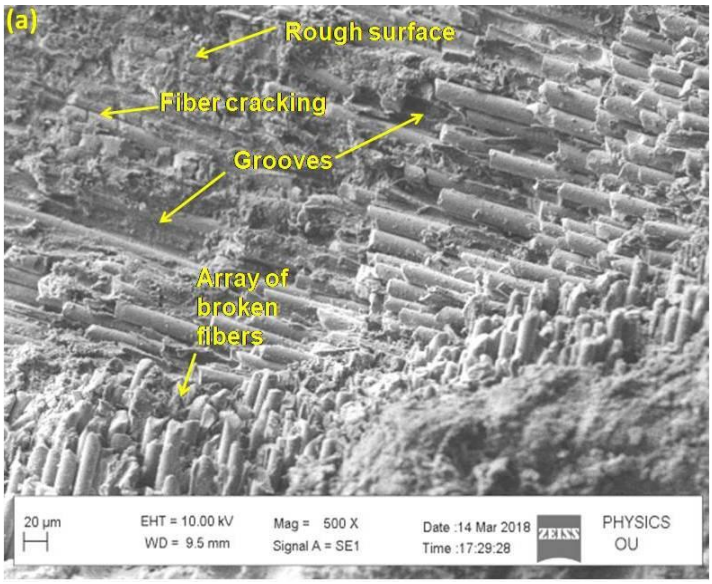

Figure 5.9 (a). SEM image of specimen tested at 2gm/min, 30°impinging angle, 2 bar pressure, 1 min holding period, 30 mm stand-off distance for a composition of 0 wt.%, 10.5 vol.%, 0˚/90˚

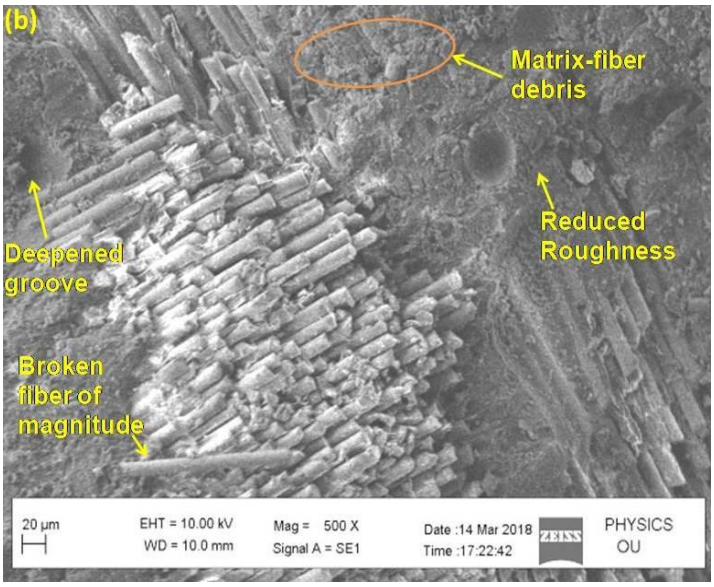

Figure 5.9 (b). SEM image of specimen tested at 2gm/min, 30°impinging angle, 2 bar pressure, 1 min holding period, 30 mm stand-off distance for compositions 0.5 wt.%, 21 vol.%, 45˚/-45˚

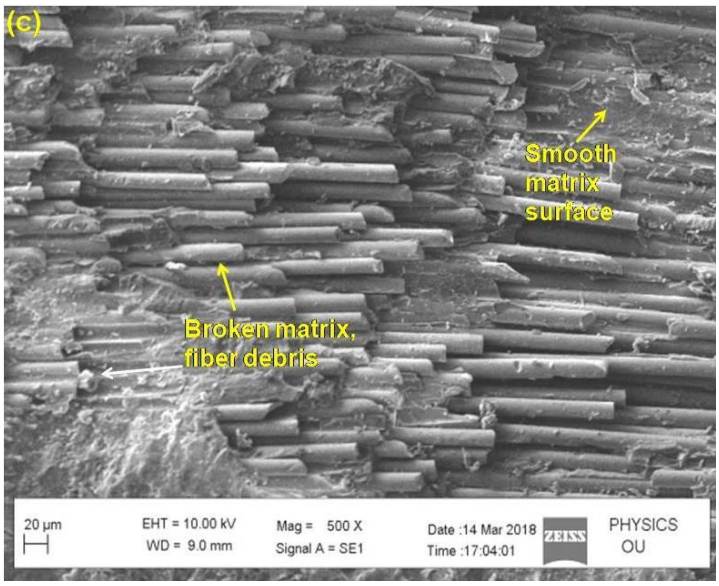

Figure 5.9 (c). SEM image of specimen tested at 2gm/min, 30°impinging angle, 2 bar pressure, 1 min holding period, 30 mm stand-off distance for compositions 2.5 wt.%, 21%, 45˚/-45˚

Fig. 5.9(a) is the SEM image of the tested neat GRE specimens and Fig. 5.9(b) - 5.9(c) are of EGCN are tested at the fixed erosion testing conditions as follows: 2gm/min, 30° impinging angle, 2 bar pressure, 1 min holding period, 30 mm stand-off distance. The mechanism of deformation of the FRPs subjected to erodent particles is as follows; the abrasive particles striking the surface remove the matrix layer first and the fibers are exposed to airstream creating high bending moments on the fibers forming cracks resulting in fracture and ejection of broken fibers forming grooves. If the bombardment persists, it results in the formation of craters. The decreased surface roughness in Fig. 5.9(b)-5.9(c) indicates that the composites containing nanoclay demonstrated critical deformation, which means that the nanoclay has good compatibility with the epoxy resin and glass fiber, forming a strong bond between fiber and matrix thereby slowing down the erosion of EGCN. The neat GFRP in Fig. 5.9(a) shows the rough surface which is comparatively rougher than EGCNs shown in Fig. 5.9(b)-5.9(c). The size of the broken fiber in Fig. 5.9(b) indicates how fast the failure of the fibers occurred, unlike the

matrix which takes more time since it breaks slowly into small debris. In Figure 3, it shows that with increase in fiber volume E_r increased.

Fig. 5.10(a) - 5.10(b) show that at 15° impingement angle, deformation of EGCN occurred due to the ploughing effect caused by hitting sand particles. However, the E_r at 15° angle of impingement is low when compared to E_r value obtained at 60° angle of impingement as the ploughing effect is considerably low. The deformation of the material due to the ploughing effect indicates the semi-brittle nature of the composite. This effect increases with an increase in angle from 15° - 60° and decreases from 60° - 90° [136]. The increase in the sand flow rate increases the number of particles hitting the unit surface area, thereby increasing E_r. Table 37 shows that *f* is the highest contributing factor to E_r. As the air stream pressure increases, the kinetic energy of the sand particles increases resulting in the intense formation of cracks followed by breaking of matrix and fibers, and it is the third highest contributing factor to E_r [14, 15, 27]. Fig. 5.10(c) – 5.10(d) show that

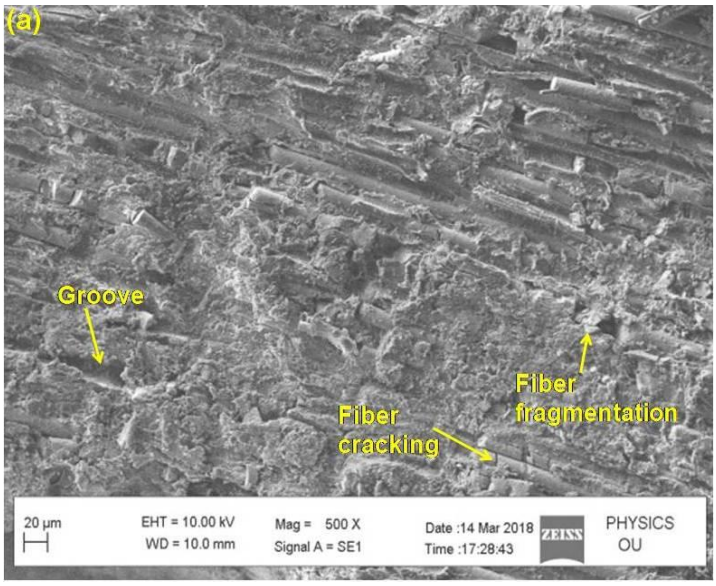

Figure 5.10(a) SEM image of test specimen tested at 2 gm/ min, 15° angle, 2 bar, 1 min,10 mm

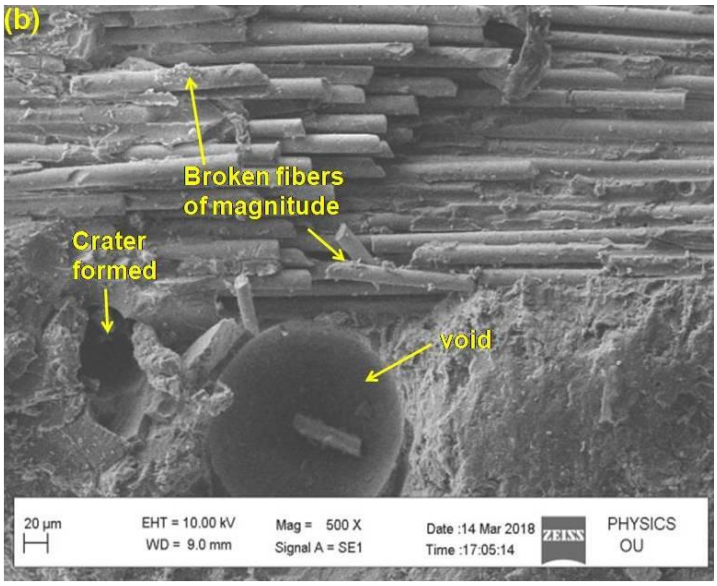

Figure 5.10(b) SEM image of test specimen tested at 2 gm/min, 15° angle, 2 bar, 3 min, 30 mm

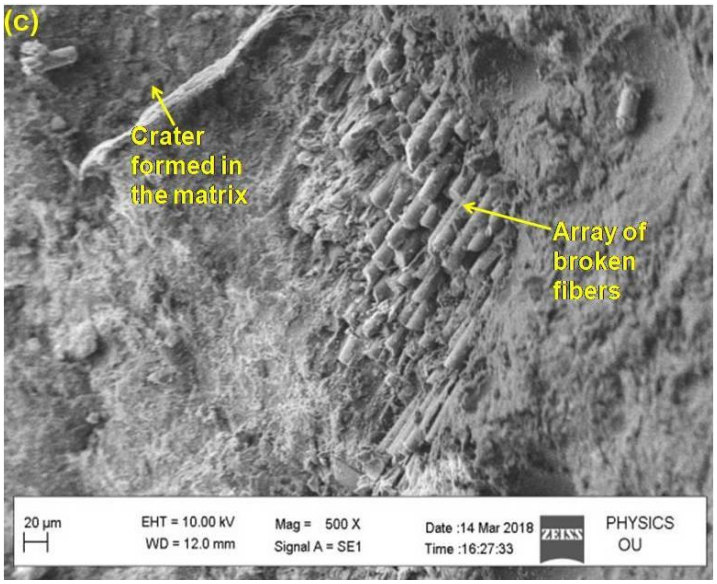

Figure 5.10(c) SEM image of test specimen tested at 4 gm/min, 60° angle, 6 bar, 1 min, 10 mm

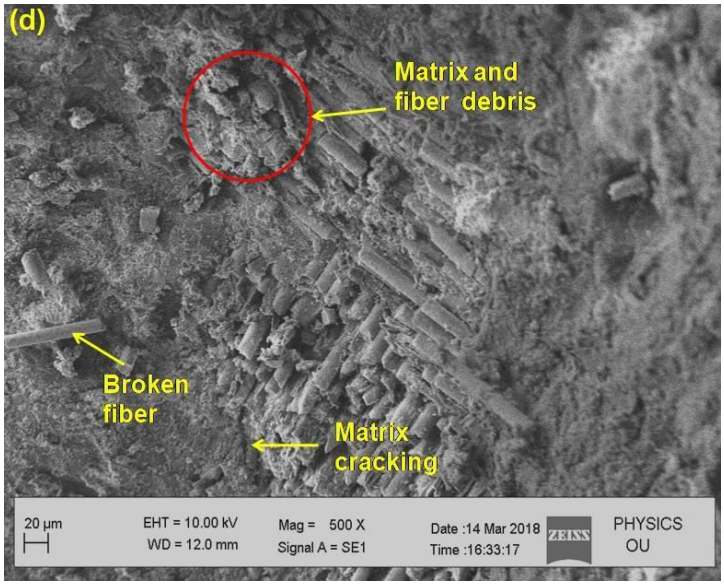

Figure 5.10(d) SEM image of test specimen tested at 4 gm/min, 60° angle, 6 bar, 3 min, 30 mm

the combined effect of all the three major contributing factors at their maximum levels resulted in the deeply eroded region compared to the partially eroded surface shown in Fig. 5.10(a) - 5.10(b), where lower levels of the same factors were used. From Fig. 5.10(c) – 5.10(d) it is obvious that at 6 bar pressure, the deformation is more pronounced on the surface as deeper grooves are formed unlike the shallow grooves observed in Fig. 5.10(a) – 5.10(b). The effect of the parameters *t, d* was low compared to the first three, which is also confirmed by the low percentage contributions exhibited by these factors shown in Anova Table 37.

5.3.3 Summary

In the present study, E_r of EGCN consisting of 2.5 wt% of nanoclay, 10.5 vol% glass fiber, and fibers oriented at 45°/-45° has been investigated. Taguchi method was used to analyze the data and fit a linear model for predicting the E_r. ANOVA analysis was done which showed that all the five parameters were effectively influencing the E_r of EGCN. The optimized result obtained indicated that the best E_r obtained was 1690.44 mg/kg occurred at a sand flow rate of 2 gm/min, impingement angle of 15°, airstream pressure of 2 bar, holding time of 1 min, and stand-off distance of 30 mm. The result is confirmed by preparing and testing five samples at the optimum conditions and the average value of E_r obtained was 1646.41 mg/kg. The fracture

morphology has shown that at high pressure, high sand flow rate, high testing period, low stand-off distance and at 60° impinging angle, the surface has shown deeply eroded zones.

Chapter 6

Conclusions

6.1 Introduction

In this work, mechanical properties and E_r of the EGCNs have been investigated. Glass fiber is reinforced in the range of 10.5 - 31.5 vol.%, nanoclay Cloisite 15A was reinforced in the range of 0.5 - 2.5 wt.%, and glass fibers orientation is changed in between 0°/90° – 45°/-45°. Taguchi and RSM methods were used to design experiments, analyze the data, and present the fitted models. ANOVA analysis was done using both methods to find the effect of each parameter on the responses. The fitted models were used to find the optimum value of response at the optimum conditions determined through the analysis. The results obtained through fitted models at the optimum conditions were confirmed by preparing and testing five samples at the same conditions. The fracture morphology was studied for EGCNs and GRE after each test using scanning electron micrography. The obtained results for EGCNs at the optimum conditions were compared with the GRE reinforced with same volume of glass fiber.

6.2 Overall Conclusions

The following results were obtained after performing all the experiments and analysis done as stated above:

1. New epoxy-glass composites reinforced with Cloisite 15A are fabricated using hand layup method according to Taguchi experimental design and central composite design which is a commonly used response surface method. The selected parameters are nanoclay content in the range of 0.5 wt% to 2.5 wt%, glass fiber volume in the range of 10.5 vol% to 31.5 vol%, and fiber orientation in the range of 0°/90° to +45°/-45°. Tensile strength, flexural strength, plane strain fracture toughness, microhardness, and erosive wear resistance of the composites are evaluated.

2. Taguchi method was used to study the linear effects of parameters and response surface method was used to study the quadratic and interaction effects of parameters on the mechanical properties and erosive wear rate. ANOVA analysis done in both methods revealed the significance of parameters. A linear regression model is fitted by the Taguchi method and a quadratic model is fitted by the response surface method. The properties were optimized in both the methods and validated.

3. The optimized σ_{UTS} obtained in Taguchi and RSM methods are 270.29 MPa and 262.37 which occurred at 2.5 wt% of nanoclay, 31.5 vol% of fiber, and 0°/90° of fibers orientation. The experimentally obtained σ_{UTS} at those conditions was 262 MPa. When compared to GRE 30.8% improvement is observed in σ_{UTS} for EGCN. ANOVA analysis done using both methods showed that all three parameters were effectively influencing the σ_{UTS}. While only glass fiber volume has shown the quadratic effect and the remaining two parameters shown only linear effect and there are no significant interactions are present between parameters.

4. The optimized flexural strength obtained in Taguchi and RSM methods is 215.43 MPa and 215.31 MPa, respectively, which occurred at 2.5 wt% of nanoclay, 31.5 vol% of fiber, and 0°/90° of fibers orientation. The experimentally obtained flexural strength at these conditions is 208.43 MPa. When compared to GRE, 36.3% improvement is observed in flexural strength for EGCN. ANOVA analysis done using both methods showed that all three parameters were effectively influencing the flexural strength. There are no quadratic effects present and no interaction effects are present between parameters.

5. The optimized plane strain fracture toughness obtained in Taguchi and RSM methods is 14.46 MPa-$m^{1/2}$ which occurred at 2.5 wt% of nanoclay, 31.5 vol% of fiber, and 0°/90° of fibers orientation. The experimentally obtained plane strain fracture toughness at these conditions was 14.28 MPa-$m^{1/2}$. When compared to GRE about 29.46% improvement in plane strain fracture toughness was observed for EGCN. ANOVA analysis done using both methods showed that all three parameters are effectively influencing the plane strain fracture toughness. Glass fiber volume and fiber orientation have shown quadratic effect and nanoclay content did not have a quadratic effect. There are no interactions between parameters were observed.

6. The optimized Vickers microhardness obtained in Taguchi and RSM methods are 27.44 HV and 24.68 HV occurred at 2.5 wt% of nanoclay, 31.5 vol% of fiber, and 0°/90° of fibers orientation. The experimentally obtained microhardness at these conditions is 26.73 HV. When compared to GRE, about 50.57% improvement in microhardness was observed for EGCN. ANOVA analysis was done using both methods and showed that nanoclay content and glass fiber volume were effectively influencing the hardness. Glass fiber volume and fiber orientation have shown quadratic effects, whereas nanoclay content did not show quadratic effect. There are no interactions observed between parameters.

7. In case of optimization of the composite parameters for erosion wear, the predicted value of E_r obtained at optimum conditions using regression equation fitted in Taguchi analysis is 1828 mg/kg and predicted E_r obtained at optimum conditions using regression equation obtained RSM analysis is 1743.2 mg/kg. These occurred at 2.5 wt% of nanoclay, 10.5 vol% of fiber, and 45°/-45° of fibers orientation. The experimentally obtained E_r at these conditions was 1865 mg/kg. When compared to GRE, about 29.5% decrease in E_r was observed for EGCN. ANOVA analysis done using both methods showed that all three parameters were effectively influencing the erosive wear rate of EGCN. All three parameters had quadratic effects but there were no interactions between parameters.

8. In case of optimization of the testing parameters for erosion wear, the predicted value of E_r obtained at optimum conditions using regression equation fitted in Taguchi analysis is 1690.4 mg/kg occurred at a sand flow rate of 2 gm/min, impingement angle of 15°, airstream pressure of 2 bar, holding time of 1 min, and stand-off distance of 30 mm. The experimentally obtained E_r at these conditions was 1586 mg/kg. When compared to GRE, about 29.8% decrease in E_r was observed for EGCN. ANOVA analysis done showed that all five parameters were effectively influencing the erosive wear rate of EGCN.

9. The fracture morphology in each mechanical property testing had shown the strong bond between fiber and matrix when nanoclay was added. The matrix morphology of EGCN is rough

in broken specimens because of the restricted crack propagations in the matrix by the clay platelets, whereas GRE has shown smooth morphology.

10. SEM micrography has shown that with an increase in nanoclay content, the surface roughness of the eroded surface greatly reduced indicating slow erosion. Irrespective of increase in hardness with addition of glass fiber, the erosion rate is increased because the fibers broke into sizes much bigger than the matrix and expelled from the zone. At high pressure, high sand flow rate, high testing period, low stand-off distance, and at 60˚ impinging angle, the surface has shown deeply eroded zones.

6.3 Recommendation for Further Research

1. In the present investigation glass fabric was used to prepare the composites. However, there exists other natural fibers like bamboo, bagasses, etc. and commercial fibers such as carbon fiber, aramid fiber, etc. which could be tried and a final conclusion can be drawn there after.

2. The hand-lay-up technique is used to fabricate the composite in the present work. However, there exist other manufacturing processes like compression molding, vacuum bag molding, and pultrusion method, etc. for polymer matrix composite. They could be tried and analyzed, so that a final conclusion (highest mechanical property as well as highest erosive wear resistance) can be drawn therefrom. However, the results provided in this thesis can act as a base for the utilization of this fiber and fillers.

3. From this work, it is found that Cloisite15A significantly improves the mechanical properties and erosion wear resistance of the composite. Other ceramic or metal micro/nanofillers could be tried and a final conclusion (highest mechanical property as well as highest erosive wear resistance) can be drawn after that.

4. In the erosion test, silica sand particles of 200 μm size have been used. This work can be further extended to other particle size and types of particle such as silicon carbide to study the effect of particle size and type of particles on wear behavior of the composite.

References

[1] K. JW, P. K, and W. W., "The production and application of metal matrix composite materials," *J. Mater. Process. Technol.*, vol. 106, pp. 58–67, 2000.

[2] D. B. Miracle, "Metal matrix composites – From science to technological significance," *Compos. Sci. Technol.*, vol. 65, no. 15–16, pp. 2526–2540, 2005.

[3] A. Mortensen and J. Llorca, "Metal Matrix Composites," *Annu. Rev. Mater. Res.*, vol. 40:243-270, 2010.

[4] F. J. McGarry, "Polymer Composites," *Annu. Rev. Mater. Sci.*, vol. 24, pp. 63–82, 1994.

[5] D. N. Saheb and J. P. Jog, "Natural fiber polymer composites: A review," *Adv. Polym. Technol.*, vol. 18, pp. 351–363, 1999.

[6] K. P. Matabola, A. R. De Vries, F. S. Moolman, and A. S. Luyt, "Single polymer composites: A review," *J. Mater. Sci.*, vol. 44, no. 23, pp. 6213–6222, 2009.

[7] H. Ku, N. Wang, H., Pattarachaiyakoop, and M. Trada, "A Review on the Tensile Properties of Natural Fiber Reinforced Polymer Composites," *Compos. Part B Eng.*, vol. 42, no. 4, p. 856–873., 2011.

[8] S. Das, J. Warren, D. West, and S. Schexnayder M., "Global Carbon Fiber Composites Supply Chain Competitiveness Analysis," 2016.

[9] A. P. Chakraverty, "SOME ASPECTS OF EVALUATION OF GFRP COMPOSITE," National Institute of Technology, Rourkela, 2015.

[10] F. P. Reding, "The stiffness modulus of polyethylene as a function of temperature and structure," *J. Polym. Sci.*, vol. 32, no. 125, 1958.

[11] N. Okui and J. H. Magill, "Crystallinity of poly(tetramethyl-p-silphenylenesiloxane) and (tetramethyl-p-silphenylenesiloxane)-(dimethyl siloxane) copolymers," *Polymer (Guildf).*, vol. 18, no. 11, pp. 1152–1156, 1977.

[12] M. N. Huda, H. Dragaun, S. Bauer, and H. Muschik, "A Study of the Crystallinity Index of Polypropylene Fibres," *Colloid Polym. Sci.*, vol. 263, no. 9, pp. 730–737, 1985.

[13] M. Krumova, D. López, R. Benavente, and C. J. M. Mijangos, "Effect of crosslinking on the mechanical and thermal properties of poly(vinyl alcohol)," *Polymer (Guildf).*, vol. 41,

no. 26, pp. 9265–9272, 2000.

[14] A. El-Hadi, R. Schnabel, E. Straube, G. Müller, and S. Henning, “Correlation between degree of crystallinity, morphology, glass temperature, mechanical properties and biodegradation of poly (3-hydroxyalkanoate) PHAs and their blends,” *Polym. Test.*, vol. 21, no. 6, pp. 665–674, 2002.

[15] J. Keeler and P. Wothers, *Chemical Structure and Reactivity An Integrated Approach*, Second Edi. Oxford University Press, 2013.

[16] I. Fraga, J. M. Hutchinson, and S. Montserrat, “Vitrification and devitrification during the non-isothermal cure of a thermoset: A TOPEM study,” *J. Therm. Anal. Calorim.*, vol. 99, no. 3, pp. 925–929, 2010.

[17] B. Katerska, G. Exner, E. Perez, and M. N. Krasteva, “Cooling rate effect on the phase transitions in a polymer liquid crystal: DSC and real-time MAXS and WAXD experiments,” *Eur. Polym. J.*, vol. 46, no. 7, pp. 1623–1632, 2010.

[18] L. A. Khan, A. Kausar, and R. J. Day, “Aerospace composite cured by quickstep and autoclave processing techniques: Evaluation and comparison of reaction progress,” *Aerosp. Sci. Technol.*, vol. 65, pp. 100–105, 2017.

[19] R. J. J. Williams, M. A. Benavente, R. A. Ruseckaite, M. S. Churio, and H. G. Hack, “Criteria for selecting cure cycles in autoclave processing of graphite/epoxy composites,” *Polym. Eng. Sci.*, vol. 30, no. 18, pp. 1140–1145, 1990.

[20] G. Jungang, L. Deling, S. Shigang, and L. Guodong, “Curing kinetics and thermal property characterization of a bisphenol-F epoxy resin and DDO system,” *Appl. Polym. Sci.*, vol. 83, no. 7, pp. 1586–1595, 2002.

[21] V. L. Zvetkov, “Mechanistic modeling of the epoxy–amine reaction: Model derivations,” *Thermochim. Acta*, vol. 435, no. 1, pp. 71–84, 2005.

[22] L. Banks and B. Ellis, “The glass transition temperature of an epoxy resin and the effect of absorbed water,” *Polym. Bull.*, vol. 1, no. 6, pp. 377–382, 1979.

[23] J. S. Nakka, K. M. B. Jansen, and L. J. Ernst, “Effect of chain flexibility in the network structure on the viscoelasticity of epoxy thermosets,” *J. Polym. Res.*, vol. 18, no. 6, pp. 1879–1888, 2011.

[24] E. Crawford and A. J. Lesser, “The effect of netwrork architecture on the thermal and mechanical behaviour of epoxy resins", *J. Polym. Sci. B. Polym. Phys.*, vol. 36, no. 8, pp.

1371–1382, 1998.

[25] L. LG, L. H, E. JE, S. JW, and B. CN., "The effect of cure rate on the mechanical properties of dental resins," *Dent. Mater.*, vol. 17, no. 6, pp. 504–11, 2001.

[26] C. Nightingale and R. J. Day, "Flexural and interlaminar shear strength properties of carbon fibre/epoxy composites cured thermally and with microwave radiation," *Compos. Part A Appl. Sci. Manuf.*, vol. 33, no. 7, pp. 1021–1030, 2002.

[27] H. Sun, Y. Liu, Y. Wang, and H. Tan, "Curing behavior of epoxy resins in two-stage curing process by non-isothermal differential scanning calorimetry kinetics method," *J. Appl. Polym. Sci.*, vol. 131, no. 17, pp. 1–8, 2014.

[28] L. L., Z. B.M., W. D.F., and W. Z.J., "Effect of cure cycles on void content and mechanical properties of composite laminates," *Compos. Struct.*, vol. 73, no. 3, pp. 303–309, 2006.

[29] Z. I, P. M, and D. L. ML, "Influence of crosslinker and ionic comonomer concentration on glass transition and demixing/mixing transition of copolymers poly(N-isopropylacrylamide) and poly(sodium acrylate) hydrogels," *Colloid Polym. Sci.*, vol. 292, pp. 485–492, 2013.

[30] E. B, *Chemistry and technology of epoxy resins*. 1993.

[31] T. Lan and T. J. Pinnavaia, "Clay-reinforced epoxy nanocomposites," *Chem. Mater.*, vol. 6, no. 12, pp. 2216–2219, 1994.

[32] K. L. Loewenstein, "The Manufacturing Technology of Continuous Glass Fibers," *Platin. Met. Rev.*, vol. 19, no. 3, pp. 82–87, 1975.

[33] "A Market Assessment and Impact Analysis of the Owens Corning Acquisition of Saint-Gobain's Reinforcement and Composites Business is out Now," 2008.

[34] U. Fritz, Wolfgang Gerhartz, Y. S. Yamamoto, B. Elvers, and J. F. Rounsaville, *Ullmann's encyclopedia of industrial chemistry. Vol. A11, Fibers. 5. synthetic inorganic to formaldehyde*, 5th ed. Germany: Wiley-VCH, 1988.

[35] V. B. Gupta and V. K. Kothari, *Manufactured Fibre Technology*, 1st ed. Springer Netherlands, 1997.

[36] V. M. B., *Technical approach to glass*. New York : Elsevier, 1990.

[37] F. W. T., J. C. Watson, and H. Li, "Glass Fibers," *ASM Handb.*, vol. 21, no. Composites (#06781G), 2001.

[38] M. Zoghi, *The International Handbook of FRP Composites in Civil Engineering,*. CRC Press, 2013.

[39] J. C. Gerdeen and R. A. Rorrer, *Engineering design with polymers and composites*. CRC Press, 2011.

[40] H. Mahmood, "Multifunctionality in epoxy / glass fibers composites with graphene interphase," 2017.

[41] M. C. Roco, "Nanoparticles and Nanotechnology Research," *J. Nanoparticle Res.*, vol. 1, no. 1, pp. 1–6, 1999.

[42] R. N. Rothon, "Particulate Fillers for Polymers," *Rapra Rev. Reports*, 2002.

[43] E. Reynaud, C. Gauthier, and J. Perez, "Nanophases in polymers," *Rev. Metall. Cah. d'Informations Tech.*, vol. 96, no. 2, pp. 169–176, 1999.

[44] M. Zhang, M. Z. Rong, H. M. Zeng, and S. Schmitt, "Atomic force microscopy study on structure and properties of irradiation grafted silica particles in polypropylene-based nanocomposites," *J. Appl. Polym. Sci.*, vol. 80, no. 12, pp. 2218–2227, 2001.

[45] S. W. Bailey, "The status of clay mineral structures," in *Clays and Clays Minerals Proceedings 14th National Conference*, 1966, pp. 1–23.

[46] U. Hoffman, K. Endell, and D. Wilm, "Kristallstruktur and Quellung von Montmorillonit," *Z. Krist.*, vol. 86, pp. 340–348, 1933.

[47] H. Van Olphen, *An introduction to clay colloids chemistry*. Wiley, New York, 1977.

[48] A. Okada, M. Kawasumi, A. Usuki, and Y. Kojima, "Nylon 6–Clay Hybrid," *MRS Online Proceeding Libr. Arch.*, vol. 171, 1989.

[49] A. Usuki, M. Kawasumi, Y. Kojima, A. Okada, T. Kurauchi, and O. Kamigaito, "Swelling behaviour of montmorillonite cation-exchanged for ω-amino acids by ε-caprolactam," *J. Mater. Res.*, vol. 8, pp. 1174–1178, 1993.

[50] A. Usuki, M. Kawasumi, Y. Kojima, A. Okada, T. Kurauchi, and O. Kamigaito, "Synthesis of nylon 6-clay hybrid," *J. Mater. Res.*, vol. 8, pp. 1179–1184, 1993.

[51] J. W. Jordan, "Organophilic Bentonites. I. Swelling in Organic Liquids.," *J. Phys. Chem.*, vol. 53, no. 2, pp. 294–306, 1949.

[52] A. Weiss, "Organic Derivatives of Mica-type Layer-Silicates," *Chemie Int. Ed.*, vol. 2, no. 3, pp. 134–144, 1963.

[53] T. Lan, P. D. Kaviratna, and P. T. J., "Mechanism of clay tactoid exfoliation in epoxy-clay

nanocomposites," *Chem. Mater. Mater.*, vol. 7, pp. 2144–215, 1995.

[54] Z. Wang and T. J. Pinnavaia, "Hybrid organic-inorganic nanocomposites: exfoliation of magadiite nanolayers in an elastomeric epoxy polymer," *Chem. Mater.*, vol. 10, pp. 1820–1826, 1998.

[55] G. Lagaly, "Interaction of alkylamines with different types of layered compounds," *Solid State Ionics*, vol. 22, pp. 43–51.

[56] M. Alexandre and P. Dubois, "Polymer- Layered Silicate Nanocomposites: Preparation, Properties and Uses of a New Class of Materials," *Mater. Sci. Eng.*, vol. 28, no. March, pp. 1–63, 2000.

[57] A. K. Dhingra, "Metals Replacement by Composites," *J. Miner. Met. Mater. Soc.*, vol. 38, no. 3, p. 17, 1986.

[58] R. Mehrabian, R. G. Riek, and M. Lemings, "Preparation and casting of metal-particulate non-metal composites," *Metall. Trans.*, vol. 5, no. 8, pp. 1899–1905, 1974.

[59] J. Eliasson and R. Sandström, "Applications of aluminium matrix composites," *Key Eng. Mater.*, vol. 104, pp. 3–36, 1995.

[60] X. Kornmann, M. Rees, Y. Thomann, A. Necola, M. Barbezat, and R. Thomann, "Epoxy-layered silicate nanocomposites as matrix in glass fibre-reinforced composites," *Compos. Sci. Technol.*, vol. 65, no. 14, pp. 2259–2268, 2005.

[61] E. Bozkurt, E. Kaya, and M. Tanoğlu, "Mechanical and thermal behavior of non-crimp glass fiber reinforced layered clay/epoxy nanocomposites," *Compos. Sci. Technol.*, vol. 67, no. 15–16, pp. 3394–3403, 2007.

[62] Y. Shi, K. Kanny, and P. Jawahar, "Hybrid nanocomposites: Processing and properties," *Adv. Compos. Mater.*, vol. 18, no. 4, pp. 365–379, 2009.

[63] K. Wang, L. Chen, M. Kotaki, and C. He, "Preparation , microstructure and thermal mechanical properties of epoxy / crude clay nanocomposites," *Compos. Part A*, vol. 38, pp. 192–197, 2007.

[64] C. L. Wu, M. Q. Zhang, M. Z. Rong, and K. Friedrich, "Tensile performance improvement of low nanoparticles filled-polypropylene composites," *Compos. Sci. Technol.*, vol. 62, no. 10–11, pp. 1327–1340, 2002.

[65] A. Yasmin, J. J. Luo, J. L. Abot, and I. M. Daniel, "Mechanical and thermal behavior of clay/epoxy nanocomposites," *Compos. Sci. Technol.*, vol. 66, no. 14, pp. 2415–2422, 2006.

[66] A. Yasmin, J. L. Abot, and I. M. Daniel, “Processing of clay/epoxy nanocomposites by shear mixing,” *Scr. Mater.*, vol. 49, no. 1 SPEC., pp. 81–86, 2003.

[67] X. Liu and Q. Wu, “PP / clay nanocomposites prepared by grafting-melt intercalation,” vol. 42, pp. 10013–10019, 2001.

[68] P. C. Lebaron, Z. Wang, and T. J. Pinnavaia, “Polymer-layered silicate nanocomposites: An overview,” *Appl. Clay Sci.*, vol. 15, no. 1–2, pp. 11–29, 1999.

[69] S. Ganguli, D. Dean, K. Jordan, G. Price, and R. Vaia, “Mechanical properties of intercalated cyanate ester –layered silicate nanocomposites,” vol. 44, pp. 1315–1319, 2003.

[70] D. Dean, A. M. Obore, S. Richmond, and E. Nyairo, “Multiscale fiber-reinforced nanocomposites: Synthesis, processing and properties,” *Compos. Sci. Technol.*, vol. 66, no. 13, pp. 2135–2142, 2006.

[71] S. Gurusideswar and R. Velmurugan, “Strain rate sensitivity of glass/epoxy composites with nanofillers,” *Mater. Des.*, vol. 60, pp. 468–478, 2014.

[72] G. C. Jacob, J. M. Starbuck, J. F. Fellers, S. Simunovic, and R. G. Boeman, “Strain rate effects on the mechanical properties of polymer composite materials,” *J. Appl. Polym. Sci.*, vol. 94, no. 1, pp. 296–301, 2004.

[73] Y. Ou *et al.*, “Mechanical Characterization of the Tensile Properties of Glass Fiber and Its Reinforced Polymer (GFRP) Composite under Varying Strain Rates and Temperatures,” *Polymers (Basel).*, vol. 8, no. 5, p. 196, 2016.

[74] R. Velmurugan and T. P. Mohan, “Epoxy-clay nanocomposites and hybrids: Synthesis and characterization,” *J. Reinf. Plast. Compos.*, vol. 28, no. 1, pp. 17–37, 2009.

[75] A. S. Zerda and A. J. Lesser, “Intercalated clay nanocomposites: Morphology, mechanics, and fracture behavior,” *J. Polym. Sci. Part B Polym. Phys.*, vol. 39, no. 11, pp. 1137–1146, 2001.

[76] A. Haque, M. Shamsuzzoha, F. Hussain, and D. Dean, “S2-glass/epoxy polymer nanocomposites: Manufacturing, structures, thermal and mechanical properties,” *J. Compos. Mater.*, vol. 37, no. 20, pp. 1821–1838, 2003.

[77] O. Okoli and G. Smith, “High Strain Rate Characterization of a Glass/Epoxy Composite,” *J. Compos. Technol. Res.*, vol. 22, no. 1, p. 3, 2000.

[78] T. Govaert, L. E., Schellens, H. J., De Kok, J. M. M., and Peijs, “Micromechanical Modelling of Time Dependent Failure in Transversely Loaded Composites,” *Proceedings,*

3rd In- ternational Conf. Deform. Fract. Compos. IoM, pp. 77–85, 1995.

[79] F. Fereshteh-Saniee, G. H. Majzoobi, and M. Bahrami, "An experimental study on the behavior of glass-epoxy composite at low strain rates," *J. Mater. Process. Technol.*, vol. 162–163, no. SPEC. ISS., pp. 39–45, 2005.

[80] M. M. Shokrieh and M. J. Omidi, "Tension behavior of unidirectional glass/epoxy composites under different strain rates," *Compos. Struct.*, vol. 88, no. 4, pp. 595–601, 2009.

[81] F. Hussain, "Polymer-matrix Nanocomposites, Processing, Manufacturing, and Application: An Overview," *J. Compos. Mater.*, vol. 40, no. 17, pp. 1511–1575, 2006.

[82] B. Chen and J. R. G. Evans, "Impact and tensile energies of fracture in polymer-clay nanocomposites," *Polymer (Guildf).*, vol. 49, no. 23, pp. 5113–5118, 2008.

[83] R. K. Bharadwaj, A. R. Mehrabi, C. Hamilton, C. Trujillo, and M. Murga, "Structure - property relationships in cross-linked polyester - clay nanocomposites," *Polymer (Guildf).*, vol. 43, pp. 3699–3705, 2002.

[84] B. A. Bhanvase, D. V. Pinjari, P. R. Gogate, S. H. Sonawane, and A. B. Pandit, "Synthesis of exfoliated poly(styrene-co-methyl methacrylate)/montmorillonite nanocomposite using ultrasound assisted in situ emulsion copolymerization," *Chem. Eng. J.*, vol. 181–182, pp. 770–778, 2012.

[85] I. Zaman *et al.*, "Interface-tuned epoxy/clay nanocomposites," *Polymer (Guildf).*, vol. 52, no. 2, pp. 497–504, 2011.

[86] X. Li, Z. J. Zhan, G. R. Peng, and W. K. Wang, "Nano-disassembling method-A new method for preparing completely exfoliated epoxy/clay nanocomposites," *Appl. Clay Sci.*, vol. 55, pp. 168–172, 2012.

[87] G. J. Withers *et al.*, "Improved mechanical properties of an epoxy glass-fiber composite reinforced with surface organomodified nanoclays," *Compos. Part B Eng.*, vol. 72, pp. 175–182, 2015.

[88] S. Gurusideswar and R. Velmurugan, "High Strain Rate Sensitivity of Glass / Epoxy / Clay Nanocomposites," *10th Int. Conf. Compos. Sci. Technol.*, no. September, pp. 1–12, 2015.

[89] K. A. Brown, R. Brooks, and N. A. Warrior, "The static and high strain rate behaviour of a commingled E-glass/polypropylene woven fabric composite," *Compos. Sci. Technol.*, vol. 70, no. 2, pp. 272–283, 2010.

[90] S. Zainuddin, M. V. Hosur, Y. Zhou, A. T. Narteh, A. Kumar, and S. Jeelani, "Experimental and numerical investigations on flexural and thermal properties of nanoclay-epoxy nanocomposites," *Mater. Sci. Eng. A*, vol. 527, no. 29–30, pp. 7920–7926, 2010.

[91] R. Jeyakumar, P. S. Sampath, R. Ramamoorthi, and T. Ramakrishnan, "Structural , morphological and mechanical behaviour of glass fibre reinforced epoxy nanoclay composites," *Int. J. Adv. Manuf. Technol.*, vol. 93, pp. 527–535, 2017.

[92] P. P. Binu, K. E. George, and M. N. Vinodkumar, "Effect of Nanoclay, Cloisite15A on the Mechanical Properties and Thermal Behavior of Glass Fiber Reinforced Polyester," *Procedia Technol.*, vol. 25, no. Raerest, pp. 846–853, 2016.

[93] U. A. Kini, P. H. Manjunath Shettar, Sathyashankara Sharma, G. M. C, A. Hegde, and D. Siddhartha, "Effect of hygrothermal aging on the mechanical properties of nanoclay- glass fiber-epoxy composite and optimization using full factorial design," *Mater. Res. Lett.*, pp. 1–13, 2019.

[94] K. Prabhakar, S. Debnath, M. Anwar, and K. Palanikumar, "Experimental Analysis on the Effect of Surface Treatment of Glass Fibers & Nanoclay on Mechanical Properties of Glass Fiber Reinforced Polymer Nanocomposites Experimental Analysis on the Effect of Surface Treatment of Glass Fibers & Nanoclay on Mechanical," 2019.

[95] L. B. Manfredi, H. De Santis, and A. Vázquez, "Influence of the addition of montmorillonite to the matrix of unidirectional glass fibre/epoxy composites on their mechanical and water absorption properties," *Compos. Part A Appl. Sci. Manuf.*, vol. 39, no. 11, pp. 1726–1731, 2008.

[96] S. Sinha Ray and M. Okamoto, "Polymer/layered silicate nanocomposites: A review from preparation to processing," *Prog. Polym. Sci.*, vol. 28, no. 11, pp. 1539–1641, 2003.

[97] V. Mittal, "Polymer layered silicate nanocomposites: A review," *Materials (Basel).*, vol. 2, no. 3, pp. 992–1057, 2009.

[98] B. Sharma, S. Mahajan, R. Chhibber, and R. Mehta, "Glass Fiber Reinforced Polymer-Clay Nanocomposites: Processing, Structure and Hygrothermal Effects on Mechanical Properties," *Procedia Chem.*, vol. 4, pp. 39–46, 2012.

[99] M. Zulfli and W. Chow, "Mechanical and thermal behaviours of glass fiber reinforced epoxy hybrid composites containing organo-montmorillonite," *Malaysian Polym. J.*, vol.

7, no. 1, pp. 1–8, 2012.

[100] N. A. Siddiqui, R. S. C. Woo, J. Kim, and C. C. K. Leung, “Mode I interlaminar fracture behavior and mechanical properties of CFRPs with nanoclay-filled epoxy matrix,” vol. 38, pp. 449–460, 2007.

[101] J. J. Karippal, H. N. N. Murthy, K. S. Rai, M. Sreejith, and M. Krishna, “Study of mechanical properties of epoxy/glass/nanoclay hybrid composites,” *J. Compos. Mater.*, vol. 45, no. 18, pp. 1893–1899, 2011.

[102] S. U. Khan, A. Munir, R. Hussain, and J. K. Kim, “Fatigue damage behaviors of carbon fiber-reinforced epoxy composites containing nanoclay,” *Compos. Sci. Technol.*, vol. 70, no. 14, pp. 2077–2085, 2010.

[103] J. M. L. Reis, J. L. V. Coelho, A. H. Monteiro, and H. S. Da Costa Mattos, “Tensile behavior of glass/epoxy laminates at varying strain rates and temperatures,” *Compos. Part B Eng.*, vol. 43, no. 4, pp. 2041–2046, 2012.

[104] K. Kanny and T. P. Mohan, “Resin infusion analysis of nanoclay filled glass fiber laminates,” *Compos. Part B Eng.*, vol. 58, pp. 328–334, 2014.

[105] K. Krushnamurty, D. Rasmitha, I. Srikanth, K. Ramji, C. Subrahmanyam, and A. R. Materials, “Effect of Volume Fraction of Fibre on the Mechanical Properties of Nanoclay Reinforced E-Glass-Epoxy Composites,” *Int. J. Mater. Metall. Eng.*, vol. 10, no. 1, pp. 98–101, 2016.

[106] M. H. G. Wichmann, J. Sumfleth, and F. H. Gojny, “Glass-fibre-reinforced composites with enhanced mechanical and electrical properties – Benefits and limitations of a nanoparticle modified matrix,” vol. 73, pp. 2346–2359, 2006.

[107] I. Srikanth, S. Kumar, V. Singh, and B. Rangababu, “Effect of carbon nanofibre addition on the mechanical properties of different Vf carbon-epoxy composites,” *Bull. Mater. Sci.*, vol. 38, no. 2, pp. 309–317, 2015.

[108] M. Najafi, A. Darvizeh, and R. Ansari, “Effect of Nanoclay Addition on the Hygrothermal Durability of Glass / Epoxy and Fiber Metal Laminates,” *Fibers Polym.*, vol. 19, no. 9, pp. 1956–1969, 2018.

[109] G. Swaminathan and K. Shivakumar, “Thermomechanical and fracture properties of exfoliated nanoclay nanocomposites,” *J. Reinf. Plast. Compos.*, vol. 30, no. 3, pp. 256–268, 2011.

[110] J.-L. Tsai and M.-D. Wu, "Organoclay Effect on Mechanical Responses of Glass/Epoxy Nanocomposites," *J. Compos. Mater.*, vol. 42, no. 6, pp. 553–568, 2008.

[111] L. F. P. Santos and B. Ribeiro, "Influence of nanoclay on interlaminar shear strength and fracture toughness of glass fiber reinforced nanocomposites Influence of nanoclay on interlaminar shear strength and fracture toughness of glass fiber reinforced nanocomposites," *IOP Conf. Ser. Mater. Sci. Eng.*, vol. 346, 2018.

[112] W. Steinmann and A.-K. Saelhoff, "Essential Properties of Fibres for Composite Applications," in *Fibrous and Textile Materials for Composite Applications*, Springer, 2016, pp. 39–73.

[113] P. Jawahar and M. Balasubramanian, "Influence of nanosize clay platelets on the mechanical properties of glass fiber reinforced polyester composites.," *J. Nanosci. Nanotechnol.*, vol. 6, no. 12, pp. 3973–3976, 2006.

[114] X. Wang, X. Zhao, Z. Wu, Z. Zhu, and Z. Wang, "Interlaminar shear behavior of basalt FRP and hybrid FRP laminates," *J. Compos. Mater.*, p. 0021998315587132-, 2015.

[115] A. Wang, D. Xia, G. Xian, and H. Li, "Effect of Nanoclay Grafting onto Flax Fibers on the Interfacial Shear Strength and Mechanical Properties of Flax / Epoxy Composites," *Polym. Compos.*, pp. 1–11, 2019.

[116] L. J. W, H. A, R. A. R, and W. M. U, "Morphology, thermal and mechanical behavior of polypropylene nanocomposites toughened with poly (Ethylene-Co-Octene)," *Polym. Int.*, vol. 55, no. 2, pp. 204–215, 2006.

[117] J.-C. Lin, L. C. Chang, M. H. Nien, and H. L. Ho, "Mechanical behavior of various nanoparticle filled composites at low-velocity impact," *Compos. Struct.*, vol. 74, no. 1, pp. 30–36, 2006.

[118] C. Basara, U. Yilmazer, and G. Bayram, "Synthesis and characterization of epoxy based nanocomposites," *J. Appl. Polym. Sci.*, vol. 98, no. 3, pp. 1081–1086, 2005.

[119] A. C. T. A. J. Kinloch, "Mechanical and Fracture Properties of Epoxy/Inorganic Micro-and Nano-composites," *J. Mater. Sci. Lett.*, vol. 22, pp. 1439–1442, 2003.

[120] S. Mishra *et al.*, "Studies on mechanical performance of biofibre/glass reinforced polyester hybrid composites," *Compos. Sci. Technol.*, vol. 63, no. 10, pp. 1377–1385, 2003.

[121] A. Rafiq, N. Merah, R. Boukhili, and M. Al-qadhi, "Impact resistance of hybrid glass fiber reinforced epoxy/nanoclay composite," *Polym. Test.*, vol. 57, pp. 1–11, 2017.

[122] S. U. Khan, K. Iqbal, A. Munir, and J. K. Kim, "Quasi-static and impact fracture behaviors of CFRPs with nanoclay-filled epoxy matrix," *Compos. Part A Appl. Sci. Manuf.*, vol. 42, no. 3, pp. 253–264, 2011.

[123] H. Khanjanzadeh, T. Tabarsa, A. Shakeri, and A. Omidvar, "Effect of organoclay platelets on the mechanical properties of wood-plastic composites formulated with virgin and recycled polypropylene," *Wood Mater. Sci. Eng.*, pp. 1–6, 2011.

[124] G. K. Idiyatullina, S. I. Vol'fson, R. K. Sabirov, and R. S. Yarullin, "Effect of the montmorillonite cloisite 15A on the structure and properties of poly(1-butene)," *Polym. Sci. Ser. A*, vol. 54, no. 6, pp. 493–498, 2012.

[125] P. K. Mallick, *Fiber-reinforced composites: materials, manufacturing, and design*, 3rd ed. CRC Press, 2007.

[126] E. Petrie, *Epoxy adhesive formulations*. McGraw Hill Professional, 2005.

[127] A. A. Azeez, K. Y. Rhee, S. J. Park, and D. Hui, "Epoxy clay nanocomposites - Processing, properties and applications: A review," *Compos. Part B Eng.*, vol. 45, no. 1, pp. 308–320, 2013.

[128] ASTM E 384, "Standard Test Method for Microindentation Hardness of Materials," *ASTM Int.*, vol. USA, 2017.

[129] M. Bagci, H. Imrek, and O. Mashi Khalfan, "Optimization of Test Parameters That Influence Erosive Wear Behaviors of Glass Fiber-Reinforced Epoxy Composites by Using the Taguchi Method," *J. Tribol.*, vol. 137, no. 1, p. 011602, 2014.

[130] H. K. Kumar, S.M., Satsangi, P.S. and Sardana, "Optimization of surface roughness in turning unidirectional glass fiber reinforced plastics (UD-GFRP) composites using polycrystalline diamond (PCD) cutting tool," *Indian J. ofEngineering Mater. Sci.*, vol. 19, no. 3, pp. 163–174, 2012.

[131] W. Liu, S. V. Hoa, and M. Pugh, "Organoclay-modified high performance epoxy nanocomposites," *Compos. Sci. Technol.*, vol. 65, no. 2, pp. 307–316, 2005.

[132] A. Patnaik, A. Satapathy, S. S. Mahapatra, and R. R. Dash, "A modeling approach for prediction of erosion behavior of glass fiber-polyester composites," *J. Polym. Res.*, vol. 15, no. 2, pp. 147–160, 2008.

[133] S. S. Mahapatra, A. Patnaik, and A. Satapathy, "Taguchi method applied to parametric appraisal of erosion behavior of GF-reinforced polyester composites," *Wear*, vol. 265, no.

1–2, pp. 214–222, 2008.

[134] T. Alomayri and I. M. Low, “Synthesis and characterization of mechanical properties in cotton fiber-reinforced geopolymer composites,” *J. Asian Ceram. Soc.*, vol. 1, no. 1, pp. 30–34, 2013.

[135] M. Bagci and H. Imrek, “Solid particle erosion behaviour of glass fibre reinforced boric acid filled epoxy resin composites,” *Tribol. Int.*, vol. 44, no. 12, pp. 1704–1710, 2011.

[136] A. P. Harsha and S. K. Jha, “Erosive wear studies of epoxy-based composites at normal incidence,” *Wear*, vol. 265, pp. 1129–1135, 2008.

[137] V. K. Srivastava and A. G. Pawar, “Solid particle erosion of glass fibre reinforced flyash filled epoxy resin composites,” *Compos. Sci. Technol.*, vol. 66, no. 15, pp. 3021–3028, 2006.

[138] S. Biswas and A. Satapathy, “Tribo-performance analysis of red mud filled glass-epoxy composites using Taguchi experimental design,” *Mater. Des.*, vol. 30, no. 8, pp. 2841–2853, 2009.

Publications

1. Z. Shanti Kiran, V. Suresh Babu, K.V. Sai Srinadh, **Effect of Nanoclay, Glass fiber volume, and orientation on tensile strength of epoxy-glass composite and optimization using Taguchi method", World journal of Engineering**, vol. 15, no. 2, pp: 312-320, 2018. doi: 10.1108/WJE-08-2017-0286.

2. Z. Shanti Kiran, V. Suresh Babu, K.V. Sai Srinadh, **Investigation of the microhardness and solid particle erosive wear of organoclay filled glass-epoxy nanocomposites and Optimization using Taguchi method**, Australian Journal of Mechanical Engineering, 2018. doi: 10.1080/14484846.2018.1527076.

3. Z. Shanti Kiran, V. Suresh Babu, **Study of the microhardness and erosive wear behavior of organo-modified nanoclay filled glass-epoxy composites and Optimization**. Journal of Mechanical Engineering and Sciences, vol. 13, no. 2, pp: 4793-4814, 2019. doi: 10.15282/jmes.13.2.2019.03.0400

4. Z. Shanti Kiran, V. Suresh Babu, K.V. Sai Srinadh, **Mechanical and Thermo-mechanical properties of Epoxy-Nanoclay-Glass fiber composites: A Review**, Under Review, Polymer Composites.

5. Z. Shanti Kiran, V. Suresh Babu, **Investigation of tensile strength of Epoxy-Glass composite with addition of Cloisite 15A nanoclay and its Optimization**, Under Review, Arabian Journal for Science and Engineering.

Conferences

1. Z. Shanti Kiran, V. Suresh Babu, K.V. Sai Srinadh, **Tensile characteristics of epoxy/glass/clay composite with polyamine based hardener**, National Symposium of Mechanical Engineering Research Scholars, NITW, 7th October 2016.